# Ocean / Ice sheet interactions : toward a coupled model system

Nacho Merino

Communauté
UNIVERSITÉ Grenoble Alpes

# THÈSE

Pour obtenir le grade de

## DOCTEUR DE LA COMMUNAUTÉ UNIVERSITÉ GRENOBLE ALPES

Spécialité : Sciences de la Terre et de l'Univers et de l'Environnement (CESTUE)

Arrêté ministériel : 25 mai 2016

Présentée par


## Nacho MERINO

Thèse dirigée par **Gaël DURAND**, cnrs
et codirigée par **Julien LE SOMMER**, Chargé de Recherche, CNRS

préparée au sein du **Laboratoire de Glaciologie en Géophysique de l'Environnement (LGGE)**
dans **l'École Doctorale Terre, Univers, Environnement**


# Interactions calotte polaire/océan : vers la mise en place d'une modélisation couplée

# Ocean / Ice sheet interactions: toward a coupled model system

Thèse soutenue publiquement le **2 décembre 2016**,
devant le jury composé de :

**Monsieur JULIEN LE SOMMER**
CHARGE DE RECHERCHE, CNRS DELEGATION ALPES, Co-directeur de thèse
**Monsieur GILLES REVERDIN**
DIRECTEUR DE RECHERCHE, CNRS DELEGATION PARIS, Rapporteur
**Madame MARIE-NOËLLE HOUSSAIS**
DIRECTRICE DE RECHERCHE, CNRS DELEGATION PARIS, Examinateur
**Monsieur JEAN-BASPTISTE SALLEE**
CHARGE DE RECHERCHE, CNRS DELEGATION PARIS, Rapporteur
**Monsieur XYLAR STORM ASAY-DAVIS**
CHARGE DE RECHERCHE, PIK - ALLEMAGE, Examinateur **Monsieur MICHEL FILY**
PROFESSEUR, UNIVERSITE GRENOBLE ALPES, Président

# Contents

Chapter 1

# Introduction

Contents



## 1 Antarctic Polar Region

The challenging Antarctic Polar Region is the most isolated, the most extreme region on Earth and the last to be touched by human beings. It has attracted the attention of navigators in the $XVIII^{th}$ century, explorer expeditions in the $XIX^{th}$ century, and scientists since the early $XX^{th}$ century to nowadays. The last continent to be sighted by the explorers, like James Cook, John Davis or Bellingshausen; the playground of the last big expedition race between Amundsen and Scott; and today, one of the last places on Earth to find some of the missing pieces of the most complex of puzzles: the climate.

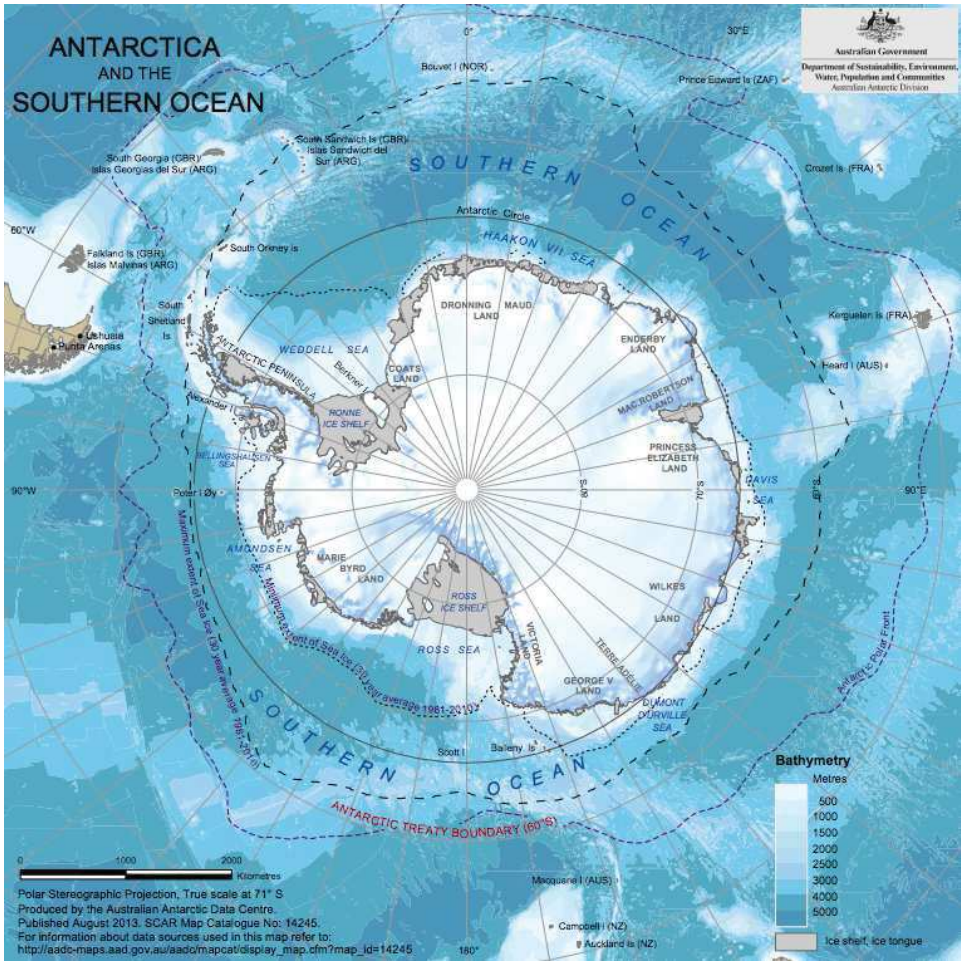


Figure 1.1: Map of the Antarctic Polar Region from the Australian Antarctic Division.

## 1.1 Definition

The Antarctic Polar Region (APR) covers, by definition the surroundings of the South Pole. Its northern boundary is the Antarctic Polar Frontal, which separates the subtropical and sub-antarctic waters. It is composed basically of the Antarctic Ice Sheet (AIS) and the subpolar Southern Ocean (SO), two crucial components of the global climate system, as they strongly participate in setting the global atmospheric and oceanic circulations and in the heat and carbon cycles, among many other processes.

### 1.1.1 The Southern Ocean

**Topographical definitions.**

The SO is the youngest ocean in the world, formed 30 millions years ago with

the opening of the Drake passage between Antarctica and South America. It is commonly defined, as proposed by the International Hydrographic Organization, as the sea south of 60°S. However, in physical oceanography, the Antarctic Polar Front is widely used as as the northern bound of the SO (see in Figure 1.1). The northern bound of the SO has the particularity of not crossing any land, and therefore the SO connects the Indian, Pacific and Atlantic oceans. The strong wersterly winds drive the Antarctic Circumpolar Current (ACC) across the three oceanic basins. The ACC is the largest (100 times the flow of all the world rivers) and the longest ($21 \times 10^3$ km) current in the world, and contributes to the particular isolation of the APR from the rest of the planet.

South of the ACC, recirculation gyres in the Ross and Weddell Seas are strongly constrained by the bathymetry in the Antarctic Continental Shelf. The Antarctic Continental Shelf is in average 80 km away from the AIS coastline, peaking in distance in Ross and Weddell Seas, and presents an average depth of about 200 m and 500 m at its edge. However, the bathymetry of the continental shelf is very complex, with deep glacial channels and canyons reaching 2000 m deep. Sloping northwards, the steep Antarctic Continental Slope, connects the continental shelf with the Atlantic, Pacific and Indian basins of the SO with depths ranging between 4000 and 5000 m. The geometry of the Antarctic Continental Shelf and Slope participate in the formation of dense water masses, important drivers of the global oceanic circulation.

**Antarctic sea ice.**

In winter, the SO surface freezes due to the extremely cold, dry and windy conditions, forming the Antarctic sea ice. The Antarctic sea ice has some particularities as compared to the other main sea ice platform on Earth, the Arctic sea ice. For instance, the Antarctic sea ice shows a strong sea ice extent seasonality, a larger maximum extent, and is much thinner. In winter, sea ice extents about $18 \times 10^6$ km$^2$, however, in summer, strong sea ice melting occurs and only $3 \times 10^6$ km$^2$ remain. Antarctic sea ice is between 1 m and 2 m thick, which is about half of the thickness of the Arctic sea ice, mostly because the expansion of the Antarctic sea ice is not constrained by any continental boundary. The latter contributes, in addition, to the fact that in the APR almost all the sea ice is removed from one season to the other.

In winter, the ice pack is very concentrated, homogeneous and relatively symmetric around AIS. However, under the action of continental winds flowing seawards, Antarctic sea ice opens and forms coastal polynyas, vast ocean surfaces relatively free of sea ice, which affect the ocean stratification and the ocean exchanges with the atmosphere. Coastal polynyas appear regularly at the same location with about 50 frequent locations around AIS (see Figure 1.2) where coastal polynyas form every year (Nihashi and Ohshima, 2015).

In summer, sea ice cover is less homogeneous and the SO only remains covered or

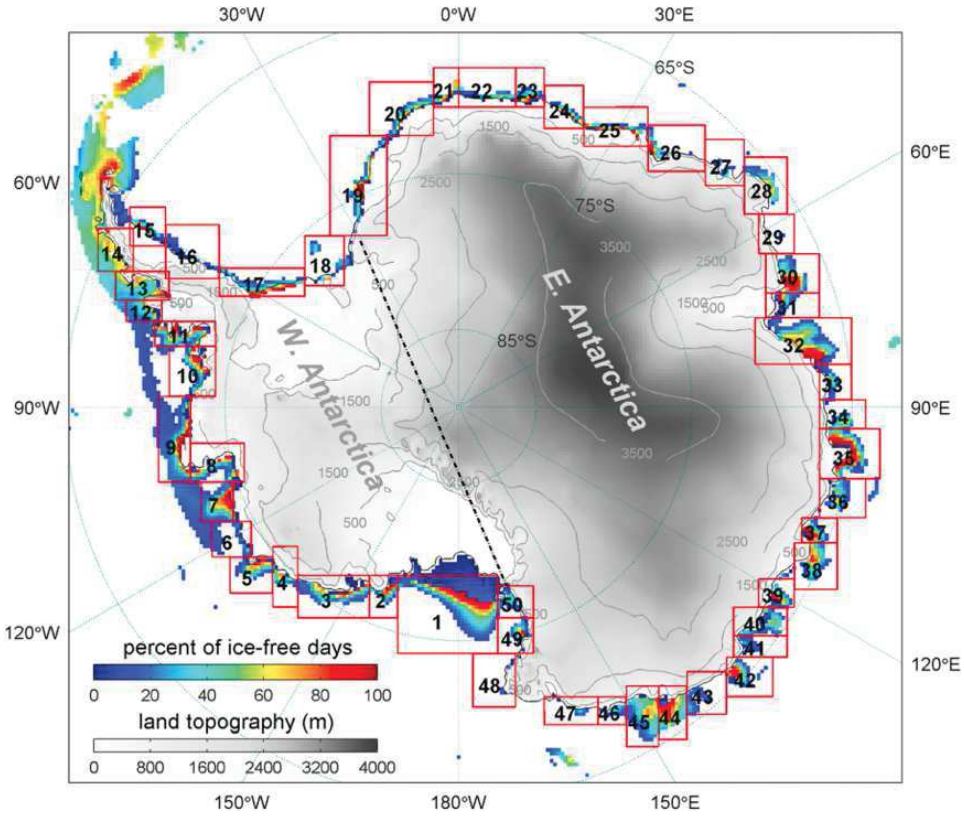


Figure 1.2: Representation of the most recurrent coastal polynyas around the Antarctic Ice Sheet (red squares). Rainbow colorbar represents the percentage of ice free days and grey colorbar the surface elevation of the Antarctic Ice Sheet. This figure is reproduced from Li et al. (2016b) .

partially covered (more than 50% of sea ice concentration) at particular locations. These are the Weddell Sea adjacent to the Antarctic Peninsula, the coast from Bellingshausen to the East Ross ice shelf and some parts in Adelie Lands in the West Pacific sector. Other locations are almost free of sea ice in summer (Figure 1.3).

### 1.1.2 The Antarctic Ice Sheet

The AIS is the coldest, highest continent and has the driest climate on Earth. Ninety-eight percent of its surface is covered by ice, which reflects about 80% of all the radiation received from the sun. The AIS is the largest ice sheet on Earth with an extension of about $14 \times 10^6$ km$^2$, and contains about $30 \times 10^6$ km$^3$, able to raise sea level by 58 m (Fretwell et al., 2013). Mean annual temperature scales from -57 °C in the interior to -26 °C in coastal areas like in McMurdo station, much colder than the other ice sheet on Earth, Greenland. This is why in most of AIS, contrary to Greenland, the melting of ice in the surface is negligible year-round.

The average elevation of AIS is above 2000 m high, with about 4000 m of altitude

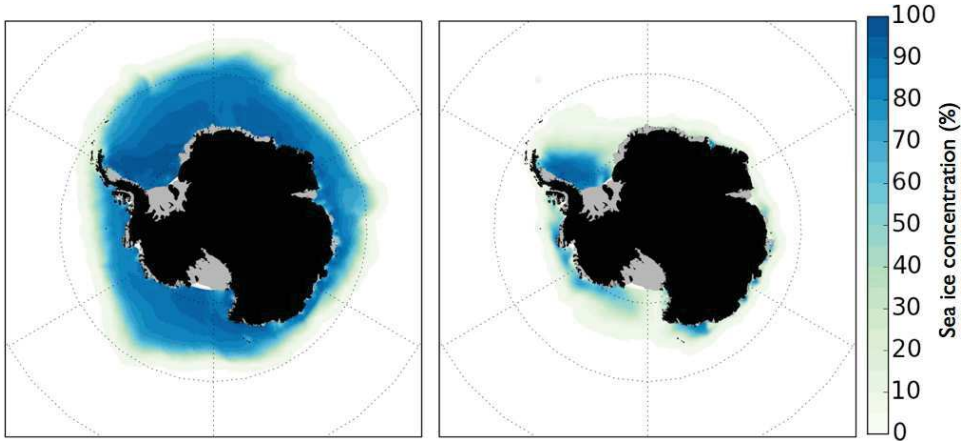


Figure 1.3: Climatology of winter (left) and summer (right) sea ice concentration over the period 1979-2010 extracted from the NSDIC database. Summer climatology includes months from January to March both included, and winter climatology includes months from July to September both included.

in the center of the continent where elevation is more regular and much higher than in coastal areas. This configuration makes the penetration of weather fronts far into the continent difficult, and this is why precipitation rates are low far inland. The AIS is technically considered to be the largest desert on Earth with an average of 166 mm of precipitation per year (Vaughan et al., 1999), ranging from averages of 300 mm per year in coastal regions to just averages of 50 mm per year at the interior.

### Subdivisions of the Antarctic Ice Sheet

Geographically, AIS is usually divided into the East Antarctica Ice Sheet (EAIS) and West Antarctica Ice Sheet (WAIS) separated by the Transantarctic Mountains, a very high mountain range which divides the flow of ice eastwards or westwards and contributes to isolating one region from the other.

EAIS is commonly defined to lie between 45° W and 168° E longitude. It is the largest ice sheet and contains most of ice of the continent, even thicker than 4 km in some parts. In general, the EAIS is colder and dryer than the rest of AIS, its mass content is more stable and its climate experiences less inter-annual variability. In addition, most of its extension rests on a bedrock above the sea level.

WAIS differs substantially from EAIS. It is smaller, lower in altitude and flows faster than its counterpart. It is classified as a marine-ice sheet since most of its ice is grounded below sea level, sometimes even 2500 m below sea level. This is why WAIS mass content is considered much less stable than in EAIS (Weertman, 1974). The WAIS contains about a 10% of the total ice volume of AIS, able to raise sea level by 3.3 m in an hypothetical collapse (Bamber et al., 2008). It contains some of the fastest glaciers on Earth, specifically in the Amundsen sector, where Thwaites

Glacier and Pine Island Glacier flow at speeds up to 4000 m per year and drain about 5% of the total AIS mass output.

Finally, the Antarctic Peninsula Ice Sheet (APIS), even if it technically belongs to WAIS, is commonly considered to be a third Antarctic region due to its special climate conditions and particularities, being the northernmost part of AIS and the warmest. APIS shows positive average temperatures in summer, indeed, It is the only Antarctic region, so far, presenting significant surface melting of ice in summer and significant ice free regions at the coastal margins.

#### Antarctic ice shelves

About a 75% of the Antarctic coastline is formed by ice shelves. Ice shelves are vast floating extensions of outlet glaciers confined into an embayment. In the case of Antarctica, various ice streams and glaciers may flow into the same ice shelf. This is, for instance, the case of the largest ice shelves of AIS, the Ross and the Filchner-Ronne Ices Shelves, covering a surface of more than $4 \times 10^5$ km$^2$. Ice shelves form in many locations in AIS when the ice reaches the ocean and continue floating away because the very cold ocean and air conditions. The space beneath the ice shelf, which is filled up with ocean water, is called an ice shelf cavity. It has a very particular oceanic circulation inside, which contributes to ice shelf melting and impacts the upstream glacier flow. At the front of the ice shelves, commonly called the calving front, ice fractures and forms icebergs. Both processes (the calving of icebergs and the melting under the ice shelves) are the two main Antarctic mass loss processes, since surface melting of ice has a significantly smaller contribution (Stocker et al., 2013). However, the ice shelf volume loss does not contribute directly to sea level rise (though it does contribute indirectly as we will see in section 1.3) since most of the ice shelf is in hydrostatic balance with the ocean.

### 1.2 Role in the climate system

The APR, even if isolated from the rest of the world by the ACC and the strong westerlies, is a very important component of the climate system. In this section we will detail some of the particularities shared by the SO and AIS that make the APR an important point of interest for climate scientists.

The SO participates actively in the climate system with various mechanisms impacting the heat and carbon cycle and the global oceanic circulation. The ACC, the only current connecting the Pacific, Atlantic and Indian oceans, redistributes heat, freshwater and nutrients between all the oceanic basins, influencing weather patterns (temperature and storms) and water masses formation. The regulation of the carbon and heat content of the atmosphere, driven by the SO, mitigates the effect of global warming. About a 40% of the anthropogenic Carbon Dioxide ($CO_2$) (Caldeira and Duffy, 2000) and a 75% of the all the heat absorbed by the oceans from the atmosphere is captured by the surface of the SO, where dense waters form and sink into the deep ocean. Those dense waters are the precursors of the Antarctic

Bottom Waters (AABW), which also participate in the global oceanic circulation. AABW form at three main areas in the APR, the Weddell Sea, the Ross Sea and the seas adjacent to Adelie Land, interacting with the Antarctic Continental Slope and feeding the deep waters of the Atlantic, Pacific and Indian oceans respectively. The AABW is an important contributor to the global oceanic overturning circulation (Broecker et al., 1991; Iudicone et al., 2008) (see Figure 1.5) and controls the global stratification and distribution of heat and carbon sequestered from the atmosphere between the world oceans. The production of AABW and the heat and carbon absorption by the SO is affected by the freezing of the SO surface. When the Antarctic sea ice forms, it becomes an efficient insulator between atmosphere and ocean water. The sea ice cover affects the atmospheric heat content due to the effect of sea ice albedo, and impacts the sea ice volume via the *ice-albedo feedback* (Curry et al., 1995; Nihashi and Cavalieri, 2006). Sea ice also impacts the capacity of the ocean surface to absorb CO2 (Le Quéré et al., 2007; Takahashi et al., 2009) and regulates the mechanical exchanges between the atmospheric winds and the ocean surface, therefore affecting ocean mixing and heat advection of the ocean surface. Indeed, the opening of large sea ice free regionscalled polynyas in the middle of the ice pack, are actively investigated because of their potential impact on global climate through air-sea fluxes (Gordon, 1978; Bersch et al., 1992; Holland, 2001; Beckmann et al., 2001).

The AIS contributes to about 10% of the total Sea Level Rise (SLR) observed today (about 3 mm per year (about 3 mm per year, Stocker et al., 2013)). The role of AIS in SLR is commonly the most important concern to the global public opinion, mostly because it is the largest potential contributor in the future, since it contains about 58 m of ice in sea level equivalent (Fretwell et al., 2013). However, interest in the AIS is not only motivated by SLR: its location surrounding the South Pole and its high mean altitude confer to Antarctica an essential role in the atmospheric circulation, it is the largest sink of atmospheric heat on Earth, and contributes actively to various oceanic processes. This is why the impact of AIS and SO are interconnected and our understanding of the climate system would augmented by improving the coupling between this two components.

The AIS lies under the center of the atmospheric polar cell, and contributes to the warming of the air flowing poleward in the tropopause from norther latitudes. In the high inland surface of Antarctica the air experiences a strong cooling and becomes much denser than the air located in the coastal regions. This results in strong katabatic winds descending seaward, pushing the sea ice, and forming large coastal polynias (see Figure 1.2). Coastal polynias make a significant contribution to two processes very important in climate:

- First, they are very efficient ”factories” of sea ice. The cold atmosphere and the katabatic winds contribute to freeze the ocean surface. The newly formed sea ice is pushed by the winds away from the coast towards the ice pack, therefore maintaining the polynya opened and allowing yet more sea ice to form.

- Second, due to the strong sea ice production in coastal polynyas, extremely cold and salty waters are formed resulting in High Salinity Shelf Water (HSSW), which sinks to the sea bottom and forms the AABW (see Figure 1.2).

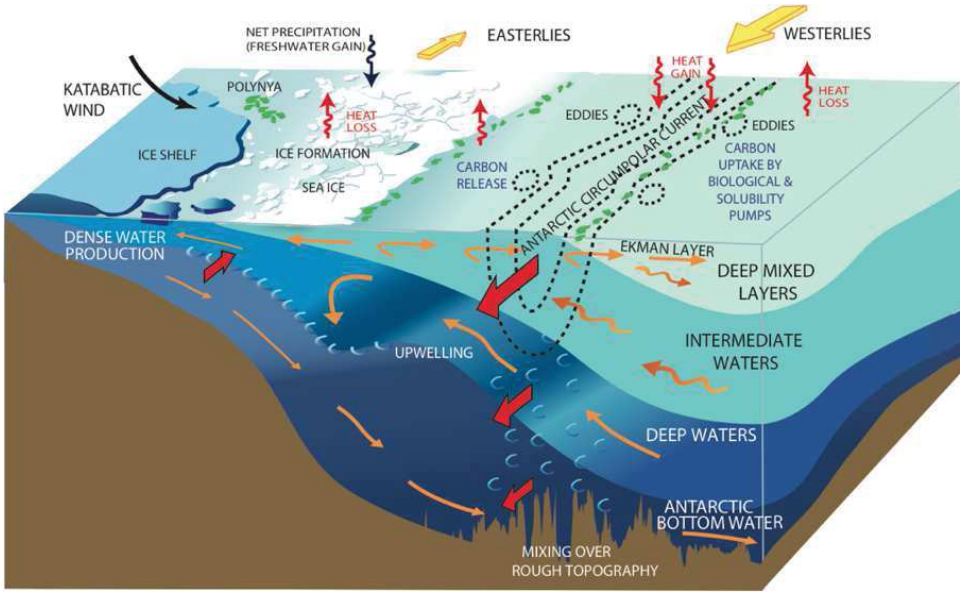


Figure 1.4: Schematic representation of the water masses formation in the Southern Ocean and the interactions with the Antarctic Ice Sheet and ice shelves. This figure is extracted from Lynne Talley lectures material (http://www-pord.ucsd.edu/ ltalley/sio210/Southern/index.html) as an adaptation from Williams et al. (2015) and based on Olbers et al. (2004).

The formation of AABW is an example of the role of AIS in climate through interactions with the SO. This thesis is interested in other possible interactions between AIS and the SO (or vice versa) that may be affecting global climate, or will potentially affect it in the near future. The impact of surface freshwater fluxes on the SO properties, such as the sea ice cover or the density stratification of the ocean surface have been investigated (Marsland and Wolff, 2001) but the role of the glacial freshwater in these mechanisms needs further analysis. (Bintanja et al., 2013; Swart and Fyfe, 2013; Pauling et al., 2016). In addition, the impact of the SO on the mass balance of the AIS due to outlet glacier acceleration driven by the melting of ice shelves (Rignot et al., 2011) is another example of the interaction between the APR components that may affect future climate. Those interactions still require further investigations to be adequately accounted for in climate projections. This is one of the main motivations behind this thesis.

## 1.3 Observed changes in the Antarctic Polar Region

The APR is affected by ongoing global changes. As seen in the previous section, the APR is also an important component of the climate system and its changes may

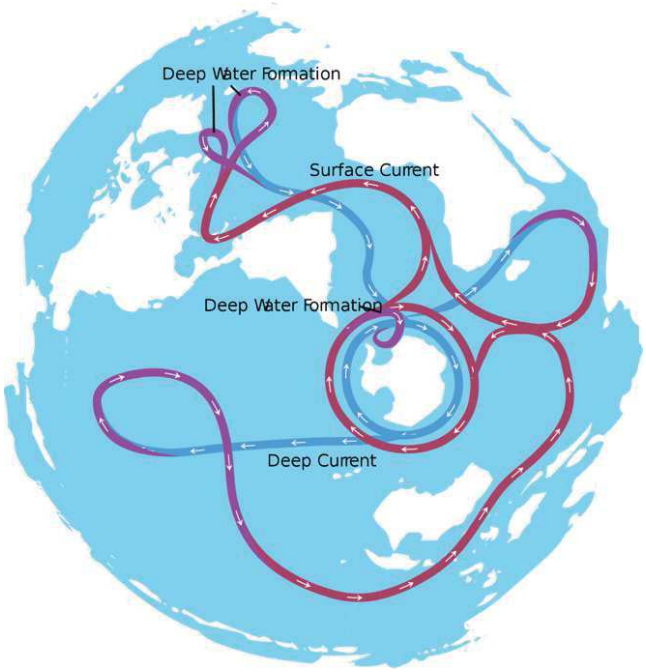


Figure 1.5: Schematic representation of the global overturning circulation showing the prominent role played by the circulation and water mass formation in the SO (figure extracted from Wikipedia).

therefore have a large impact on atmospheric and oceanic properties over the globe. This is why monitoring and understanding changes in the APR are so important in order to improve our knowledge of the climate system.

Changes in the APR have been observed not only in the SO and the AIS, but also in the polar atmosphere, the main driver of the variability in the APR. In this section we will see the main changes that the APR and its atmospheric conditions are experiencing in recent years.

### 1.3.1 Atmospheric changes, the main variability of the Antarctic Polar Region

The principal mode of variability in the Southern Hemisphere, and consequently in the APR, is known as the Southern Annular Mode (SAM). It is mainly a zonal symmetric structure with a zonal mode three wave pattern superimposed on it. Basically, the SAM is the normalized difference in the zonal mean sea surface pressure between 40°S and 65°S. It is directly associated with a southward (northward) displacement of the main belt of subpolar westerly winds when SAM presents positive (negative) phases.

Since 1960s, there is a statistically significant positive trend in the SAM phase (Marshall, 2003; Bindoff et al., 2013) which is consistent with the intensification of the circumpolar westerlies. This trend is likely the result of the human-made halon

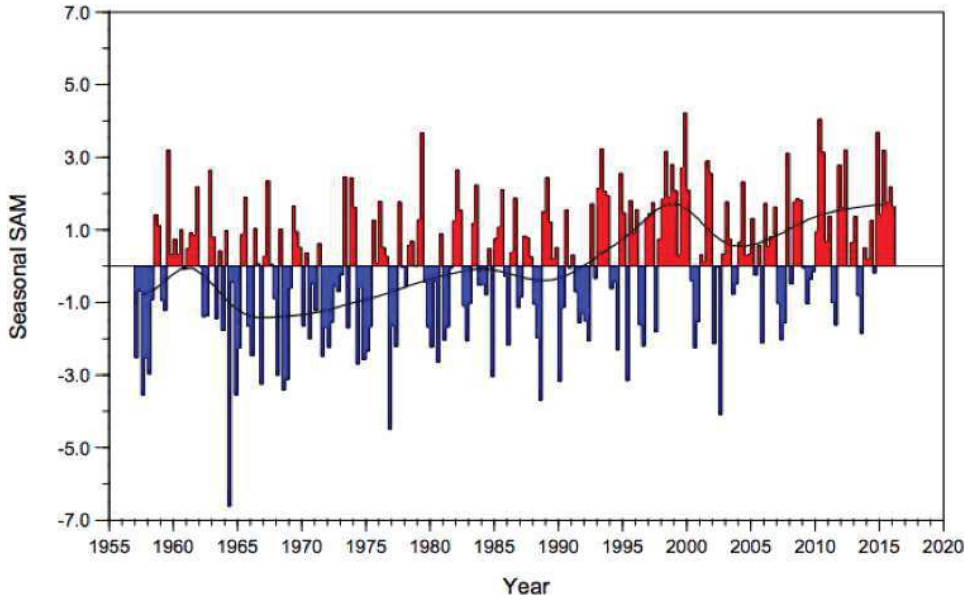


Figure 1.6: Mean seasonal observational-based SAM index. The black curve shows decadal variations. This figure, an updated version from Figure 3.32 in Trenberth et al. (2007), has been updated by Marshall, Gareth & National Center for Atmospheric Research Staff. Retrieved from https://climatedataguide.ucar.edu/climate-data/marshall-southern-annular-mode-sam-index-station-based.

gases, particularly chlorofluorocarbons (CFCs), which weaken the ozone layer in the stratosphere and reduces the absorption of the solar ultra-violet radiation (Arblaster and Meehl, 2006). During the late winter, the marked depletion of stratospheric ozone produces the cooling of the Antarctic stratosphere and a consequent warming of the troposphere, which is also associated to the increasing greenhouse effect due to the increassing greenhouse gas (GHG) emissions (Shindell and Schmidt, 2004; Simpkins and Karpechko, 2012). As a consequence, there are changes in the tropospheric circulation affecting the sea level pressure above the polar SO, resulting in the positive trend in the SAM, in annual average and in particular during the summer and autumn seasons.

Positive phases of the SAM index lead to a poleward shift of the westerlies and a subsequent strengthening of the zonal winds and the ACC. This produces an increase in the insulation of the APR, leading to lower heat exchanges of the APR with the tropics (Turner et al., 2005). Wind changes are associated with an increase in the precipitations (Kang et al., 2013), and regional sea ice trends (Fan et al., 2014; Holland and Kwok, 2012a). In addition, SAM trends have been also discussed to play a role in the CO2 uptake capacity of the Southern Ocean (Le Quéré et al., 2007; Lovenduski et al., 2013; Lenton et al., 2013). In combination with the El Ni'no Southern Oscillation (ENSO), positive phases of the SAM have a strong impact in another atmospheric feature. It contributes to the deepening of the Amundsen Low (AL) (Baines and Fraedrich, 1989; Bertler et al., 2004), a

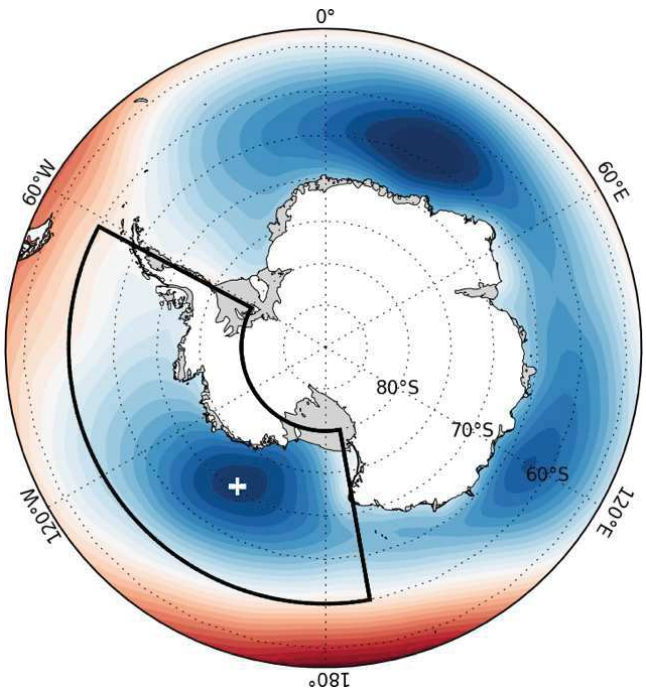


Figure 1.7: Example of the average sea level pressure around Antarctica. The + symbol marks the estimated mean location of the Amundsen Sea Low. This figure was produced by Hosking, Scott & National Center for Atmospheric Research Staff and retrieved from https://climatedataguide.ucar.edu/climate-data/amundsen-sea-low-indices.

low pressure anomaly situated in the Amundsen Sea sector with many implications in the regional climate variability of West Antarctic Region (Hosking et al., 2013; Raphael et al., 2016; Turner et al., 2016). For instance, it is associated with the observed warming of the APIS and the Amundsen and Bellinghausen Seas sectors as well as the wind variability observed in the Ross Sea (as it will discussed in Section 2).

### 1.3.2 Changes in the Southern Ocean

From the second half of the past century, the SO has experienced rapid changes. Warming, freshening, acidification of the surface, changes in the AABW production, and regional changes in the sea ice cover have been observed during the last decades. Those changes may impact the role of the SO in controlling the heat and anthropogenic CO2 content of the atmosphere, ocean ventilation, and the biodiversity of the Southern Hemisphere. Relatively isolated from the rest of the oceans by the ACC, changes in the SO are mostly controlled by atmospheric trends and internal feedbacks, as will be deeply analyzed in Section 2. For instance, this isolation contributes to a delay in the SO warming with respect to the other regions on the Earth, although, observations suggest a mean warming of the ocean surface

of about $0.02°C$ per decade (Armour et al., 2016). A significant warming of the continental shelf waters with a very distinctive regional pattern has also been observed, mostly located in the Amundsen sector (Jacobs et al., 2011). This is one of the factors impacting the formation of the AABW, which are experiencing a warming and freshening (Purkey and Johnson, 2013), leading to a volume contraction of about 50% between the periods 1969-1971 and 2008-2012 (Wijk and Rintoul, 2014). Changes in AABW are also impacted by the observed trends in Antarctic sea ice. Sea ice extent in Antarctica experienced a global positive increase of 1.2% per decade from the combination of positive and negative regional trends in the Ross and the Amundsen-Bellingshausen sectors respectively (Zwally et al., 2002; Cavalieri and Parkinson, 2008; Parkinson and Cavalieri, 2012a; Comiso et al., 2011). The drivers of the sea ice trends in a global warming context and the changes and consequences of the AABW production remain unclear and a subject of ongoing study due to the potential impact in the future climate. This, and other changing ocean properties in the SO are more thoroughly analyzed in Section 2 and partially motivate this thesis.

### 1.3.3 Mass changes of AIS

As commented in Section 1.2, AIS is the largest potential contributor to SLR (it contains about 58 meters of sea level equivalent) and contributes up to 10% to the ongoing rate of sea level rise. However, AIS is strongly isolated by the strong westerlies winds and the SO (specifically by the ACC) and until recent years it has been thought to remain unaffected by global climate changes, contrary to its counterpart in the Northern Hemisphere, Greenland. First suggestions concerning the mass imbalance of AIS and the concern about future SLR projections started in the 1970s with the works of Mercer, Hugues and Weertman (Mercer, 1968; Hughes, 1973; Weertman, 1974). Today, changes in AIS are widely observed and accepted, supported by satellite observations since the early 1990s. In general, Antarctica is thinning, losing volume and its ice flow is accelerating, but changes depends strongly on the region and the estimates present large uncertainties.

The most widely accepted estimate proposes an average AIS mass loss of 71 Gt/yr for the two most recent decades (Shepherd et al., 2012) with an acceleration of 14.5 $Gt/yr^2$ (Rignot et al., 2011). More recent estimates propose a mean global mass loss for the period 2003-2014 of 92 Gt/yr (Harig and Simons, 2015). This result is the combination of strong mass imbalance in WAIS and a mass gain in EAIS. In particular, the most significant changes are observed: in APIS, with a mass change of -27 Gt/yr, the rest of WAIS with -121 Gt/yr, Wilkes Land Region in EAIS with -17 Gt/yr, and a mass gain of 62 Gt/yr in Dronning Maud Land Region (Sasgen et al., 2013; Harig and Simons, 2015). Mass losses in WAIS are associated with dynamical changes in the ice flow producing ice discharge acceleration of the outlet glaciers. The largest acceleration has been observed in the Amundsen sector where Pine Island Glacier and Thwaites Glacier have exhibited strong acceleration and thinning over recent decades (Mouginot et al., 2014). In APIS, an acceleration

of the tributary glaciers of Larsen B ice shelf has been observed after the ice shelf collapses in the sector (Scambos et al., 2004; Wouters et al., 2015). In the EAIS, the most significant acceleration is registered in Totten Glacier sector (Li et al., 2016a). The mass gain observed for some regions in EAIS is mostly related to changes in snow accumulation near coastal areas (Boening et al., 2012; Gorodetskaya et al., 2014; Frieler et al., 2015). Indeed, changes in surface elevation by precipitation have been proposed recently to balance the dynamical mass losses in Antarctica (Zwally et al., 2015), however, this result has been strongly questioned (Scambos and Shuman, 2015; Richter et al., 2015).

## 1.4 The Antarctic Polar region in the context of this work

As mentioned previously, the APR, even if isolated from the rest of the world, hosts several processes playing a key role in setting the current global climate. Sea level, the heat and anthropogenic carbon content of the oceans, and the global oceanic and atmospheric circulation are significantly affected by the components of the APR. Therefore, the future climate will depend strongly of the evolution of the APR in the context of a changing climate. Significant changes in the SO and the AIS have been observed from the 1960s, but their drivers are not completely understood yet. Atmospheric changes are suggested to play an important role in the variability of the APR but other mechanisms are recently being more and more regarded in the study of causes and effects of the observed changes in the region. In the following sections we will see the main mechanisms controlling those changes, as suggested in scientific literature, but with a special regard for other yet unknown potential contributors like the role of the internal interaction between the SO and the AIS in the observed and future changes in the region. Indeed, the interaction of AIS with the SO has been omitted most of time in climate studies and is typically misrepresented in climate models. *This thesis aims at understanding the role of those interactions in setting the observed changes in the APR, and improving their representation in the standalone ocean and standalone ice sheet models with an eye toward a potential future coupling of the models in order to improve climate projections.*

# 2 A changing Southern Ocean on a changing planet

Because of the strong link of the SO with the climate system, the evolution of the SO on a changing planet is tightly followed and studied by climate scientists. A significant warming of the global oceans, dramatic changes in the general ocean circulation controlled by changes in bottom waters formation, significant changes in the uptake of heat and anthropogenic CO2 due to regional sea ice changes, changes in ocean surface properties, and a large impact on the biodiversity of the Southern Hemisphere are just a few examples of the potential impact of the SO on the current and future climatic conditions. But the drivers of those changes, and its impact on the future climate, are not fully understood.

Most of the observed changes in the SO has been linked to atmospheric trends, in particular to the trends in the Southern Annular Mode index (see Section 1.3.1). Indeed, atmospheric forcing is a crucial driver of most of the changes, but an important part of the variability can not be entirely explained simply by interaction of the SO with the atmosphere. This section aims to explain, the triggers and drivers of the observed changes in the SO, not only in the context of current climate, but also regarding the role of the different mechanisms in the future variability of the SO.

## 2.1 A cascade of changes in the ocean water column

### 2.1.1 Sea surface properties.

From 1950s, the ocean surface in the APR has experienced a mean warming rate of $0.02°C$ per decade, much smaller than the global warming rate of about $0.08°C$ per decade (Armour et al., 2016). Global oceans warming is associated to the global atmospheric warming as a consequence of the increase in greenhouse gas emissions. However, whether the delayed warming of the SO (others observational studies even proposed a slight insignificant cooling Maheshwari et al., 2013)) is taking place or not, has been controversial and seems to be the combination of many factors:

- The enhancement of the Ekman advection of cold surface waters northwards driven by the strengthen of the ACC linked to the positive trend in SAM (Oke and England, 2004; Fyfe et al., 2007).
- The consequence of deep-ocean warming, affecting surface properties through convective and isopycnal mixing (Li et al., 2013).
- The SO meridional overturning circulation, which may bring old, cold pre-industrial waters (ocean waters that have not been exposed to the atmosphere since pre-industrial times) to the surface (Armour et al., 2016).
- A consequence of the increasing freshwater released by AIS, as the freshening of the ocean surface may reduce the convective heat flux from the subsur-

face waters by reinforcing the ocean stratification (Marsland and Wolff, 2001; Bintanja et al., 2013).

Projections of the Sea Surface Temperature (SST) during the coming century are very uncertain due to the numerous processes involved and their poor representation in GCMs. Most of General Circulation Models (GCMs) differ in their projections for the impact of the SAM trends on the SST of the SO (Kostov et al., 2016), and the freshening of the ocean surface is not well reproduced in model due to the a misrepresentation of the glacial freshwater fluxes in climate models up to date.

### 2.1.2 Deep shelf waters.

Antarctic Continental Shelf Waters in the SO present a strong dipolar structure around Antarctica (see Figure 1.8). The Weddell and Ross shelf seas contain cold waters at around the surface freezing temperature (-1.9 °C) (Jacobs et al., 1970; Gill, 1973; Orsi and Wiederwohl, 2009; Petty et al., 2013), while the Amundsen and Bellingshausen shelf seas are strongly influenced by Circumpolar Deep Waters (CDW), which is relatively warm ( +1 °C) (Talbot, 1988; Hellmer et al., 1998; Jenkins and Jacobs, 2008; Jacobs et al., 2011). The Weddell and Ross shelf waters are cooled by persistent coastal polynyas, opened by the cold katabatic winds, which form HSSW that sinks to the bottom of the oceanic shelf. In the Amundsen and Bellingshausen Seas, the warm shelf waters are related to the proximity with the ACC.

Intrusions of modified CDW into the ice shelf cavities have been observed in connection with steep gradients in bathymetry at the continental shelf (Klinck et al., 2004; Moffat et al., 2009; Wåhlin et al., 2010; Castagno et al., 2016). This mechanism is strongly influenced by winds (Thoma et al., 2008; Dinniman et al., 2011), but the exact contributors are not yet well understood. The volume of CDW on the continental shelf is increasing (Jacobs et al., 2011), likely driven by the strengthen of the westerlies due to the positive trend in SAM (Thoma et al., 2008; Wåhlin et al., 2010; Dinniman et al., 2015). This is happening in the Bellingshausen (Dinniman et al., 2011), the Amundsen Sea (Thoma et al., 2008; Nakayama et al., 2015) and the western Antarctic Peninsula (Dinniman et al., 2012), but also cold locations like the Ross shelf (Kohut et al., 2013; Castagno et al., 2016).

The increasing presence of CDW on the continental shelf is suggested to be the driver of the increasing basal melting of the Amundsen sector ice shelves (Jacobs et al., 1996; Hellmer et al., 1998; Dutrieux et al., 2014), with many implications in the observed acceleration of the outlet glaciers in the sector (Rignot et al., 2011; Pritchard et al., 2012a; Cook et al., 2016) and future SLR (DeConto and Pollard, 2016). However, evolution of the continental shelf waters and the presence of CDW remains unclear, and the mechanisms involved are not well understood yet.

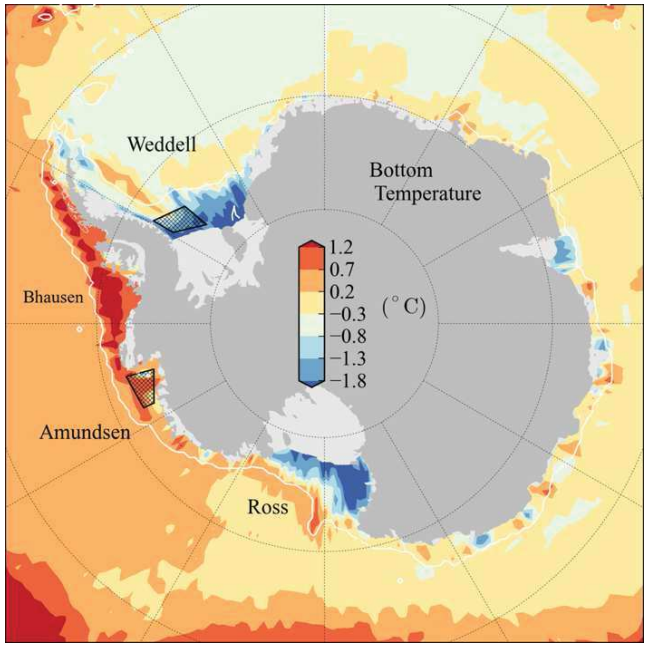


Figure 1.8: Southern Ocean bottom potential temperature. White line represents the 1000-m bathymetry contour. This figure is extracted from Petty et al. (2013).

### 2.1.3 Acidification

The observed acidification of the SO has been associated to the increasing absorption of $CO_2$ from the atmosphere at the SO surface. Indeed, the SO is particularly sensitive to the increasing anthropogenic CO2 emissions, since it absorbs about a 40% of all the CO2 taken up by the all the oceans on Earth. Today, atmospheric CO2 has reached levels of 391 ppm, the highest level of at least the last 25 million years (Dolman et al., 2010), and it might reach the 1000 ppm in 2100 (Raupach et al., 2007). Ocean pH has changed from 8.2 to 8.1 since the pre-industrial era (Howard et al., 2009), due to the increase in anthropogenic CO2 emissions. Changes in acidity of the SO surface have two significant implications:

- The acidification of the SO affects its capacity to continue taking up CO2 from the atmosphere. This may dramatically increase the CO2 content of the atmosphere and therefore accelerate the climate warming.
- The acidification of the SO notably affects the biological production of the entire Southern Hemisphere (Doney et al., 2009; Shi et al., 2010; Yang et al., 2016). In general, the $CO_2$ absorption negatively impacts the calcium extraction of some species, and consumes carbonate ions, very important in the shell-forming marine organisms production.

The melting of Antarctic glacial ice (ice shelves and icebergs) is suggested to affect

the ocean surface acidification and its impact on biodiversity. This is due to the dilution effect of the freshwater in some regions (Fransson et al., 2014) and the iron content of the glacial ice, which may impact acidity by different processes. For instance, the iron from glacial ice has been estimated to contribute to up to a fifth of the total downwards carbon sink to the the deep ocean, due to an increase in the pytoplankton fertilization (Duprat et al., 2016). Additionally, iron is suggested to have a role in modulating the impact of changes in carbonate ions on primary production (Hoppe et al., 2013). Accordingly, projections of acidification and biological production in the SO can be affected by future increase in freshwater fluxes from AIS. This means that projections for carbon and biological cycles may require a realistic representation of the iron flux from the melting of glacial ice.

## 2.2 Changes in Antarctic Bottom Waters

Concerning future climate, the most relevant observed change in the Southern Ocean might be the freshening, the warming and the loss in volume of the AABW. The estimated warming below 4000 m for the Amundsen-Bellingshausen, Australian-Antarctic and Weddel-Enderby basins corresponds to heat fluxes of 0.14, 0.11 and 0.23 $\mathrm{Wm}^{-2}$ respectively for the period from 1990-2000 (Purkey and Johnson, 2013). Warming of deep waters is accelerating, since lower rates of warming were estimated for the preceding period from the 1970s to the 1990s. Regionally, the warming is stronger in the Weddel Sea sector, where Weddel Deep Water feeds the AABW. Hydrographic sections across the eastern Weddell gyre suggest a warming of about $0.1°C$ of the AABW of the Indian basin in the SO for the period mid 1990s-late 2000s (Couldrey et al., 2013). This may be associated with the entrainment at mid-depth of CDW in the sector due to a southwards shift of the ACC (Fahrbach et al., 2011), which suggests a relation between the SAM trend and the Weddel Deep Water (Meredith et al., 2011; Jullion et al., 2010).

The freshening of the AABW presents a distinctive spatial pattern (see Figure 1.9). In the Ross Sea, the shelf water, the precursor of the bottom water, have freshened at a rate of 0.03 PSU (Practical Salinity Units) per decade since the 1960s (Jacobs and Giulivi, 2010). Between the 1990s and mid 2000s, freshening of about 0.03 PSU per decade of the bottom waters formed in Adelie Land has been reported (Rintoul, 2007). However, there is no significant evidence of freshening in the Weddel Sea-formed AABW (Fahrbach et al., 2011). The driving mechanism of the freshening of the AABW in Ross and Adelie Land is suggested to be the enhanced glacial freshwater fluxes into the shelf waters (Jacobs and Giulivi, 2010), due to an increase in glacier melting in West Antarctica (Purkey and Johnson, 2013). This mechanism is likely to continue freshening the AABW in the future as projections predict more basal melting of glaciers in the region over the next century (Stocker et al., 2013). This might also occur in the Weddell sector, where ocean circulation changes caused by the receding of sea ice in response to atmospheric perturbations may enhance basal melting of glaciers in the southern Weddell Sea (Hellmer et al., 2012). This may have an impact in a future freshening of the Weddell

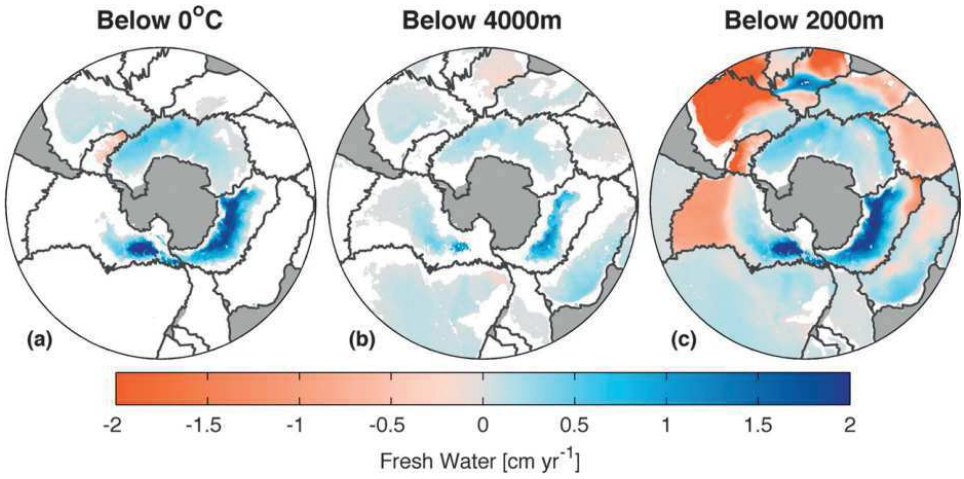


Figure 1.9: Vertical freshwater fluxes below (a) 0°C, (b) 4000 m deep (b) and (c) 2000 m deep (c) from observed water mass salinity changes. This Figure is extracted from Purkey and Johnson (2013).

Bottom Water as has been suggested in Jullion et al. (2013). However, estimates of regional freshening of AABW do not match observations exactly (Heuzé, 2015). This might be due to the misrepresentation in models of the freshwater transported by icebergs around the Antarctic continent and the evolution of ice shelf melting in recent decades.

All these changes may have a dramatic impact in the world oceans, and small changes have started to be reported far away from the Antarctic region. Indeed, a warming of the AABW in the North Atlantic (Johnson, 2008), and also in the North Pacific (Fukasawa et al., 2004) have been observed. The observed reduction in density due to the freshening and warming of AABW affects the global ocean overturning circulation with potentially dramatic consequences for the future climate. In the most pessimistic scenario, freshening and warming of AABW could stop the thermohaline circulation (Broecker et al., 1991). More realistic projections, but based on low resolution models, estimated a weakening by 20-50% (Rahmstorf and Ganopolski, 1999). Recent works estimates a volume reduction of the AABW of about 50 % between 1969-1971 and 2008-2012 and a thinning of 100 m per decade (Wijk and Rintoul, 2014). In addition, the volume of water with potential temperature below $\theta = 0°C$ has decreased at a rate of 8.2 $\times 10^6 m^3 s^{-1}$ over the last two decades (Purkey and Johnson, 2012) .

Climate models do not always reproduces correctly the formation of AABW nor its trends in the present context. A good representation of AABW formation would need a good representation of the shelf-deep ocean processes, shelf waters response to SAM trends, and future projections of the freshwater fluxes in Antarctica.

## 2.3 Changes in sea ice

The response of the Antarctic sea ice to global climate change is counter-intuitive and unexpected. While the Artic sea ice is decreasing in response to atmospheric warming, the Antarctic sea ice extent is showing a weak but statistically significant global increase of 1.2% per decade (Comiso et al., 2011; Parkinson and Cavalieri, 2012a), with its maximum extent being registered in recent years (Reid et al., 2015). The response of the Antarctic sea ice extent in the present warming context is being an area of a large amount of active research due to its strong connection with bottom waters formation and heat and carbon uptake processes. Understanding the changes in Antarctic sea ice and their impact on climate is a significant and important scientific challenge (Kennicutt II et al., 2015).

The significance of the increase recorded in Antarctic sea ice has been questioned (Polvani and Smith, 2013a; Screen, 2011), though there is broad consensus in the community that the regional trends are occurring (Comiso et al., 2011). In Ross Sea, annual mean Sea Ice Extent (SIE) shows an increase of 5% per decade, while in the Amundsen-Bellingshausen Seas sector, a decrease in SIE up to 7% per decade has been recorded since the late 1970s (Turner et al., 2009a). In summer and autumn the largest positive trend in Sea Ice concentration (SIC) is observed in Weddel and western Ross Sea (Meier et al., 2013), and a negative trends is observed in Bellingshausen and Amundsen Sea (Holland et al., 2014), particularly strong along the western coast of the Antarctic Penninsula. In winter, the SIC trend is weaker in magnitude and significance, and a significant positive trend can be founded only near the ice edge in Ross Sea.

Most of the observed changes in sea ice area have been associated to atmospheric changes (Lefebvre and Goosse, 2008; Holland and Kwok, 2012a; Raphael and Hobbs, 2014; Matear et al., 2015). For instance, positive phases of SAM contribute to the atmospheric warming in the Antarctic Peninsula and in the Amundsen Bellingshausen Seas sector, contributing actively to the observed reduction in sea ice concentration in the region. Paradoxically, intensification of westerly winds related to positive SAM, should contribute to sea ice expansion due to the northwards export of the sea ice, and a subsequent increase in sea ice production (Hall and Visbeck, 2002; Sen Gupta and England, 2006). However, over longer timescales the intensification of westerlies may also leads to Ekman pumping of CDW and impacts regional sea ice cover, and thus reducing SIC (Sigmond and Fyfe, 2010; Ferreira et al., 2015).

The regional dipole observed in the sea ice trends between Ross and the Amundsen-Bellingshausen sector is suggested to be mainly controlled by the deepen of the AL, which is closely related to the SAM trends. The cyclonic flow associated with the AL increases the warm flow polewards to the Amundsen-Bellingshausen sector and the northwards cold continental air to the Ross Sea sector (Lefebvre et al., 2004; Holland and Kwok, 2012a; Hosking et al., 2013; Turner et al., 2015b). The contribution of wind-driven sea ice motion to the observed trends in autumn-winter has also been suggested (Holland and Kwok, 2012a; Haumann et al., 2014). In addition, there is a complex regional response in eastern Ross and Amundsen-Bellingshausen

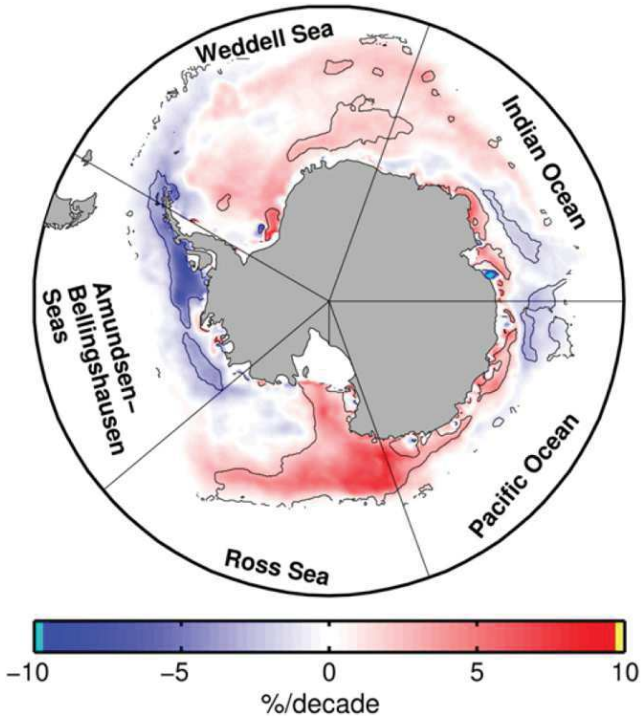


Figure 1.10: observed trends in Antarctic sea ice concentration for the period 1980-2008 derived from the monthly anomalies with respect to the 1980-2008 mean seasonal cycle. Black lines enclose the trends that have a statistically significant difference from zero ($p < 0.05$). This figures is extracted from Massonnet et al. (2013).

to tropical SST annomalies due to ENSO (Gloersen, 1995; Simmonds and Jacka, 1995; Turner, 2004; Meehl et al., 2016). Pacific atmospheric anomalies propagate into the region by atmospheric Rosby waves, peaking in the late winter and spring (Mo and Higgins, 1998; Simpkins et al., 2012), and decreasing sea ice cover.

Therefore sea ice trends in the Amundsen-Bellingshausen and eastern Ross sectors seems largely to be explained by atmospheric trends. However, the strong trend observed in the western Ross seems not to be fully explained by atmospheric forcing. An eastward shift of the Amundsen Low has been recently observed, leading to a decrease in the meridional winds, which were believed to be the responsible of the sea ice trend of the region (Coggins et al., 2015). The shift in Amundsen Low should therefore produce a weakening of the observed sea ice trend, but this is not what it is observed. Because of this unexpected trend of the sea ice in the western Ross region, this particular sector has been suggested to be particularly affected by a positive ice-ocean feedback associated with changes in the ocean surface stratification induced by the sea ice production or melting (Stammerjohn et al., 2012a; Holland et al., 2014). The ice-ocean feedback has been attributed to two mechanisms:

- Zhang (2007) proposed that a reduction in the sea ice production in autumn

decreases the brine rejection, consequently increasing the stratification. This may negatively affect the heat supply from the subsurface into the winter mixed layer during the next spring, and therefore reduce the sea ice melting.

- By contrast, when the ice pack is established, the sea surface tends to be fresher with a greater sea ice coverage, and this may lead to an increased stratification and a reduction of the heat upwelling from the subsurface and the consequent sea ice melting (Goosse and Zunz, 2014a).

The role of these two competing mechanisms in setting the local sea ice trends depends strongly on the ocean and mixed layer conditions. In addition, more recently, other external factors have been proposed to affect the mixed layer stratification and contribute to the ice-ocean feedback. The impact of precipitation and the freshening of the surface in the sea ice production were firstly proposed in Marsland and Wolff (2001). Several works have recently investigated this mechanism and its impact on sea ice production due to the increasing glacial freshwater flux to the SO from AIS (Bintanja et al., 2013; Swart and Fyfe, 2013; Pauling et al., 2016). However their results and conclusions differ. Bintanja et al. (2013) find that trends in glacial freshwater may have a significant impact on regional sea ice, but their regional distribution of the sea ice cover changes does not correspond to observations. Swart and Fyfe (2013) and more recently Pauling et al. (2016), obtain a much smaller response of the regional sea ice to an even larger glacial freshwater perturbations compared to Bintanja's study. This might be related to problems in capturing the coastal circulation due to a relatively coarse ocean model resolution. Anyway, all these works are based on a simplified representation of the freshwater fluxes and the spatial distribution of the freshwater perturbation introduced.

As seen so far in this section, projections of future sea ice trends are suggested to be mostly controlled by atmospheric trends. However ocean modeling is needed to correctly capture correctly the ice-ocean feedbacks and the impact of glacial freshwater sources. Even if the role of glacial freshwater remains limited according to recent works, AIS is expected to further contribute to the freshening of the ocean surface in the next century. This makes AIS a potentially significant contributor to sea ice trends in the future. Quantifying the impact of AIS mass changes on observed sea ice changes is therefore much needed. This may require more efforts in the representation of the glacial freshwater sources and the understanding of the associated mechanism.

## 2.4 Summary and open questions

Numerous properties in the SO are changing in response to a number of different physical processes. A quick overview of these processes indicates that the atmospheric trends control the changes of the SO, but not entirely. Internally, the stratification of the ocean might be crucial in setting the response of the system to the external atmospheric forcing. Glacial ice discharge from AIS has been suggested to contribute significantly to set the water column properties in the SO, and the

observed recent acceleration of the AIS volume loss may be having a non negligible role in the ongoing observed changes of the SO.

Historically, climate scientists have been interested in understanding the link between the atmospheric and oceanic trends. More recently, new studies reveal that the variability of the region cannot be entirely explained by atmospheric features, but that internal interactions between SO and AIS should be considered. Neglecting these interactions might not be so dramatic nowadays, but the observed acceleration of the ice discharge from AIS and projections of an increasing volume loss rate suggest that the contribution of the AIS to future variability of the SO may significantly increase in the future. *Understanding the potential role of the ice/ocean interactions on current and future ocean properties seems very important in order to project future global climate. However, the representation of the glacial freshwater sources have not been a priority in the development of ocean models, and the seasonal and regional distribution of the glacial freshwater fluxes need further investigation in order to perform model studies and predictions.*

# 3 Mass changes of the Antarctic Ice Sheet: a sea level concern

Despite the fact that AIS mass discharge has an influence on properties of the SO, as seen in the previous section, monitoring of the AIS volume is mostly focused in sea level rise predictions. Historically, AIS has been believed to be more or less stable and concerns related to sea-level rise were mostly focused to other components like the Greenland Ice Sheet (GrIS) and continental glaciers. Today, its potential contribution to future sea level rise and its rapid acceleration have increased the focus of scientists on the AIS. This section explores the role of AIS on the current rate of sea level rise, and analyzes the associated uncertainities related to the projections of its future contribution, in particular due to the ice/ocean interactions.

## 3.1 Sea-level rise and the contribution of the Antarctic Ice Sheet

The potentially rapid rate of SLR within the next century in among the largest global concerns about the consequences of climate change (Stocker et al., 2013). In the First Intergovernmental Panel in Climate Change (IPCC) Assesment Report in 1990 (Houghton et al., 1990), a projected SLR during the 21th century was accepted with high degree of confidence. Indeed, sea level has found an inflection point in the last century after being very stable during the last three or two millenia. After a peak of sea level of about 120 m higher that today at the end of the last ice age (approximately 21000 years ago), the oceans level stabilized between 3000 and 2000 years ago. From then until the late 19th century, no evidence of any significant change in sea level has been observed. However, the estimations for the 20th century show a robust mean rate of SLR of about 1.7 mm/yr (Stocker et al., 2013). More recently, satellite measurements since the early 1990s have provided estimates of about 3 mm/yr for the period 1993-2010, which has also been confirmed by coastal measurements (Stocker et al., 2013). The projections for the next century indicate (with high confidence according to the Fifth IPCC report) that sea level will continue to rise at increasing rates for all the Representative Concentration Pathway explored (Stocker et al., 2013). However the quantification of the future rates of sea-level rise remains unclear due to the large uncertainities associated with projection of some SLR contributors.

Sea level is mainly affected by the thermal expansion of the oceans and the melting of the land-based ice: the continental glaciers, the GrIS and the AIS. Thermal expansion due to ocean warming is estimated to contribute to SLR to about 1.1 mm/yr for the period 1993-2010. The cumulative contribution of the cryosphere has been estimated in about 1.7 mm/yr for the same period. More than half of this estimate corresponds to the melting of glaciers other than AIS and GrIS Ice Sheet. GrIS contributes with about 0.45 mm/yr, and AIS with 0.27 mm/yr (Stocker et al., 2014; Broeke et al., 2016). Although, polar ice sheets (AIS and GrIS) contribute relatively smaller rates compared to the other contributors, the concern about their potentially larger contribution in the future is increasing for several reasons. Firstly,

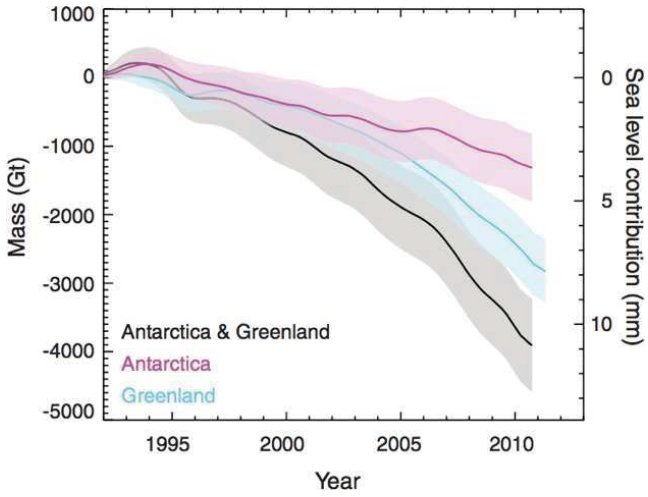


Figure 1.11: Estimated cumulative mass loss of Greenland, Antarctica and the combination of both Ice sheets, expressed as cumulative sea level contribution on the right-end vertical axis, and cumulated mass change in gigatones on the left-end vertical axis. This figure is extracted from Shepherd et al. (2012).

they are the largest potential contributors accounting together for 70 m of ice in Sea Level Equivalent (SLE) (continental glaciers only accumulate 35 cm of ice in SLE Grinsted, 2013). Secondly, a significant acceleration of their ice mass discharge has been observed (Velicogna et al., 2014) which suggests that the polar ice sheets may be the driving contributors to SLR in the near future (see Figure 1.11).

Projections of GrIS estimate a cumulative contribution of 27 cm to sea level at the end of the 21th century (Yan et al., 2014). In the case of Antarctica, some estimations project a contribution ranging from 28 cm to 98 cm at the end of 2100 (Church et al., 2013) while others project SLR of more than a meter (DeConto and Pollard, 2016). The large uncertainty in this estimate has been particularly noted by the last IPCC assessment. This is due to problems in modelling *"the dynamical response of marine-terminating glaciers and marine-based sectors of the Antarctic ice sheet"* and the low confidence in *"projecting the onset of large-scale grounding line instability in the marine-based sectors of the Antarctic ice sheet"* (Stocker et al., 2013). The combination of these AIS-related uncertainties and the strong potential contribution of more than 15 m to the sea level by 2500 (DeConto and Pollard, 2016), have increased the interest of the ice-sheet modelers in estimating the role of AIS in future sea level change.

## 3.2 Projecting the Antarctic contribution to Sea Level Rise

Projecting the mass balance of AIS and its contribution to SLR differs substantially from the study of the mass balance of the continental glaciers or GrIS. The mass balance of most of continental glaciers (out of the polar regions) is mainly dependent on snow accumulation in the high parts of the glacier and ablation at their terminus

due to the warmer atmospheric or oceanic conditions. Mass balance of those glaciers is almost entirely driven by precipitations and surface atmospheric temperature, and the ice dynamics has a limited impact on the mass budget of most of those glaciers. In constrast, in the case of GrIS and some other tidewater glaciers in polar regions, there is a non-negligible component of the mass loss associated to the ice dynamics (up to the 50% of total mass loss in GrIS van den Broeke et al., 2009). The acceleration of those glaciers increases the ice discharge into the ocean, enhances the iceberg production and the ice melted by the ocean, and therefore their contribution to SLR. In the case of AIS, the impact of ice dynamics on the mass balance has a much larger importance than in GrIS and continental glaciers. On average, the surface melting of ice in AIS represent only 1% of the total mass gain by snowfall (Stocker et al., 2013). This low rate of surface melting in AIS is likely to continue in the future since there are not projections of any significant change in surface melting during the next century, as meltwater and rain are projected to continue to freeze in the snowpack (Ligtenberg et al., 2013). As a consequence, AIS mass balance, and therefore its contribution to SLR, is basically estimated as the balance between the snow accumulation gains and the ice outflow losses through the outlet glaciers.

In AIS, the small ablation rate in the coastal areas results in the formation of large ice shelves floating on the ocean surface. The impact of the volume changes in the ice shelves on SLR can be neglected (Jenkins and Holland, 2007) since they already displace ocean water. As a consequence, for a SLR purpose, Antarctic mass outflow may be assumed to be the flux of ice traversing the boundary between the bedrock-grounded ice and the ice-shelf floating ice, i.e. the Grounding Line (GL). The ice outflow in AIS is mainly affected by two processes:

- First, changes in the snow accumulation may induce driving stress changes in the outlet glaciers, therefore affecting to the ice velocity and the ice flux.

- Second, a change in the ice shelf volume may trigger an acceleration of the upstream part of the glacier due to the buttressing effect (Gagliardini et al., 2010; Gudmundsson et al., 2012a; Fürst et al., 2016). This is the impact on the upstream ice dynamics exerted by laterally confined ice shelves, to which the grounded parts of the glacier (generally due to pinning points or ice rises in the middle of the ice shelf) transfer lateral shear slowing down the ice stream or the outlet glacier

Observations have shown a decrease of the ice shelf volume during recent decades (Pritchard et al., 2012a; Paolo et al., 2015). There are two main processes reducing the volume of an ice shelf: the calving of icebergs at the ice shelf front, and the basal melt of ice by the ocean at the upper surface of the ice shelf cavity. According to recent studies, both processes represent an almost similar contributions to the ice shelf volume loss (Rignot et al., 2013; Depoorter et al., 2013), but their indirect impact on SLR is difficult to quantify and project.

Calving events of unbuttressed parts of ice shelves have no significant impact on

upstream grounded glacier dynamics (Fürst et al., 2016). However, the relatively less frequent calving of big tabular icebergs or ice shelves collapses may produce a significant loss of buttressing and induce strong acceleration of the upstream tributary glaciers, therefore increasing the ice outflow. The latter has been the case for Larsen B ice shelf (Scambos et al., 2004), the collapse of which was likely produced by a substantial warming of the Antarctic Peninsula (Cook and Vaughan, 2010). However, the warming needed for similar collapses of the main Antarctic ice shelves (the Ross and Flitchner-Ronne ice shelves) is not expected to be approached in the next century (Stocker et al., 2014). Anyway, ice shelves collapses around AIS remains unpredictable and their impact in the ice outflow of the glacier is one of the big challenges of the SLR projections.

Basal melting below the ice shelves has been increasing in the last decades. The associated thinning of the ice shelves (Paolo et al., 2015) is suggested to have triggered the observed glacier acceleration and GL retreats observed in many locations around Antarctica (Rignot et al., 2002, 2014; Li et al., 2016a; Joughin et al., 2016; Scheuchl et al., 2016). This may be a direct consequence of the observed warming in shelf waters of the SO as seen in Section 2 and the intrusion of warm waters into the ice shelves cavities (Jacobs et al., 1992; Hellmer et al., 2012; Kusahara, 2016). However, there are still large uncertainties in the ocean temperature projections in the interior of ice shelf cavities and what will be the impact of this in the upstream glacier dynamics. Main reason for the latter is a possible feedback in the melt rates produced by a changing ice shelf draft. Strong melting-induced GL retreats lead to significant changes ice shelf draft, affecting the ocean circulation in the cavity, and therefore to the melt rates at the ocean/ice interface (De Rydt et al., 2014). This feedback suggests the need for the coupling between ocean and ice sheet models in order to better account for the melting processes, and a new generation of coupled model are currently under development. In particular, those new models are mostly focused in the Amundsen Sea sector of WAIS, where this feedback seems currently to be the most important (De Rydt and Gudmundsson, 2016). As we will see in next section, the rapid ocean warming, the strong observed ice shelf thinning, and the observed GL retreat of the sector, indicate the necessity of improving the representation of the ocean-ice shelf interactions in ice-sheet models in order to improve SLR projections.

## 3.3 The uncertain future of the Amundsen sector and the Marine Ice Sheet Instability

Projections of the AIS contribution to SLR are mostly focused on the evolution of WAIS and the Amundsen Sea sector in particular. This is mainly due to an observed regional ocean warming associated with the presence of relatively warm Circumpolar Deep Water on the continental shelf of Amundsen Sea (see Section 2). In addition, the specific topography below WAIS makes the ice dynamics of the region particularly sensitive to perturbations, giving the sector its strong potential role in future SLR. This is related to the fact that WAIS is mostly resting over a

bedrock below sea level (it is a marine ice sheet) with GL commonly resting on an upward-sloping bed, and therefore sensitives to the so-called Marine Ice Sheet Instability (MISI).

MISI is the name given to a theoretical instability applying to marine ice sheets with GL resting on upward-sloping beds. There is a long history of discussions about MISI since it was mathematically formulated by Weertman (1974) and further explored by Thomas and Bentley (1978). Today, many refinements have been made to the initial theory, and satellite observations from 1990s, partially confirming the theoretical projections for the Amundsen sector, have relaunched the needs for a better understanding of this instability. MISI states that, theoretically, in a two-dimensional ice-sheet neglecting lateral stresses (only considering vertical and ice flow horizontal direction dimensions), GL positions resting on upward-sloping beds are unstable. It is based on the hypothesis proposed by Weertman (1974) suggesting a positive feedback between the retreat of the GL and a subsequent increase in the Grounding Line Flux (GLF), which depends strongly on the local ice thickness. Basically, an initial retreat of the grounding line on a seaward bed slope, leads to an increase in the ice thickness and therefore an increase in the ice flux in the vicinity of the GL. Weertamn demonstrated, for a two dimensional problem and based on some simplifications, that an increase in the outflow ice flux should produce further GL retreat. Accordingly, such an ice-sheet configuration (grounding line position resting on an upward-sloping bed) will inexorably lead to the retreat of the GL until a downward-sloping bed were found by the GL (see Figure 1.12). In downwards-sloping bed, the positive GL-retreat/ GLF-increase feedback is no longer applied and the solution becomes stable.

In the initial MISI theory, the relationship established between the GLF and the GL position has been controversial (Hindmarsh, 1993, 1996) due to the simplistic description of the mass fluxes in the transition zone between the grounded and floating ice assumed in Weertman (1974). The findings of Hindmarsh (2006) suggested that some steady states might be stable in seaward bed slopes, but any numerical studies could not find any stable solutions (Pattyn et al., 2006; Schoof, 2007a). The works of Schoof (2007a), based on a boundary layer theory for the transition between the grounded and floating ice, confirmed the conclusions of Weertman (1974) and Thomas and Bentley (1978). Today MISI is widely accepted by the community and it has been linked to the observed GL retreat of glaciers in the Amundsen Sector (Favier et al., 2014; Joughin et al., 2014).

MISI theory is only valid in two dimensional case, this is without considering the lateral stresses exerted by the sidewalls of an ice shelf in confined glaciers. In such configuration, a laterally confined ice shelf may play an important role in the stabilisation of GL in marine ice sheets due to the buttressing effect (Dupont and Alley, 2005; Goldberg et al., 2009; Gudmundsson et al., 2012b). This means that the stability of a marine ice sheet has a strong dependency on the glacier topography and its ice shelf configuration. Despite the theoretical work made in the study of MISI, realistic projections of SLR requires the use of numerical models in order to account for the interactions of the ice dynamics with the topography. How the

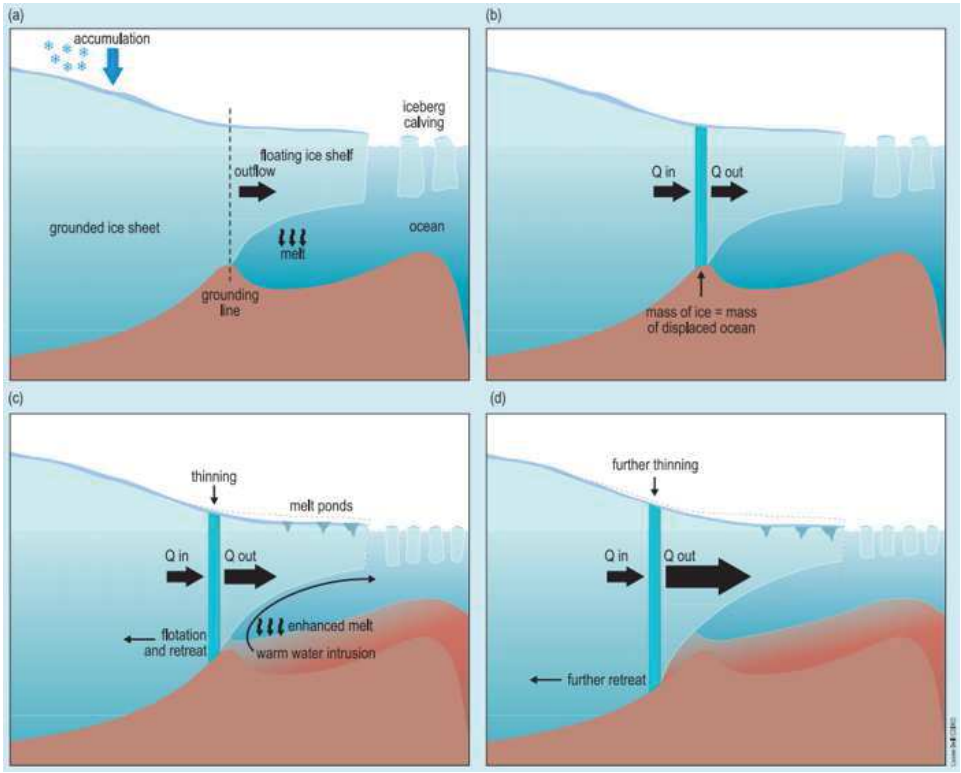


Figure 1.12: Schematic representation of the Marine Ice Sheet Instability (MISI) retrieved from Stocker et al. (2013) showing (a) the geometry and ice mass fluxes of a marine ice sheet, (b) the steady state of a grounding line, (c) climate perturbation triggering the start of a grounding line retreat, and (d) the self-sustained retreat according to MISI.

outlet glaciers of marine ice sheets will evolve in response to processes leading in ice shelf volume loss (the calving and the melting) is one of the largest uncertainties of the SLR projections. The dynamical response of glaciers to ice shelf collapses (i.e. Larsen B) or ice shelf basal melting (i.e. Pine Island and Thwaites Glaciers) have been observed and simulated with numerical models. For instance, some recent works have studied the evolution of the GL in response to melting applied under ice shelves arriving at different projections of the contribution of the sector to SLR, particularly of Pine Island and Thwaites Glaciers (Payne et al., 2004; Joughin et al., 2010; Favier et al., 2014; Seroussi et al., 2014; Joughin et al., 2014; NIAS et al., 2016). Indeed, the modeling of GL retreat in the Amundsen Sector is one of the largest challenges associated with the SLR projections. This is because the number of different parametrizations within the ice sheet models which are currently active topics of research: the grid resolution (Durand et al., 2009; Pattyn et al., 2013; Cornford et al., 2013), the basal friction laws (Gagliardini et al., 2007; Schoof, 2010; Tsai et al., 2015), the impact of englacial stresses aproximations (Favier et al., 2014), the impact of calving (Krug et al., 2015; Cassotto et al., 2015; Morlighem et al., 2016) and the need for a coupling with the oceanic circulation at the interior ice shelf-ocean interface (Martin et al., 2015; Timmermann and Goeller, 2016; De Rydt and Gudmundsson, 2016). The need for improvements in ice sheet models has motivated the creation of model inter-comparison exercises like MISMIP (Pattyn et al., 2012), MISMIP3D (Pattyn et al., 2013) and the more recent MISOMIP (Asay-Davis et al., 2016). Those exercises aim to test the ability of the existing ice sheet models to numerically reproduce the response of the marine ice sheet glaciers to different external perturbations, and identify the largest sources of uncertainties associated with the modeling of grounding line retreats in marine ice sheets.

## 3.4 Summary and open questions

The role of AIS in present-day sea level rise remains limited compared to other contributors. However, AIS is the largest potential contributor in the future and it is experiencing the fastest acceleration in SLR contribution during the last two decades. Projecting the volume changes of AIS has large uncertainties related to the limited capabilities of the ice sheet models in accurately reproducing the grounding line retreats of marine ice sheets in response to oceanic perturbations, particularly in the Amundsen sector in WAIS. Indeed, the main factor controlling the grounding line retreat in this region has been attributed to the interaction of the outlet glaciers with the ocean and the role of buttressing in the stability of the grounding line. This has suggested the necessity of ocean/ice sheet coupled models in order to accurately represent these interactions. *However, numerous physical processes related to the standalone ice sheet models remain unclear, and their impact on the ice dynamics and grounding line retreat may be as important as the coupling of ice sheet models with ocean models. For instance the impact of model resolution, the englacial stress approximation and the basal friction applied are still not well constrained and their impact on the solution is very glacier-dependent. Projections based on future ice-*

*sheet/ocean coupled models would need to be based on further understanding of the response of standalone ice sheet models to oceanic perturbations.*

## 4 Objectives of this work

Throughout this introduction we have shown the important role of the Antarctic Polar Region in the present and future climate. The two main components, the AIS and the SO, are strongly affected by climate change and are potential drivers of several climate processes that may have a large global impact in the near future. However, many of those processes are arguably not well represented in climate models, and the projections for the next century are uncertain due to the misrepresentation of several processes, interactions and feedbacks.

The largest driver of the observed changes in the APR is the trends in SAM as a consequence of ozone depletion in the troposphere and the increasing GHG emissions. The impact of SAM in the climate variability of the region is widely studied and relatively well understood. However, other mechanisms due to the interaction between the SO and the AIS have recently been suggested to also participate in the variability of the region, and therefore in the global climate of the near future.

On the ocean side, the freshening due to an increase in ice discharged by AIS is suggested to affect many properties of the SO, with particular implications for the AABW and the sea ice cover. Due to the complexity of the mechanisms participating in the production of AABW and Antarctic sea ice, projections are estimated by modeling. Unfortunately, present climate models do not account correctly for the glacial freshwater sources from melting icebergs and ice shelves, leading to a misrepresentation of many of the processes expected to impact the SO.

On the ice sheet side, melting of the ice shelves by the ocean is suggested to drive glaciers retreat and increasing ice discharge, mainly in the Amundsen sector, with important consequences in future sea level rise. The mechanism driving those changes in the ice dynamics of the Antarctic outlet glaciers are not fully understood and contribute to the large uncertainity associated with the sea level rise projections. Improvements in ice sheet modeling are needed in particular in the interactions with the oceans and the melting-induced grounding line retreats.

New ice-sheet/ocean coupled models have recently appeared in order to better reproduce the ice sheet-ocean interactions. On the ocean modeling side, coupling with an ice sheet model is expected to improve the representation of temporal and spatial evolution of the glacial freshwater fluxes coming from the ice discharged into the ocean. This may help to better reproduce regional patterns in the Antarctic sea ice through a better representation of the ice-ocean feedback (Zhang, 2007; Goosse and Zunz, 2014a) and the bottom waters formation (Heuzé, 2015). On the ice sheet side, coupling with an ocean model is expected to better capture the changes in oceanic circulation, salinity and temperature in the interior of ice shelf cavities. This is expected to lead to a better estimate of the melt rates affecting the ice dynamics and therefore the ice discharge into the ocean.

In the context of future coupled models, this thesis is focused on investigating some particularities of the standalone ocean and ice sheet models that will become components of a future coupled system. Before tackling the ambitious challenge of coupling the two models, improvements in the standalone models (either ocean or ice-sheet models) and to determine the situations for which coupling is required, need to be further investigated. This try to better address the efforts of the climate community and identify the lines of action in the development of the standalone components of the future coupled systems. On a more personal level, instead of just focusing my research in either the ocean or the ice sheet modeling, my personal objective during this thesis was to contribute to both modeling communities in order to acquire a wider view of the physical processes affected by the ice-ocean interaction, and the model particularities of both components of the coupled systems.

The pertinence of the coupled models has not been confirmed yet regarding the ocean processes of sea ice an AABW formation. Indeed, the response of the modeled Antarctic sea ice and bottom waters to perturbations in the ice discharge from AIS are still open to debate as we have seen in previous sections (Bintanja et al., 2013; Swart and Fyfe, 2013; Pauling et al., 2016; Heuzé, 2015). The first objective of this thesis is to study the impact of recent changes in glacial ice discharge on the Antarctic sea ice. In contrast to other studies, in this work special attention will be given to capturing the spatial pattern of ice discharge changes in Antarctica, as will be the case in future coupled models. However, to date, ocean models have a very poor representation of the glacial freshwater fluxes, and therefore, before studying our first objective, improvements in the inclusion of those fluxes in models are needed in particular from the melting of icebergs. This is the aim of Chapters 2 and 3.

The need for a coupled model when modeling the ice sheet dynamics (mostly in the Amundsen sector) seems widely accepted, and international projects like MISOMIP have been created in order to investigated the particularities of future models. However, without coupling, standalone ice sheet modeling of glaciers experiencing MISI and confined ice shelves, like in Pine Island Glacier, needs still further work in including required physical parametrizations or processes. The interaction with the ocean via the loss of buttressing produced by the melting of the ice shelf cavity may produce glacier acceleration in the upstream part of the glacier. In such situation and in some glacier configurations, the model choices like the friction law and the stress approximation applied may have a large impact on the ice dynamics, even larger than the coupling with an ocean model. The second objective of this thesis is to produce an estimate of the uncertainities associated with the choice of different friction laws or stress approximations when projecting the SLR contribution of a Pine-Island-like glacier. This is the aim of Chapter 4.

Chapter 2

# Improving the representation of Antarctic glacial freshwater fluxes in ocean models

Contents



## 1 Introduction

The development of numerical tools for the study of the oceans has historically been focused on better representing the general circulation patterns of the world oceans. As discussed in Chapter 1, the poles have an important role on setting this large scale global circulation through mechanisms driven by the sea ice and associated with bottom waters formation. Those processes are represented in most of ocean models, but commonly from a large scale point of view. Today, the observed regional changes in the Southern Ocean (SO) and in the Antarctic Ice Sheet (AIS), have increased the interest of ocean modelers in better accounting for the polar processes of sea ice and bottom waters formation. This is also motivated by the potential impacts of these mechanisms on a global scale. However, the regional response of the SO to the ongoing changes is not always reproduced satisfactorily by climate models (Heuzé, 2015; Shu et al., 2015). Among the reasons for this misrepresentation of SO changes in current models, is the role that the AIS may have in influencing SO properties (Bintanja et al., 2013; Marsland and Wolff, 2001). Indeed, the regional and seasonal distributions of the glacial freshwater fluxes have not been among the priorities of the ocean modelers so far, and the majority of climate models consider the glacial freshwater fluxes from a very large scale perspective. For instance, Figure 2.1 shows the glacial freshwater fluxes as they are commonly applied into the NEMO/ORCA025 simulations (Dufour et al., 2012). This flux is evenly distributed around Antarctica and is kept almost constant in time with the exception of the first

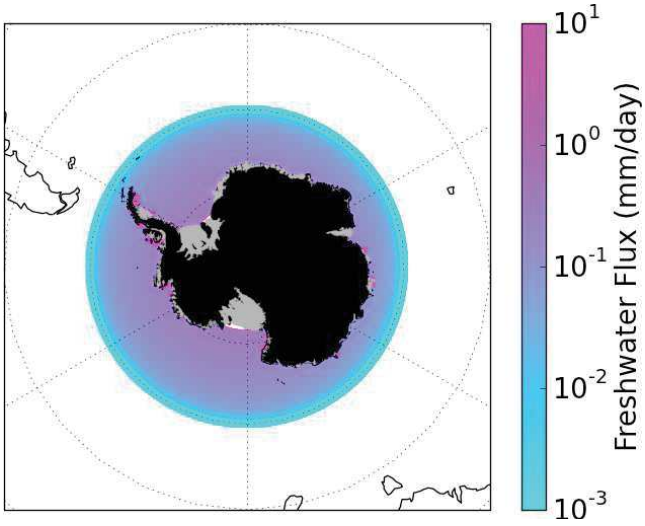


Figure 2.1: Representation of the Antarctic glacial freshwater fluxes as in Dufour et al. (2012).

three grid points adjacent to the coast, which include a slight arbitrary seasonality. In other cases (for instance in Tréguier et al. (2014)), the offshore fluxes coming from icebergs are redistributed based on satellite observations of large tabular icebergs from Silva et al. (2006). Recent observational findings from glaciological studies can be used to better constrain glacial freshwater fluxes in ocean circulation models. These observational estimates distinguish between freshwater associated with melt and calving (Rignot et al., 2013; Depoorter et al., 2013). Those estimates have confirmed the very distinctive spatial pattern associated to the basal melting of the ice shelves, which is not taken into account by global ocean models. In addition, recent radar altimetry estimates have shown the strong seasonality and the distinctive spatial pattern of the freshwater released by icebergs (Tournadre et al., 2016). According to the findings of Tournadre et al. (2015) most of iceberg meltwater is produced by the melting of small icebergs ($< 6km$ in lenght), which drift differently than big tabular icebergs.

Motivated by the weakly constrained representation of the glacial freshwater fluxes in ocean models, and the availability of new glaciological estimates, this section shows my contribution to improving the representation of glacial freshwater fluxes in ocean models. More precisely we will discuss here:

- The improvement of the spatial distribution of the ice shelf basal melting in the global ORCA025 grid of NEMO constrained by the state-of-the-art of glaciological observations.

- The Improvement of the representation of the iceberg meltwater fluxes in ocean models. To this end, I have proposed an set of improvements to the NEMO/ICB module (see Appendix A) collaborating in the publication Marsh et al. (2015a). This physical improvements have been implemented for the first

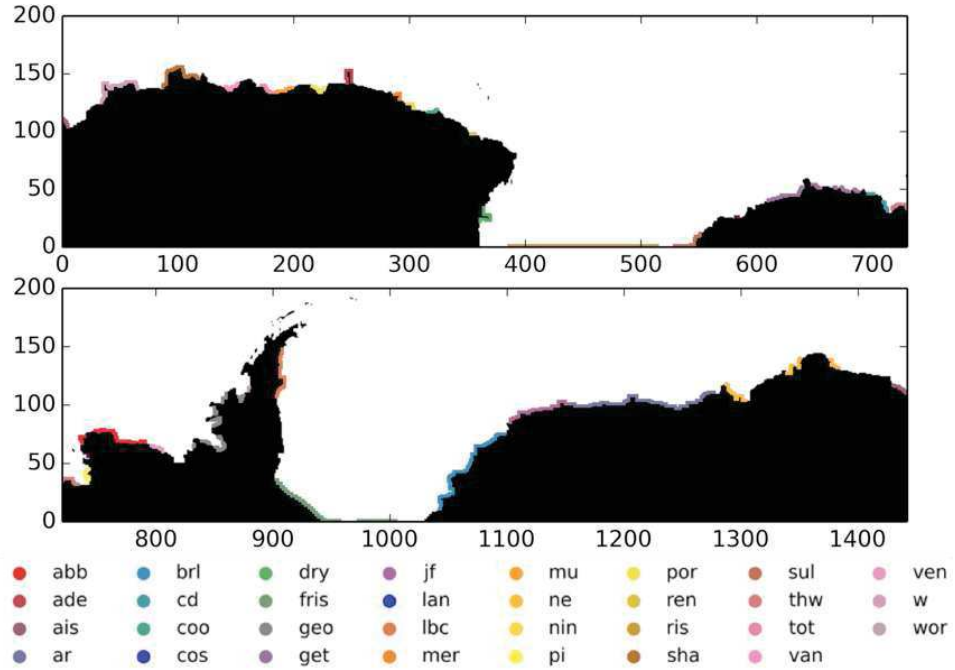


Figure 2.2: Representation of the oceanic grid points adjacent to an ice shelf in an extracted subset of the ORCA025 grid Colors code correspond to the following ice selves: Astrid-Ragnhild (AR), North-East (NE), Amery (AIS), West (W), Shackleton (SHA), Vanderford (VAN), Totten (TOT), Moscow University (MU), Porpoise (POR), Adelie (ADE), Mertz (MER), Ninnis (NIN), Cook (COO), Rennick (REN), Drygalski (DRY), Ross (RIS), Sulzberger (SUL), Land (LAN), Getz (GET), Crosson and Dotson (CD), Thwaites (THW), Pine Island (PI), Cosgrove (COS), Abbot (ABB), Venable (VEN), George VI (GEO), Wordie (WOR), Larsen B-C (LBC), Filchner-Ronne (FRIS), Brunt and Riiser-Larsen (BRL), and Jelbart and Fimbul (JF).

time in the simulations performed for this study, and set up accordingly to recent calving fluxes estimates. The main objective is to produce a model-based estimate of a monthly climatology of iceberg meltwater fluxes, that could be used for forcing ocean models at reduced numerical cost, and study the impact of the icebergs on the Antarctic sea ice.

# 2 Improving melt water

At the time of this study, the most recent estimates of Antarctic ice shelves mass loss are described in Rignot et al. (2013) and Depoorter et al. (2013). Both studies are based on similar data and methods, and therefore present very similar results. For our purpose we decided to use the results from Depoorter et al. (2013) instead of those of **?** based on the fact that the former used a more advanced ice-firn density

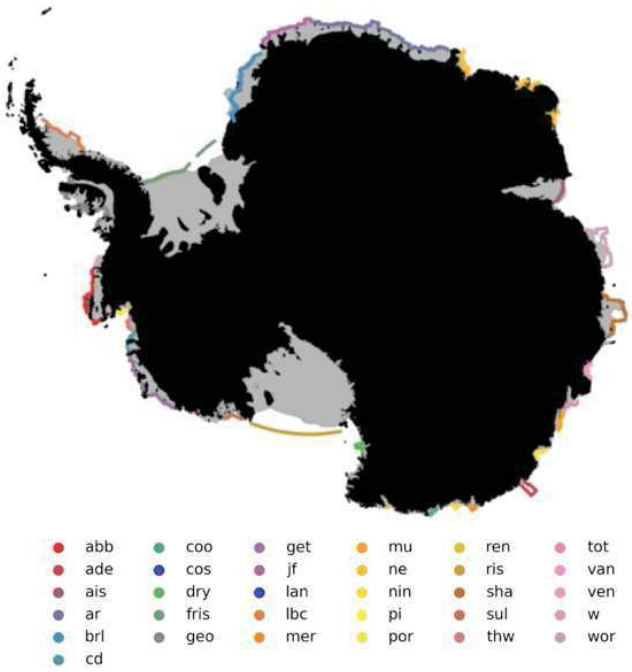


Figure 2.3: Representation of the oceanic ORCA025 grid point adjacent to the ice shelves in polar stereographic projection. Colors code are similar than in Figure 2.2.

model, the main differences between both studies..

My main contribution has been the identification in the ORCA025 grid of NEMO of all the ice shelves and sectors defined in Depoorter et al. (2013). Figure 2.2 shows the location of the first ocean grid point adjacent to each ice shelf included in Depoorters's study. Figure 2.3 presents the geo-location of those points around the Antarctic coast line. This shows that the most significant differences can be found in the front location of Ross and Ronne-Filchner Ice Shelves. This is due to the southern limit of the ORCA025 grid in order to avoid numerical problems associated with a reduce grid size in NEMO. This issue has been recently solved with the extended version of ORCA025 (eORCA025) which includes all the polar regions adjacent to ice-shelf fronts

Once the location of the main ice shelves have been identified in the model grid, the estimate of basal melt freshwater fluxes from Depoorter et al. (2013) is evenly distributed between the grid points belonging to the same ice shelf. In addition, based on BEDMAP2 (Fretwell et al., 2013), we have chosen a constant grounding line depth value per ice shelf and the ice shelf draft depth per point for applying the ice shelf parametrization of NEMO (see Appendix A).

# 3 Freshwater fluxes due to icebergs

This estimation of the freshwater fluxes due to the Antarctic icebergs is described in the study named *Antarctic icebergs melt over the Southern Ocean : climatology and impact on sea ice* accepted for publication in the journal Ocean Modelling (Merino et al., 2016).

## 3.1 Antarctic icebergs melt over the Southern Ocean : climatology and impact on sea ice (Publication)

Ocean Modelling 104 (2016) 99–110

Contents lists available at ScienceDirect

Ocean Modelling

journal homepage: www.elsevier.com/locate/ocemod

Review

# Antarctic icebergs melt over the Southern Ocean: Climatology and impact on sea ice

Nacho Merino[a,b,*], Julien Le Sommer[a,b], Gael Durand[a,b], Nicolas C. Jourdain[a,b], Gurvan Madec[c,d], Pierre Mathiot[e], Jean Tournadre[f]

[a] CNRS, LGGE, F-38041 Grenoble, France
[b] Univ. Grenoble Alpes, LGGE, F-38041 Grenoble, France
[c] LOCEAN, CNRS/MNHN/IRD/UPMC, Paris, France
[d] NOC, Southampton, UK
[e] Met Office, Exeter, UK
[f] LOS, IFREMER, Brest, France

## 1 Introduction

In contrast with the rapid sea ice loss observed in the Arctic, satellite observations show a slight overall increase in SIE around Antarctica in recent decades (Comiso and Nishio, 2008; Parkinson and Cavalieri, 2012b). The overall increase in SIE results from the integration of large regional increases and decreases in SIC around Antarctica (Turner et al., 2009b). While the amplitude of overall trend is open to debate, the geographical pattern of regional changes in SIC has been clearly detected in satellite observations (Eisenman et al., 2014). The mechanisms driving overall change in Antarctic sea ice and its regional pattern are also not fully understood as climate models generally fail to simulate these trends in a rigorous manner (Polvani and Smith, 2013b; Gagne et al., 2015; Turner et al., 2015a). Whether this is indicative of a poor representation of physical processes in climate models, for instance the modelled ice drift (Uotila et al., 2014), or reflects the fact that the observed trend in SIE results from natural variability is still unclear.

Several model and observational studies have investigated the causes of the increase in Antarctic SIE observed over recent decades. Proposed external drivers for such change include winds, air-temperature, precipitation and freshwater forcing (FWF) from Antarctica. Model experiments show that the changes in surface winds and air temperature associated with a positive trend in the Southern Annular Mode contribute to regional changes in Antarctic SIC with a spatial pattern similar to the observed trends (Lefebvre et al., 2004). The role of changing winds appears to be dominant in the regional response to changing atmospheric conditions around Antarctica, through a combination of changes in wind-driven advection of sea ice and wind-driven thermodynamic changes (Holland and Kwok, 2012b; Fan et al., 2014; Holland et al., 2014). However, changes in winds do not appear to quantitatively account for all the changes observed in SIE (Liu et al., 2004; Fan et al., 2014). Changes in Antarctic SIE may also involve ice-ocean feedback (Zhang, 2007; Goosse

and Zunz, 2014b) and ice-atmosphere feedback (Stammerjohn et al., 2008b).

It has also been suggested that the increase in Antarctic SIE may be due in part to changes in freshwater release from the Antarctic Ice sheet (AIS) (Bintanja et al., 2013; Swart and Fyfe, 2013). This hypothesis is consistent with the observed acceleration of the mass loss from the AIS (Shepherd et al., 2012; Rignot et al., 2008). The oceanic response mechanism involves freshwater-induced changes in ocean surface stratification and convection regimes (Marsland and Wolff, 2001). However, to date, there is no quantitative agreement among existing model studies regarding the impact of the accelerated mass loss from the AIS on Antarctic sea ice. This discrepancy is arguably due to the different and crude representations of freshwater forcing from AIS in ocean models.

The oceanic freshwater forcing from AIS combines the contributions of basal melt in ice-shelf cavities around Antarctica and freshwater fluxes due to melting icebergs over the Southern Ocean. While the input of freshwater due to basal melt occurs at the base of each ice-shelf, icebergs are calved at ice-shelf fronts and melt progressively as they are transported northwards over the Southern Ocean. Reliable estimates of present-day sub ice-shelf melt and calving rates are now available for each ice-shelf (Depoorter et al., 2013; Rignot et al., 2013). However, the redistribution of iceberg mass over the Southern Ocean remains imperfectly constrained, so that ocean model studies differ in their representation of iceberg melt over the Southern Ocean (Bintanja et al., 2013; Swart and Fyfe, 2013; van den Berk and Drijfhout, 2014).

Over the last decade, observations of iceberg distribution and melt rate have mostly been limited to the tracking of large tabular icebergs (i.e. longer than 18 km Silva et al., 2006). Recent methods based on radar altimetry make it possible to estimate the distribution of the annual mean volume of icebergs and the annual mean melt rates associated with smaller icebergs (up to about 3 km in length Tournadre J., 2015). However, accurate estimates of the seasonal and spatial distribution of iceberg melt rates are still not possible because it would require tracking individual icebergs to determine where freshwater release actually occurs. In addition, the altimeter detection of icebergs is limited to sea ice free water and by constraints due to satellite orbits over the southernmost latitudes. Alternatively, explicit iceberg models based on a Lagrangian representation of collections of icebergs have also been proposed as an alternative for estimating freshwater releases from icebergs over the Southern Ocean (Bigg et al., 1997; Gladstone et al., 2001). A widely used climatology of Antarctic iceberg freshwater fluxes, proposed by Silva et al. (2006), combines observations of large tabular icebergs and modelling of small icebergs.

Several Lagrangian iceberg models have recently been coupled with ocean circulation models at various grid resolutions (Martin and Adcroft, 2010; Jongma et al., 2009; Marsh et al., 2015b). These models, however, do not yet use the most up-to-date estimates of calving rates (Depoorter et al., 2013; Rignot et al., 2013). Moreover, modelled iceberg distributions have not yet been systematically compared with observations from radar altimetry. Tournadre et al. (2012) also suggest that existing models might not be able to adequately represent iceberg trajectories

across Southern Ocean subpolar gyres (especially in the Weddell Gyre). This may be due to biases in current Lagrangian iceberg models, which are driven by ocean surface fields, or to the coarse resolution of most ocean circulation models coupled with iceberg models.

In this paper, we propose a model-based estimate of iceberg melt over the Southern Ocean and study the impact of iceberg melt on ocean surface properties and sea ice. The estimate is obtained with an improved version of a Lagrangian iceberg model coupled with an eddy-permitting ocean-sea ice model, using the most recent input calving rates based on glaciological studies. The modelled iceberg distribution is shown to compare favourably with observations in most of the Southern Ocean sectors. We show the strong seasonality of iceberg freshwater releases over the Southern Ocean and discuss its impact on Antarctic sea ice. We further show that the impact of icebergs on Antarctic sea ice can be reproduced, to a large extent, by forcing the ocean-sea ice model with a climatological iceberg freshwater flux (provided as Supplementary Material). The methods are described in section 2. The modelled distribution of icebergs is presented and compared with observations in section 3. The impact of iceberg freshwater release on sea ice is discussed in section 4. Finally, section 5 draws conclusions and discusses the proposed climatology of iceberg freshwater fluxes.

## 2 Material and methods

The distribution of freshwater fluxes due to icebergs is estimated here with an interactive ocean/sea ice/iceberg model forced with recent estimates of Antarctic freshwater forcing. In this section we describe the details of the model set up and the different datasets used to perform this work.

### 2.1 Ocean/sea ice model configuration

The ocean simulation is based on NEMO v 3.5 (Madec, 2014). The model configuration uses a 0.25-degree resolution grid (ORCA025) with 75 vertical levels developed and maintained by the DRAKKAR group. Ice-shelf cavities are not explicitly represented in the model, but ice-shelf meltwater is prescribed (see section 3). The ocean component is coupled with the LIM2 sea ice model (Fichefet and Morales Maqueda, 1997) and the NEMO iceberg module (see section 3 Marsh et al., 2015b). The ocean model is forced by using core bulk formulae with a climatological repeated-year atmospheric forcing based on ERA-Interim (Dee et al., 2011b). The climatological repeated-year forcing is constructed following the same approach as Grégorio et al. (2015) itself based on Penduff et al. (2011). This forcing is built by computing 365 ERA-Interim daily averages for the period 1979-2011. The resulting atmospherical forcing is composed of the daily averages of precipitations, runoff, cloud cover, long and short wave radiation, 10 meters winds, temperature and air humidity. In addition quadratic contributions are added to air-sea fluxes in order to account for the contribution of non-linear high frequency correlations in bulk formulae. A sea sur-

face salinity restoring towards NODC WOA94 data, with a piston velocity (Griffies et al., 2009) of 50 m/300 days, is applied, except at the first coastal grid points. This is commonly practised in stand-alone ocean/sea ice DRAKKAR simulations in order to not affect the total coastal runoff in the simulations.

## 2.2 Standard NEMO-ICB and new features in NEMO-ICB

The ocean component is coupled with the NEMO-ICB iceberg module (Marsh et al., 2015b). It describes the evolution of an ensemble of Lagrangian particles. Each Lagrangian particle is meant to represent a collection of one or several icebergs. Each collection of icebergs belongs to one of the ten different size categories of the statistical distribution based on ship observations proposed by Gladstone et al. (2001). By simplicity, a constant upper bound of 250 m is considered for all the ice shelves in this study, consistently with Martin and Adcroft (2010) and Marsh et al. (2015b). This upper bound corresponds to the typical thickness of ice-shelves at their calving front. NEMO-ICB considers a fixed number of source points with constant in time iceberg production rate for each individual source location. The dynamics and thermodynamics of each collection of icebergs are prescribed according to the procedure used by Marsh et al. (2015b), which mostly follows Martin and Adcroft (2010). Freshwater fluxes to the ocean model are calculated at each time-step from the iceberg melt rate and injected at the ocean surface. However, in the present version of NEMO-ICB, heat fluxes from icebergs are not applied to the ocean model: neither sensible heat fluxes due to iceberg-ocean temperature difference, nor latent heat of fusion when melting are taken into account.

As is common in iceberg models, the model only describes the evolution of small icebergs (up to 2.2km in length). This choice is supported by the findings of Tournadre et al. (2015) indicating that the melting of large icebergs provides only a marginal contribution to total iceberg freshwater fluxes.

### 2.2.1 NEMO-ICB module modifications

Unlike previous versions of Lagrangian iceberg models (Bigg et al., 1997; Gladstone et al., 2001; Martin and Adcroft, 2010), the model used here (NEMO-ICB module, including the modifications described in section 4 of Marsh et al., 2015b) takes into account the influence of the vertical profiles of ocean currents and temperatures instead of only considering the SST and surface ocean velocities, and considers a parametrised interaction with shallow bathymetry. Those modifications (firstly implemented for this work) are described in this section and are found to significantly improve the representation of iceberg trajectories across Southern Ocean subpolar gyres (see section 3).

The first modification introduced in NEMO-ICB is the vertical integration of ocean currents that takes into account the drag exerted by the entire ocean column in contact with the iceberg, instead of the drag exerted by the ocean surface. This modification allows in particular to take into account the change in the orientation

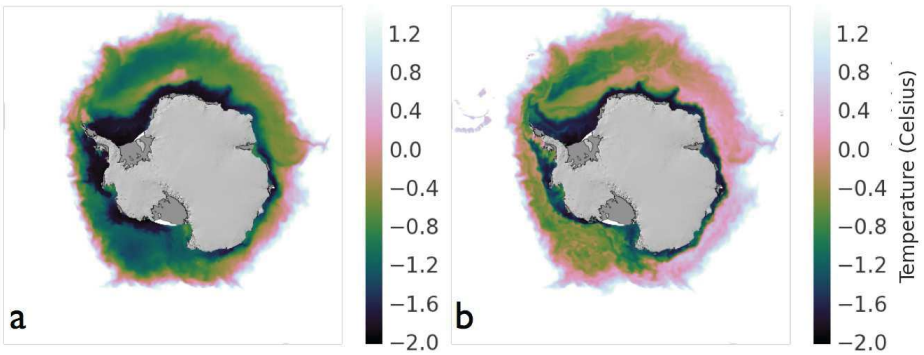


Figure 2.4: Modelled ocean temperatures of the last year of a 20-years ORCA025 simulation coupled with the NEMO-ICB module. (a) Sea Surface Temperature. (b) Averaged temperature over the first 150 m from the surface.

of wind driven currents with depth in the Ekman layer, which is approximately 100 m deep in the Southern Ocean (Lenn and Chereskin, 2009).

The second modification is the computation of melt rates using ocean temperatures at varying depths, thus taking into account the strong vertical temperature gradients in summer in the upper Southern Ocean. Modelled icebergs, according to observations, can be up to 250 m thick (Gladstone et al., 2001) and the ocean temperature profiles across the pycnocline in summer can be remarkably abrupt in shallow mixed layers. As shown in Figure 2.4, surface temperatures and first depth averaged temperatures over 0-150m can differ significantly in some regions.

The last modification introduced in this work is the parametrization of iceberg interaction with bathymetry. With the inclusion of the vertical integration of the ocean currents, the interaction of thick icebergs with shallow bathymetry needs to be explicitly taken into account. This is because, accounting for the ocean drag is needed when a thick iceberg crosses a shallow bathymetry grid cell. We choose not to stop icebergs in shallow regions because the subgrid scale bathymetry probably matters more than the model bathymetry. Nonetheless, we calculate the vertically-averaged velocity over the entire iceberg thickness, with zero velocities at depth where the iceberg is deeper than the model bathymetry, so icebergs are slowed in shallow regions (see equation 1 in Appendix). By including this interaction in the model, thick icebergs tend to stay longer in specific coastal regions instead of escaping northwards as it happened in previous versions of the iceberg model. This overall behaviour is in better agreement with observations which indicate the existence of regions with high iceberg presence due to the grounding of thick ones (Jacka and Giles, 2007).

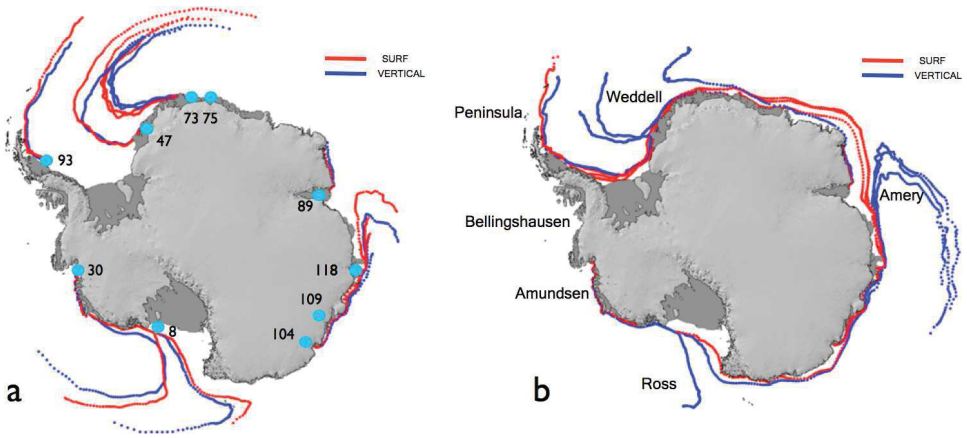


Figure 2.5: Examples of trajectories of modelled icebergs. (a) Trajectories of 73m-thick icebergs of class number 2 with their corresponding sources points (see Supplementary Material); (b) Trajectories of 133m-thick icebergs of class number 3 and the name of relevant sectors. Red dots correspond to trajectories only considering the drag exerted by the ocean surface, and blue dots correspond to icebergs considering the vertical integrated ocean drag.

### 2.2.2 Impact of vertical shear on simulated iceberg trajectories

As described in section 3 the iceberg model used in this study considers ocean currents averaged over the thickness of each iceberg in the drag formulation, instead of the ocean surface currents as commonly applied in previous iceberg modelling studies.

Figure 2.5 shows the sensitivity to this modification for individual iceberg trajectories departing from different locations and for two different size classes. Icebergs of category #1 and #2 (40m and 67m thickness respectively, Gladstone et al. (2001)) are thinner than the typical thickness of the Ekman layer and are therefore not significantly affected by the modification in NEMO-ICB (Figure 2.5-a). By contrast, larger and thicker icebergs can only cross the Weddell, Ross, and Amery Seas if the vertical integration of ocean velocities is included in NEMO-ICB (Figure 2.5-b). Icebergs following the Antarctic Coastal Current are more likely to escape before reaching the Antarctic Peninsula and to the north of the Weddell Sea. Consequently, our modification leads to a reduced presence of modelled icebergs in the Atlantic sector, and contributes to better distribute the iceberg mass between Atlantic, Indian and Pacific sectors.

## 2.3 Observation-based calving and meltwater input fluxes

The recent estimate of Antarctic freshwater forcing from Depoorter et al. (2013) is used in our simulations. Depoorter et al. (2013) provide calving rates and basal melt fluxes for 31 ice-shelves around Antarctica. The total observed mass loss from Antarctica is completed with an additional residual flux for each Southern Ocean

sector. Both the calving rates and the basal melt rates are in good agreement with another recent observational study (Rignot et al., 2013).

These recent estimates provide a major improvement over the Antarctic freshwater forcings used in previous studies (eg. van den Berk and Drijfhout, 2014). Indeed, the most recent estimates (Depoorter et al., 2013; Rignot et al., 2013) account for the observed changes in ice-shelf thickness and surface mass balance, in contrast with earlier studies (eg. Rignot and Jacobs, 2002). In addition, improved techniques for grounding line detection, thickness measurements and firn model corrections have been applied to the treatment of the most recent data (between 1994 and 2009) (Depoorter et al., 2013).

Basal melt underneath ice-shelves is prescribed as coastal run-off in our simulation set-up. Following Depoorter et al. (2013), it accounts for 1454 Gt/yr and is distributed at the ice-shelf fronts. The corresponding freshwater flux is applied at ocean grid points lying at the front of each ice-shelf and spread vertically between the base of the calving front and the minimum between the grounding line depth and the bathymetry at the calving front. The 1350 Gt/yr of calving fluxes estimated in Depoorter et al. (2013) are used as input for the NEMO-ICB module. The iceberg model then generates icebergs, which eventually distribute freshwater at the ocean surface when they melt. Calving rates are kept constant over time and their spatial distribution follows Depoorter et al. (2013). The distribution of source points for iceberg calving is provided in Supplementary Material.

## 2.4 Model experiments

Three experiments based on the described model set up have been run in this work. The *iceberg test run* (hereafter referred to as ICBT) uses the ocean/sea ice model configuration coupled with the iceberg model described above in section 3 in a 20-year simulation. The ICBT simulation initial state is free of icebergs. The first 9 years of ICBT simulation correspond to the spin-up required for the iceberg model. In steady state after the spin-up, the calving mass input matches the melted iceberg mass. In contrast, in the *control run* (hereafter CTR), the iceberg model is switched off, and consequently, the ocean/sea ice model does not include any flux from icebergs. CTR is computed for 14 years, that correspond to 9 years of spin-up and 5 years for results comparison with ICBT results. Considering the constant climatological atmospheric forcing applied, the reduced ocean/sea ice model variability allows 5-years means comparisons between both simulations. An extra simulation of 14 years (hereafter CLIM) was performed without the iceberg model but including, as an external forcing, a monthly climatology of iceberg freshwater flux. This climatology (available in Supplementary Material) has been computed from the monthly means of the ICBT simulation (see section 3)

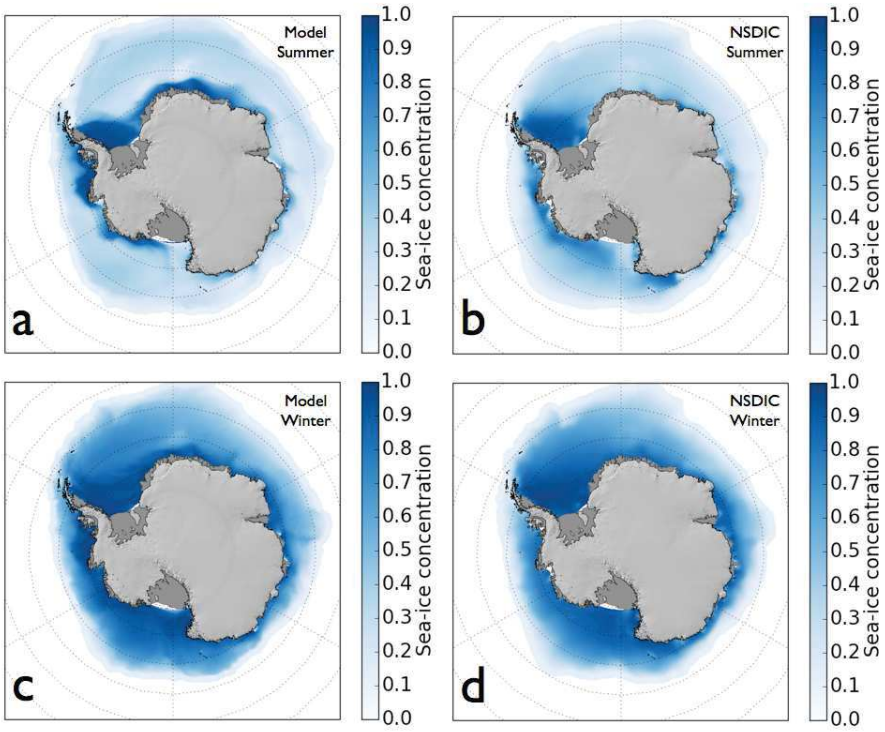


Figure 2.6: Sea ice concentration means for: (a) Summer in model results, (b) summer from observations, (c) winter in model results, and (d) winter from observations. Summer means include months from October to March. Winter means includes months from April to September. Model results correspond to ICBT (simulation with explicit icebergs) monthly means of the first 5 years after the 9-year spin up. Observations correspond to the National Snow and Ice Data Center (NSDIC) (Peng et al., 2013) sea ice concentration climatology of the period 1979-2010. Concentrations lower than 10% are not show.

## 3 Model evaluation

### 3.1 Ocean/sea ice model

Figure 2.6 shows the comparison of the modelled sea ice with observations. Modelled SIC is computed from monthly means of ICBT simulation after spin-up. Observations of sea ice concentration come from NSDIC monthly means for the period 1979-2010. Summer means includes the months from October to March, and winter means include months from April to September. ICBT simulation presents more sea ice concentration than observations in the Bellingshausen Sea in both summer and winter seasons. In summer, sea ice concentration gradients are overall stronger in the model. Besides, simulated summer sea ice is more concentrated in coastal regions of the Atlantic and East Indian sectors and less concentrated in Ross Sea.

The choice of comparing 5-years sea ice means between the different simulations

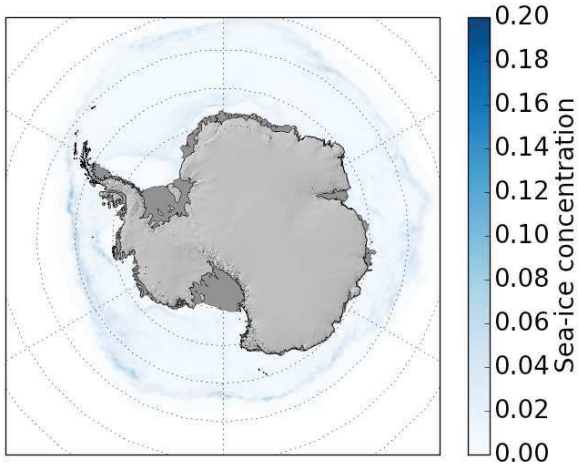


Figure 2.7: Standard deviation of the yearly mean sea ice concentration for the first 5 years after the 9-year spin up of ICBT (simulation with explicit icebergs).

(see section 3) is supported by the Figure 2.7. It shows the standard deviation of the sea ice concentration for the 5-year period after the 9-years spin-up of the ICBT simulation. As shown in Figure 2.7, the inter annual variability of the sea ice for ICBT simulation is mostly negligible. Large standard deviations are obtained near sea ice margins where year to year variability in SIC is expected to be large.

## 3.2 Iceberg model

### 3.2.1 On the model-observations comparison of iceberg presence

Iceberg model results are compared to ALTIBERG database (Tournadre J., 2015). This database uses the method described in Tournadre et al. (2012) applied to Jason-I and 9 other satellites covering various time periods from 1992 to 2014. The database provides a single estimate of iceberg volume per grid cell for icebergs of 0.1 to 3 km in length. It is based on the assumption of a constant iceberg thickness of 247 m. Our study divides this volume by the thickness (247 m) to obtain the area covered by icebergs in each grid cell. Taking into account grid cell area, we can compute the ratio between the surface covered by icebergs and the ocean surface. This can also be understood as the probability of detecting an iceberg of 0.1 to 3 km in length in a grid cell. A similar estimation can be made from model results. The total area covered by modelled icebergs is integrated over the same grid as the observations and averaged over a year.

Satellite detection of icebergs with radar altimetry is limited by the presence of sea ice. Icebergs can only be detected in sea ice free water and the comparison in regions with high annual sea ice concentration needs to be carefully considered. In order to highlight those sectors, we decided to mask in Figure 2.8 the regions

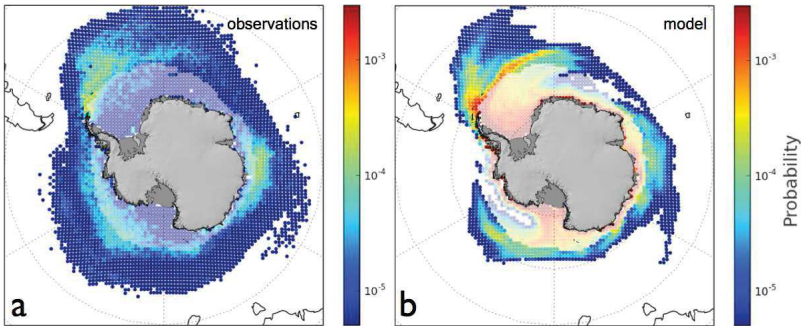


Figure 2.8: Probability of iceberg detection in a 100 km x 100 km grid cell during a year. (a) Observations from ALTIBERG database (Tournadre J., 2015), (b) Model results. Points where annual mean sea ice cover is larger than 40% are shaded.

with sea ice concentration greater than 40%, consistently with the ALTIBERG data treatment. We use observations of mean sea ice cover provided by the NSIDC (Peng et al., 2013) instead of our modelled sea ice concentrations, so as to be more consistent with ALTIBERG detections.

The quantitative comparison of modelled and observed icebergs should be considered with caution because of the specificities of iceberg detections and model settings. On the observation side, the method of Tournadre et al. (2012) only detects small icebergs of up to 3 km in length. Therefore a significant fraction of the total volume of icebergs, corresponding to icebergs longer than 3 km, is not directly observed with radar altimetry. On the model side, the distribution of iceberg class sizes, which follows Gladstone et al. (2001), assumes that the total annual volume of icebergs is distributed in iceberg classes of up to 2.2km in length. Given that the thickness of icebergs depends on the category, the model probably overestimates the area covered by small icebergs.

### 3.2.2 Qualitative model-observations comparison

Figure 2.8 compares the iceberg distribution in the model with observations from the ALTIBERG database (Tournadre J., 2015). It shows the probability of detecting an iceberg in a grid cell of 100 km x 100 km over a year following the method described in section 3. To our knowledge, this is the first qualitative comparison between an iceberg model and the distribution of small icebergs estimated from radar altimetry observations. Patterns of the probability of iceberg presence is overall well reproduced by the model. Indeed, the model correctly computes highly probability of finding icebergs in offshore branches of Antarctic subpolar gyres. The model also reproduces the observed pattern of iceberg presence in the eastward flowing branch of the Weddell Gyre. This pattern is consistent with the observations of Tournadre et al. (2012) (see their Figure 16), whereas most existing iceberg models show major discrepancies in this region (Tournadre et al., 2012). As shown in Figure 2.9, the presence of icebergs in this region significantly increases the freshwater flux in the

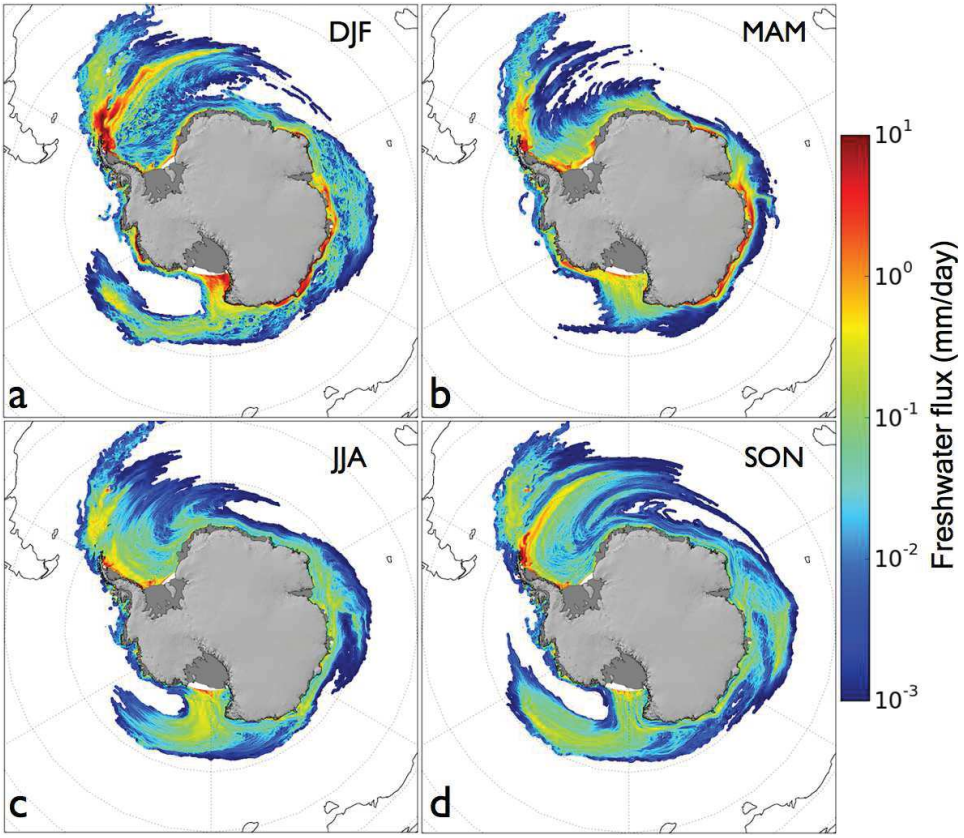


Figure 2.9: Climatology of iceberg freshwater flux over the Southern Ocean in mm/day for (a) summer, (b) autumn, (c) winter and (d) spring seasons. The flux is computed from 11 years of ICBT (simulation with explicit icebergs) after 9 years of spin-up.

Atlantic sector of the Southern Ocean. The improved distribution of icebergs in this region compared with previous studies is likely due to the depth integration of ocean currents as discussed in section 3

Several differences between the model and observations can also be identified. First, the model suggests a higher probability of iceberg presence in coastal regions compared with observations. It should be noted that most of the iceberg detections in those coastal sectors have been dismissed from ALTIBERG database based on their sea ice criteria (Tournadre J., 2015). However, synthetic aperture radar images (Wesche and Dierking, 2015) confirm the high presence of small and medium size icebergs trapped in the Antarctic Coastal Current in the Indian and Atlantic sectors. Second, in the model, the Weddell Sea sector presents a relatively larger iceberg-covered area than that found in the Amery or Ross sectors, whereas observations indicate roughly similar probabilities of iceberg presence in all three Antarctic subpolar gyres. This might indicate that the modelled icebergs are too often trapped within the Antarctic Coastal Current. Indeed, the Antarctic Peninsula

is the last escape route for icebergs transiting along the Antarctic Coastal Current. Model misrepresentation of the ability of icebergs to escape coastal regions would therefore result in an increase in iceberg presence north of Weddell Sea. This happens even if, as shown in section 3, modifications of the iceberg model used in this study tend to decrease the number of icebergs that eventually reach the Antarctic Peninsula. A further misrepresentation of escape routes from coastal regions in the model could also be associated with the representation of iceberg interaction with sea ice, firstly suggested by Lichey and Hellmer (2001), proposed by Hunke and Comeau (2011) and observed by Schodlok et al. (2006). In addition, mesoscale variability in the Antarctic Coastal Current is significant (Stewart and Thompson, 2015), but probably too weak in the model, which may contribute to limit the escape of modelled icebergs from coastal regions. The model also shows a lack of icebergs in open ocean waters of the South-East Pacific sector. This could be related to the fact that the model only considers coastal sources of icebergs, whereas observations suggest that large icebergs, which are not represented in the model, break into small icebergs in open ocean waters (Tournadre et al., 2015). These resulting smaller icebergs are then transported by the ACC and reach the west Antarctic Peninsula and the South Atlantic sectors before melting. Neglecting the formation of small icebergs associated with the breaking of large ones is therefore likely to contribute to discrepancies in the South-East Pacific and in the South Atlantic.

## 4 Results

### 4.1 Iceberg freshwater flux climatology

Starting from an initial state free of icebergs, the iceberg model takes about 9 years to reach equilibrium, when iceberg melt water balances the calving flux. At model equilibrium in ICBT run, the Southern Ocean presents a yearly mean iceberg mass close to 3000 Gt, more than twice the iceberg mass input and the melted mass released over one year. This indicates that, on average, model icebergs are transported for more than one year before melting. We find in particular that icebergs usually follow the Antarctic Coastal Current for more than one year before reaching the open ocean. This is also consistent with recent estimates of the volume of icebergs near the coast of Antarctica (Wesche and Dierking, 2015). Icebergs eventually leave coastal regions carried by offshore flows associated with the three Antarctic subpolar gyres in the Weddell, Ross and Amery sectors (see Figure 2.8). Such iceberg behaviour in the model is consistent with satellite observations (Tournadre et al., 2012) and was previously reported in the eastern Weddell Sea by Schodlok et al. (2006).

The 11-years climatological estimate of iceberg freshwater release over the Southern Ocean are shown in Figures 6 and 7. This estimate confirms that iceberg melt over the Southern Ocean is very heterogeneous. For instance, since most of the iceberg mass is concentrated in the Weddell Sea sector, this is where most of the freshwater release occurs. In contrast, iceberg freshwater release appears to be rel-

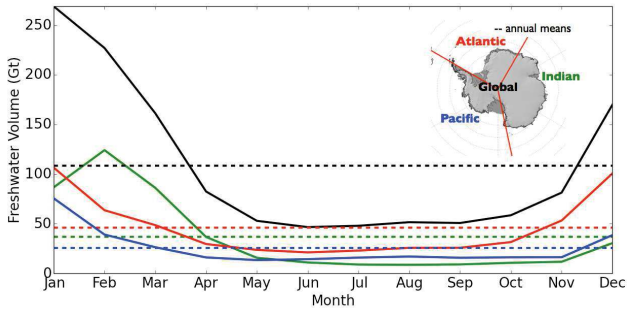


Figure 2.10: Spatial and monthly Integration of the iceberg freshwater fluxes per Southern Ocean sector. Dashed lines correspond to annual means. Red, green, blue and black lines correspond to Atlantic, Indian, Pacific and global sectors respectively.

atively limited in the Bellingshausen Sea, west of the Antarctic Peninsula, most probably because this region is not fed by icebergs flowing from upstream sources along the Antarctic Coastal Current. Our estimate also confirms that iceberg melt exhibits strong seasonality over the Southern Ocean, as suggested by Tournadre et al. (2012) and shown in Figure 2.10. The freshwater flux is indeed usually below the annual mean value for more than two thirds of the year, with about 43% of annual fresh-water release occurring from December to February. The strongest seasonality is observed in the Ross Sea and Amundsen Sea sectors in the Pacific, where January and February account for almost half of the net annual freshwater flux. Surprisingly, the seasonality of the freshwater flux in the Indian sector is slightly delayed as compared to other regions, with a maximum flux occurring in February and relatively weak fluxes in December and January.

## 4.2 Sensitivity of sea ice to icebergs

Figure 2.11 shows the differences in annual mean sea ice concentration and thickness for ICBT and CTR simulations. It considers the first 5 years after the 9 years of spin up. It reveals that the freshwater release due to icebergs increases sea ice concentration and thickness over most of the Southern Ocean with the exception of the Bellingshausen Sea. Those results are discussed in section 3. The sea ice volume seasonal cycles of both ICBT and CTR simulations are compared in Figure 2.12. As shown in Figure 2.12, both simulations present a very similar minimum of sea ice volume with remarkable differences in their maximum in most of the Southern Ocean sectors. In addition, there is no shift between the sea ice cycle of both simulations, so the maximum and the minimum happen at the same time of the year for all the analysed sectors. Overall, iceberg freshwater release therefore increases the amplitude of the seasonal cycle of sea ice with larger net production and sea ice melting. These changes lead to an increase of 10% in the annual mean sea ice volume. However, in terms of relative quantities, the largest relative global

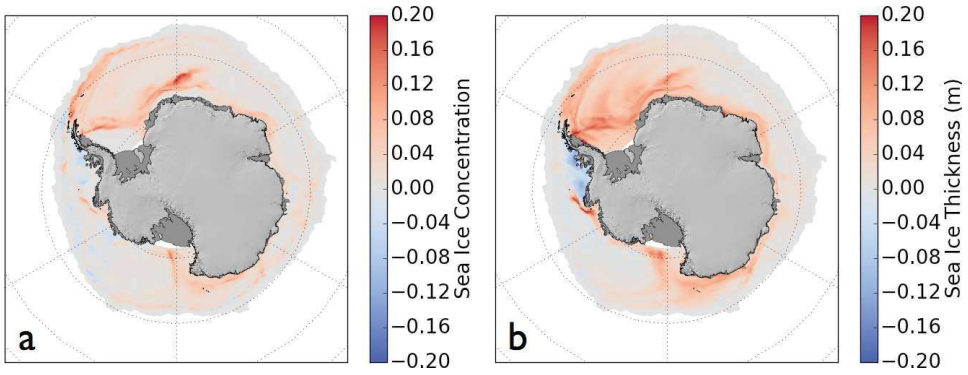


Figure 2.11: (a) Anomalous sea ice concentration in ICBT (simulation with explicit icebergs) versus CTR (simulation without icebergs fluxes).. (b) Anomalous sea ice thickness in ICBT versus CTR.. Results are computed from sea ice monthly means obtained for the first 5 years of simulations after the 9-years spin-up.

difference between ICBT and CTR occurs in mid-April, at the beginning of the sea ice production period, with a 14.3% larger sea ice volume with icebergs (ICBT). In summer, when sea ice volume is at a minimum, it is 10% larger with icebergs (sea ice extent is 13.5% larger). In winter, when sea ice volume reaches a maximum, it is 8.3% larger with icebergs (sea ice extent is only 2.5% larger). Overall, iceberg freshwater release therefore increases the amplitude of the seasonal cycle of sea ice volume with larger net production and the melting of sea ice.

The CLIM experiment (see section 3) was performed to study the ability of the ocean model to account for the iceberg freshwater fluxes with a reduced CPU cost as compared to ICBT simulation. For instance, the first year after spin-up takes 47% less CPU time for CLIM than for ICBT. Figure 2.13 shows the difference in annual mean sea ice concentration and thickness for ICBT and CLIM simulations. It considers the first 5 years after 9 years of spin up. This result reveals strong similarities in the solution obtained when an external forcing is applied at the ocean surface instead of explicitly solving the icebergs dynamics and thermodynamics. This result shows that most of the impact on the sea ice can be captured with the inexpensive approach applied for the CLIM simulation. Differences obtained in most of the Southern Ocean are indeed negligible compared to the differences between ICBT and CTR simulations (see Figure 2.11).

## 5 Discussion of the impact of icebergs on sea ice and ocean surface

Freshwater fluxes at the ocean surface directly affect surface salinity, ocean stratification and mixed layer depth through changes in bouyancy fluxes at the ocean surface. These changes in surface properties can also indirectly affect sea surface temperature (SST) and sea ice cover (as it is shown in section 3). Two important mechanisms can be expected to play a role in the response of Antarctic sea ice to iceberg freshwater release. Firstly, during fall and winter months, when the

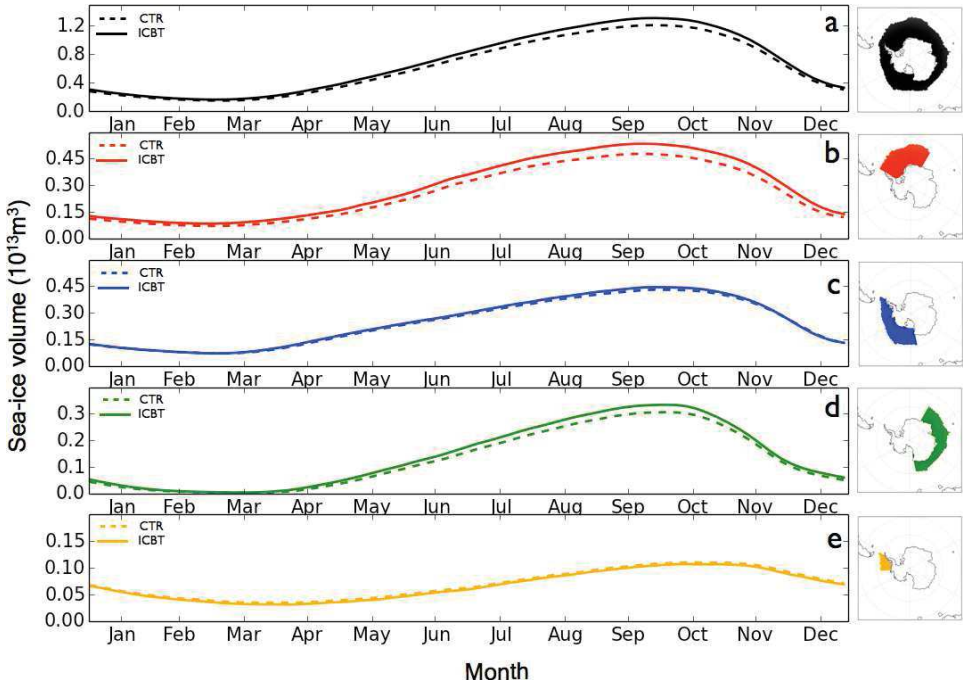


Figure 2.12: Climatological seasonal cycles of sea ice volume in ICBT (simulation with explicit icebergs) (solid line) and CTR (simulation without icebergs fluxes) (dashed line), for all the Southern Ocean, Atlantic, Pacific, Indian and Bellingshausen Sea sectors respectively.

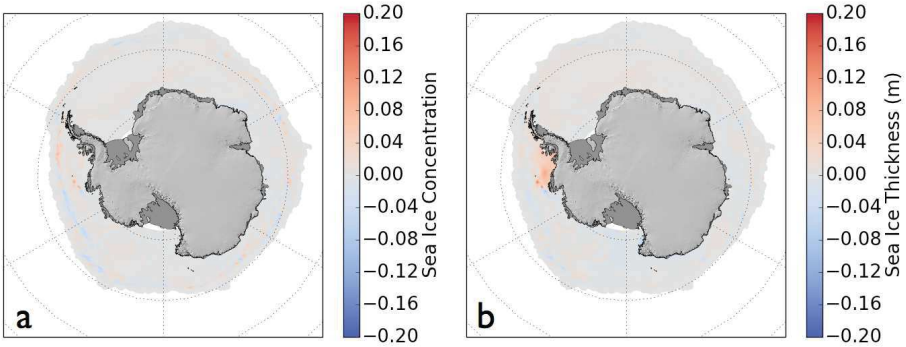


Figure 2.13: (a) Anomalous sea ice concentration in ICBT (simulation with explicit icebergs) versus CLIM (simulation forced with icebergs fluxes) . (b) Anomalous sea ice thickness in ICBT versus CLIM. Results are computed from sea ice monthly means obtained for the first 5 years of simulations after the 9-years spin-up.

atmosphere extracts heat from the ocean, a freshening of ocean surfaces enhances thermohaline stratification, thereby weakening the rate of convective overturning and therefore the supply of heat to the surface layers from deeper layers. This leads to an increase in net sea ice production because the heat supply from the deep ocean no longer limits sea ice production (Marsland and Wolff, 2001). Secondly, a freshening of the ocean surface also contributes to create shallower mixed layers, thus decreasing the effective heat capacity of ocean surface layers. Ocean surface layers are then more sensitive to air-sea heat fluxes. Under a positive air-sea downward heat flux (e.g. during the melting season), the ocean surface receives more heat, thereby accelerating sea ice melt. Increased sea ice production with icebergs over most of the Southern Ocean is consistent with the mechanism involving the reduction of convective overturning in winter described by Marsland and Wolff (2001). For instance, iceberg freshwater release significantly reduces convective overturning in the Weddell Sea, delaying the seasonal opening of Maud Rise Polynia and increasing annual mean sea ice cover in this region. In addition, the model indicates that summer mixed layers (not shown) are shallower with icebergs, consistently with a reduction in the effective heat capacity of ocean surface layers. One could expect that the reduction in heat capacity in ICBT simulation would drive a surface warming during summer as compared to CTR simulation. On the contrary, model SST in the seasonal ice zone are usually considerably colder (0.5-1°C) with icebergs (see Figure 2.14). This is probably related to the difference in winter sea ice concentration and thickness between ICBT and CTR, Changes in winter sea ice concentration and thickness may cool the SST by two mechanisms: Firstly, the extra insulation exerted by the thicker or more concentrated sea ice layer may reduce the net heat flux received by the ocean surface layer in spring and summer. Secondly, larger latent heat fluxes are required to melt the extra sea ice volume of the ICBT simulation. Both mechanisms seem to notably compensate the effect of changes in heat capacity.

As noted above, modelled iceberg melt is relatively limited in the Bellingshausen Sea west of the Antarctic Peninsula, but the response of the modelled sea ice to this extra freshwater is significant and somewhat unexpected. In contrast with most of the Southern Ocean, sea ice tends to be thinner with icebergs in this region while sea ice concentration is essentially unchanged (see Figure 2.11). In addition, SSTs are found to be significantly warmer in summer upstream of the Bellingshausen Sea along the Antarctic Peninsula (see Figure 2.14). This suggests that the equilibrium state reached after spin-up in the Bellingshausen Sea may be affected by changes in heat transport by the Antarctic Coastal Current. In the model, the lateral supply of warmer water may affect the formation of sea ice in the Bellingshausen Sea so that the ocean/sea ice system eventually reaches an equilibrium state with thinner sea ice over the entire annual cycle. What drives the warming of surface layers upstream is not clear yet, but this warming could be associated with changes in effective heat capacity of ocean surface layers in coastal regions along the Antarctic Peninsula. Other processes in the model, as for instance changes in the convective supply of heat to the surface could also contribute to the unexpected response of

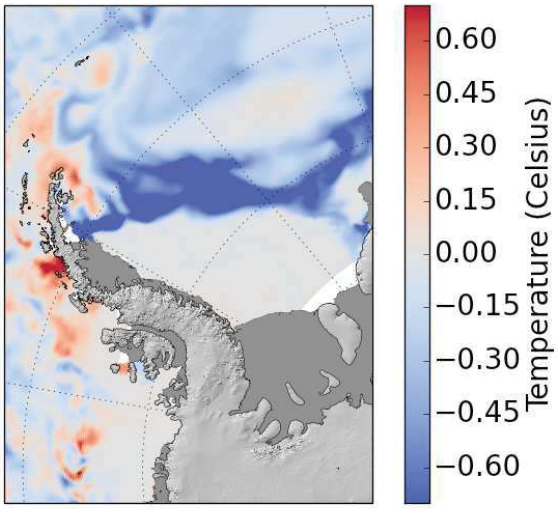


Figure 2.14: Mean sea surface temperature difference between ICBT (simulation with explicit icebergs) and CTR (simulation without icebergs fluxes) simulations averaged over January, February and March of the first five years of the simulation after spin-up. This plot shows the cold temperature anomaly in the seasonal ice zone in the Weddell and the warm temperature anomaly west of the Antarctic Peninsula.

simulated sea ice properties in the Bellingshausen Sea. But further analysis would be needed to disentangle the mechanisms involved. In conclusion, the response in terms of modelled sea ice volume in the Bellingshausen Sea illustrates how icebergs can affect ocean surface properties through a range of physical processes. Indeed, the Bellingshausen sector presents the only discrepancies between ICBT and CLIM simulations (see Figure 2.13). The forced simulation (CLIM) produces even thinner sea ice than ICBT and CTR. The three simulations notably differ in their sea ice thickness solution in the Bellingshausen sector. However, the icebergs fluxes in the sector seems to be weaker than what the observations suggests (see Figure 2.8), and the discussed mechanism producing sea ice thinning should not be considered as a realistic climate feature in the sector. Instead, the Bellingshausen Sea in the model is an example which illustrates how, under specific conditions, the way icebergs fluxes are represented in the ocean models may be crucial to model sea ice.

## 6 Conclusions

In this paper, we have studied the climatological distribution of iceberg melt over the Southern Ocean and its impact on Antarctic sea ice and ocean surface properties. To do this, we have used a Lagrangian iceberg model (Marsh et al., 2015b) coupled with a global, eddy-permitting ocean sea ice model configuration (NEMO-ORCA025). The Lagrangian iceberg model has been modified in order to explicitly take into

account the influence of ocean current and temperature vertical profiles. Ocean currents integrated along the iceberg vertical profile are shown to notably impact the trajectories of icebergs crossing the subpolar gyres in the Ross, Amery and Weddell Seas. The model is forced with recent estimates of calving rates and melt rates for the Antarctica Ice Sheet (Depoorter et al., 2013).

The distribution of Antarctic icebergs in the model is shown to be broadly consistent with satellite observations of small icebergs from radar altimetry. We have presented the first comparison of the probability of iceberg detection obtained from radar altimetry with that from an iceberg model. This comparison makes it possible to identify limitations of current Lagrangian iceberg models

For instance, modelled icebergs seem to be too confined in the Antarctic Counter Current, which impacts the equatorward transport of icebergs through the Ross and Amery subpolar gyres. In addition, modelled iceberg trajectories seem too short in the model, especially in the Pacific sector where observations suggest that iceberg are transported further east. Improving the representation of icebergs/sea ice interaction may also improve simulation results, either by producing more export of icebergs out of the Antarctic Counter Current following the drift of the sea ice pack, or by fastening iceberg close to coast within fast sea ice. Additionally, a higher ocean model resolution and the representation of the synoptic component of the wind forcing could help icebergs escaping the Antarctic Counter Current. Finally, accounting for small icebergs associated with the fracturing of large tabular, could result in trajectories extending further east and might lead to a better agreement between the model and the altimetry observations. This could be reproduced in the model by adding offshore calving sources in the model according to a probabilistic estimation of the tabular iceberg fracturing.

Iceberg melt over the Southern Ocean is found to show a significant seasonality and to be mostly concentrated in offshore flowing branches of Antarctic subpolar gyres. A large fraction of the total iceberg melt is found to occur in the South Atlantic sector of the Southern Ocean. The freshwater release is found to be strongly seasonal in the Ross Sea and the Amundsen Sea where almost half of the freshwater release occurs in January and February. The monthly climatology of iceberg melt over the Southern Ocean is provided as Supplementary Material.

Iceberg melt is shown to substantially increase sea ice concentration and thickness over most of the Southern Ocean, except in the Bellingshausen Sea where iceberg melt decreases sea ice thickness in the model. As suggested by previous studies, in most of the Southern Ocean, iceberg melt increases sea ice production in autumn and winter because it reduces convective overturning, thus limiting the heat supply from the deep ocean to the surface. In contrast, iceberg melt results in thinner sea ice in the Bellingshausen Sea, probably because of the advection of warmer waters flowing along the Antarctic Coastal Current.

The extra computational cost of running an explicit iceberg model can be drastically reduced by forcing the ocean model with a monthly climatology of iceberg melt. Figure 2.13 shows that this inexpensive simulation strategy succeeds in capturing the essential aspects of the response of sea ice to freshwater release in a climatolog-

ical forced ocean simulation. Whether this result still holds with an inter-annually varying atmospheric forcing needs to be further investigated. Such a forcing strategy could arguably be adopted for forced ocean simulations and possibly adapted to climate models. For climate simulations, latent heat exchanges due to iceberg melt would need to be recalculated from the freshwater fluxes in order for the model to conserve energy.

## Appendix: Modified equations of the NEMO-ICB Lagrangian iceberg model

Interested reader may refer to Martin and Adcroft (2010) for a thorough description of the dynamics and thermodynamics of the iceberg model. We only describe here our modifications and the corresponding changes in the original model equations.

The parametrized dynamics of the iceberg model from Martin and Adcroft (2010) which are based on Bigg et al. (1997), depend on the sea surface velocity. In this work we consider the following depth-integrated ocean velocity:

$$\vec{v_m} = \frac{\int_{-min(H_{bat},H_{icb})}^{0} \vec{v_o}(h)dh}{H_{icb}} \tag{2.1}$$

where $H_{bat}$ is the bathymetry depth at the grid point, $H_{icb}$ is the submerged part of the iceberg thickness, $dh$ is the differential of depth, $\vec{v_o}(h)$ is the ocean velocity depending on the depth and $\vec{v_m}(h)$ is the resulting depth-integrated ocean velocity.

Our version of NEMO-ICB model uses the equations A.2a A.2b and A.2c from Martin and Adcroft (2010) applying $\vec{v_m}(h)$ instead of the sea surface velocity.

We also modify the equations of the parametrization of basal turbulence and buoyant convection melt rates (see equations A.7 and A.9 from Martin and Adcroft (2010)) as follows:

$$M_b = 0.58|\vec{v} - \vec{v_b}|^{0.8}\frac{\tilde{T_b} - \tilde{T}}{L^{0.2}} \tag{2.2}$$

with $\vec{v_b} = \vec{v_{bat}}$ and $\tilde{T_b} = \tilde{T_{bat}}$ whenever $H_{icb} > H_{bat}$, where $\vec{v}$ is the iceberg velocity, $\vec{v_b}$ is the velocity of the ocean at the base of the iceberg, $\vec{v_{bat}}$ is the bottom ocean velocity (i.e. at sea floor depth), $\tilde{T_b}$ is the ocean temperature at the base of the iceberg, $\tilde{T_{bat}}$ is the bottom ocean temperature, $L$ is the iceberg horizontal length, and $M_b$ is the resulting basal turbulence melt rate.

Finally, the buoyant convection melt rate is integrated over the depth of the iceberg as follows:

$$M_v = \int_{-H_{icb}}^{0} (7.62 \times 10^{-3}\tilde{T_o}(h) + 1.29 \times 10^{-3}\tilde{T_o^2}(h))dh \tag{2.3}$$

with $\tilde{T_o}(h) = \tilde{T_{bat}}$ whenever $h > H_{bat}$, where $\tilde{T_o}(h)$ is the ocean temperature at depth $h$ and $M_v$ is the resulting buoyant convection melt rate.

## Acknowledgments

We would like to thank Jean Marc Molines for his invaluable help with model configuration. Numerical simulations were performed on IDRIS supercomputers (Saclay, France). The study was partially funded by the French National Research Agency (ANR) under the SUMER (Blanc SIMI 6) 2012 project, referenced as ANR-12-BS06-0018. NCJ is an Associate Investigator with the ARCCSS (ARC Centre of Excellence for Climate System Science). Finally, we would like to thank the three anonymous reviewers and the editor Stephen Griffies for their helpful and constructive contribution to this work.

## Supplementary Files

Supplementary file Iceberg-Source-Points-Merino.xls: Distribution of iceberg source points along the model coastline. The table provides the longitude, latitude and calving rate (in Gt/year) corresponding to each iceberg source point of the iceberg model. Calving rates for each ice-shelf and oceanic sector are extracted from Depoorter et al. (2013) and distributed along the corresponding ice-shelf and sector coastline on NEMO ORCA025 grid. This table can be founded in the Appendix B

Supplementary file Iceberg-Climatology-Merino.nc: Monthly climatology of iceberg meltwater flux. Monthly means are computed using the last 11 years of ICBT (simulation without icebergs fluxes) after the spin-up period. The NetCDF file contains the longitude, the latitude and the freshwater flux for each grid cell and month.

Chapter 3

# Impact of glacial freshwater flux changes on Antarctic sea ice

Contents



## 1 Introduction

One of the lines of development of the next generation of Global Climate Models (GCMs) is the inclusion of ice sheet models interacting with the ocean component (Stocker et al., 2013; Prinn, 2013; Jones and Sellar, 2016). This inclusion aims at better representing in the ocean model the freshwater and heat fluxes from the changing ice sheets and the subsequent sea level rise. So far, most Earth-System-Model do not include ice sheet dynamics. As a consequence, they can not account for the glacier acceleration and the related increase in the ice discharged to the ocean. This has been suggested to partially explain why GCMs fails in reproducing the observed trends in sea ice extent in Antarctica (Shu et al., 2015). It is not clear yet if the lack of representation of the observed ice discharge acceleration from Antarctic Ice Sheet could contribute to the observed trends in sea ice or not. First, we do not know how the ocean model components of the GCMs would response to realistic perturbation in the glacial freshwater fluxes from Antarctica. Second, we do not know how those perturbations of the Antarctic glacial freshwater fluxes have contributed to the observed trends in the Antarctic sea ice. Recent works have studied these questions with contrasting conclusions (Bintanja et al., 2013; Swart and Fyfe, 2013; Pauling et al., 2016). None of these studies were able to reproduce the magnitude and the spatial pattern of the observed trends in sea ice in response to glacial freshwater perturbations. However, the ocean model simulations were forced with a very simplistic description of the spatial and seasonal distribution of the glacial freshwater fluxes.

This chapter aims at responding to both questions, the ability of a global ocean model in responding to perturbations in the glacial freshwater forcing, and the

response of the Antarctic sea ice to a realistic decadal-scale perturbation of the glacial freshwater forcing. To do so, a set of experiments using an atmospheric-forced global eddy-permitting ocean model have been designed and performed in order to study the model sensitivity to glacial freshwater forcing perturbations corresponding to recent decades. In contrast to previous studies (Bintanja et al., 2013; Swart and Fyfe, 2013; Pauling et al., 2016), state-of-the-art of glaciological estimates and iceberg modeling have been used in order to produce a realistic spatial and seasonal distribution of the Antarctic freshwater fluxes as described in Chapter 2 of this thesis. A second freshwater fluxes scenario has been designed constrained by other glaciological estimates accounting for the decadal-long Antarctic regional mass changes in order to produce a realistic decadal perturbation of the freshwater fluxes. Additionally, the ocean model is forced for 30 years with inter-annual atmospheric forcing DFS 5.2 beginning in both 1969 and 1979 in order to compare the response of sea ice to freshwater fluxes perturbation with the response to a decadal-scale perturbation in the atmospheric conditions. The comparison between the experiments are described and analyzed here in order to investigate the impact of the current Antarctic Ice Sheet imbalance on the current sea ice variability and give insights on the importance of including Antarctic ice sheet dynamics in the future development of climate models.

# 2 Studying the impact of recent Antarctic Ice Sheet mass discharge acceleration on the Antarctic sea ice

The method and results of this study have been submitted to Ocean Modeling and is entitled *Impact of increasing Antarctic glacial freshwater release on regional sea-ice cover in the Southern Ocean.*

## 2.1 Impact of increasing Antarctic glacial freshwater release on regional sea-ice cover in the Southern Ocean

# Impact of increasing Antarctic glacial freshwater release on regional sea-ice cover in the Southern Ocean

Nacho Merino[a,b,*], Julien Le Sommer[a,b], Gael Durand[a,b], Nicolas C. Jourdain[a,b], Hugues Goose[c], Gurvan Madec[d,e], Pierre Mathiot[f]

[a] *CNRS, LGGE, F-38041 Grenoble, France*
[b] *Univ. Grenoble Alpes, LGGE, F-38041 Grenoble, France*
[c] *Universite Catholique de Louvain, Louvain-la-Neuve, Belgium*
[d] *LOCEAN, CNRS/MNHN/IRD/UPMC, Paris, France*
[e] *NOC, Southampton, UK*
[f] *Met Office, Exeter, UK*

## Abstract

The sensitivity of Antarctic sea-ice to increasing glacial freshwater release into the Southern Ocean is studied in a series of 30-year ocean/sea-ice/iceberg model simulations. Glaciological estimates of ice-shelf melting and iceberg calving are used to better constrain the spatial distribution and magnitude of freshwater forcing around the Southern Ocean. Two scenarios of glacial freshwater forcing have been designed to account for a decadal perturbation in glacial freshwater release to the Southern Ocean. For the first time, this perturbation explicitly takes into consideration changes in the volume of Antarctic ice shelves, which is found to be a key component of changes in freshwater release. In addition, glacial freshwater-induced changes in sea ice are compared to changes induced by the decadal evolution of atmospheric states. Our results show that, in general, the increase in glacial freshwater release increases Antarctic sea ice extent, but the opposite sensitivity is found in some regions. We also note that changes in freshwater forcing may induce large changes in sea-ice thickness, explaining about one half of the total change due to the combination of atmospheric and freshwater changes. Our results are a strong incentive for improving the representation of freshwater sources and their evolution in climate models.

## 1 Introduction

The Southern Ocean plays a substantial role in the Earth system. For instance, it is a significant sink for the anthropogenic origin carbon dioxide emissions (Sallée et al., 2012) and atmospheric heat (Roemmich et al., 2015), thus mitigating global warming. In addition, Southern Ocean produces the Antarctic Bottom Water (AABW), which is distributed into the three main oceanic basins (Atlantic, Pacific and Indian). The AABW, a key driver of the world's conveyor belt of ocean currents, affects the ventilation of the deep ocean due to its high oxygen content (Mantyla and Reid, 1983; Orsi et al., 1999). All these processes are directly impacted by the

Antarctic sea-ice cover, its melting and its production.

Some studies have confirmed the unexpected response of the Antarctic sea ice cover in ongoing climate trends, ( e.g. Comiso (2010)). While the Arctic sea ice extent (SIE) presents a statistically significant decrease of 3.8% per decade, the Antarctic SIE presents a small but statistically significant increase of 1.2% per decade (Comiso et al., 2011). The global increase results from the combination of positive and negative regional trends. Even if the magnitude and the significance of the global increase remains open to debate (Polvani and Smith, 2013a; Screen, 2011), the regional trend in sea ice concentration (SIC) has a larger consensus in the community (Comiso et al., 2011). For instance, Ross Sea SIE has increased by about a 5% per decade, while the Amundsen-Bellingshausen Seas sector shows a decrease in SIE of up to 7% per decade (Turner et al., 2009a). In addition, the trend in the number of annual ice covered days exhibits similar regional patterns: the Southern Ocean has gained up to 3 days per year of coverage in some locations of the Ross Sea, and has lost up to 3 days per year in sectors of the Bellingshausen Sea (Stammerjohn et al., 2008a).

While the Artic SIE response to the climate change is strongly coupled with global atmospheric warming (Perovich, 2011), Antarctic sea ice trends seem to result from much more complex processes. It has been suggested that observed atmospheric trends in the Southern Annual Mode (SAM) index (Thompson et al., 2011) and the Amundsen Low, which affect wind velocities, air temperature and humidity, may partially explain the observed changes in the Antarctic sea-ice (Turner et al., 2009a). Additionally, the coupling between SAM and the El Nino Southern Oscillation (ENSO) may also contribute to the observed regional pattern of the trend (Stammerjohn et al., 2008b). However, the amplitude of the regional trends and the global increase in SIE does not seem to be completely explained by all the changes of atmospheric origin (Lefebvre and Goosse, 2008). Some of the extra-atmospheric drivers of the observed sea-ice pattern may be related to oceanic and sea-ice feedbacks. For instance, changes in the salt rejection associated to sea ice changes and the freshening of the ocean surface may be affecting oceanic deep heat convection in some regions (Goosse and Zunz, 2014a; Zhang, 2007).

The observed increase in mass loss from the Antarctic ice sheet (Rignot et al., 2011; Shepherd et al., 2012), may be contributing to salinity changes in the Southern Ocean (Jacobs et al., 2002). Enhanced ice discharge combined with the observed thinning of ice shelves (Pritchard et al., 2012b; Paolo et al., 2015) has increased glacial freshwater injection into the ocean surface layer, at least since the beginning of the 1990s (Shepherd et al., 2012). However, the increase in glacial freshwater is not usually considered in climate models. This might be one of the reason explaining why climate models have so far failed to predict trends and regional variability in SIE. Recent studies have investigated the response of Antarctic sea ice to the recent increase in glacial freshwater input to the ocean with a coupled model (Bintanja et al., 2013; Swart and Fyfe, 2013; Pauling et al., 2016). However, they differ in their main conclusions. In some cases, the impact of perturbations in the glacial freshwater forcing on sea ice is very weak and not significant. In other cases, the

response is relevant but does not match spatially the observations. This may be due to the lack of consensus over the quantity and spatial distribution of the freshwater perturbation to be applied in such experiments. Indeed, most ocean models present large differences in their freshwater forcing protocol and neglect the spatial distribution of the sources. Recent ice-shelves mass balance estimates (Rignot et al., 2013; Depoorter et al., 2013) may help better constrain both the magnitude and the spatial distribution of glacial freshwater released into the Southern Ocean. Furthermore, recent improvements in Lagrangian particle iceberg models (Merino et al., 2016; Marsh et al., 2015b) may improve predictions of the distribution and melting of the iceberg mass around the Southern Ocean. This has been shown to affect sea ice production (Merino et al., 2016) but, as yet, it remains neglected by most ocean models.

In our study, three numerical experiments are conducted to evaluate the impact of the recent enhancement in glacial freshwater inputs on sea ice in the Southern Ocean. Two different freshwater scenarios have been proposed, based on glaciological estimates of Antarctic ice mass loss, to represent the current and pre-imbalanced Antarctic-ocean mass exchange. Both glacial freshwater scenarios are applied to an atmospheric forced eddy-permitting ocean-sea-ice model. An improved version of a Lagrangian particle iceberg model is coupled with our ocean model in order to distribute the calved mass. The two glacial freshwater scenarios are tested with the same atmospheric conditions, corresponding to the last two decades (1990-2009). The atmospheric forcing is additionally shifted back in time for the pre-imbalanced glacial freshwater scenario in order to compare our results with the impact of recent atmospheric changes on sea ice. This results in a set of three sensitivity experiments. The three model solutions are compared in order to identify the role of the recent increases in Antarctic mass loss in relation to recent sea-ice trends and ocean properties

## 2 Material and methods

### 2.1 Ocean/sea-ice model configuration

All the numerical experiments performed in this study share the same general model set up. Simulations use a coupled ocean/sea-ice/iceberg model with inter-annual atmospheric forcing. The ocean component is based on NEMO v 3.5 (Madec, 2014) with a global grid of 0.25 degrees resolution (ORCA025) developed by the DRAKKAR group. It considers 75 vertical z-levels with partial steps. A salinity restoring term towards NODC WOA94 data with a piston velocity of 50 m/300 days is applied annually to the ocean surface (Griffies et al., 2009). The ocean component is coupled every timestep with the LIM2 sea-ice model (Fichefet and Morales Maqueda, 1997) and the NEMO-ICB iceberg module (Marsh et al., 2015b) containing the most recent improvements described in Merino et al. (2016). These latter modifications consider the depth-integrated ocean velocities and depth-integrated ocean temperature instead of the ocean-surface-based physics as is commonly prac-

ticed in iceberg modeling.

The ocean/sea-ice/iceberg model is forced by the atmosphere and by rivers and glacial freshwater run-off. The atmospheric forcing corresponds to the inter-annual DFS5.2 (ERA-Interim based). The ocean model uses the CORE bulk formulations with a three-hour frequency for winds, humidity and air temperature, and daily means for the cloud cover, short- and long-wave solar radiation and liquid and solid precipitations. For the Antarctic continent, the model grid does not include ice-shelf cavities explicitly, but adopts a parameterisation for the ice-shelf basal melt runoff similar to the described in Merino et al. (2016).. It emulates the ice-shelf overturning by distributing the coastal runoff along the vertical levels between the ice-shelf front depth and the minimum between the bathymetry and the grounding line depth.

## 2.2 Freshwater forcing in the Southern Ocean

### 2.2.1 The ice shelf mass balance equation

The Ice-shelf is the name of the floating extension of outlet glaciers confined in an embayment. They form 75% of the Antarctic coastline. A schematic Antarctic ice shelf is shown in Figure 3.1, which describes the associated mass fluxes, ocean currents, and the terms and recurrent concepts that are used throughout this text. Ice shelves receive almost all of the ice outflow from the upstream grounded ice sheet since the surface melting of snow out of the glaciers is confined to regions in the northern Antarctic Peninsula (Barrand et al., 2013; van den Broeke, 2005) and commonly neglected.

The Antarctic ice-shelf mass can be affected by various processes. Mass gain is mainly associated with an ice mass inflow through the grounding line gate (imaginary surface between the floating ice and grounded ice of an outlet glacier) and precipitation in the form of snow on the ice shelf surface. However, Antarctic ice shelves can basically loose mass through different processes: calving at the ice shelf front, basal melting beneath the ice shelves at the ocean-ice interface, and wind erosion or sublimation at the ice shelves surface. In general, there may also be ice melt at the glacier surface, but this term is neglected in the case of the Antarctic ice shelves because surface melted water commonly refreezes before reaching the ocean (Irvine-Fynn et al., 2011) and it is not significant compared to the other processes contributing to mass loss.

The glacial freshwater input from the Antarctic ice sheet to the Southern Ocean is mainly determined by the mass budget of the ice shelves. This imput may be due to a flux of icebergs, the Calving Flux (CF), or to the injection of basal melt water, the Basal Mass Balance (BMB). In the ice-shelf mass balance equation these two terms (the loss of ice shelf mass) offset the input of ice mass due to the Surface Mass Balance (SMB) (this considers snow accumulation and melt, sublimation, wind erosion, and transport at the surface) and the GLF). The difference between the inputs (GLF, SMB) and outputs (CF, BMB) results in the mean thickening

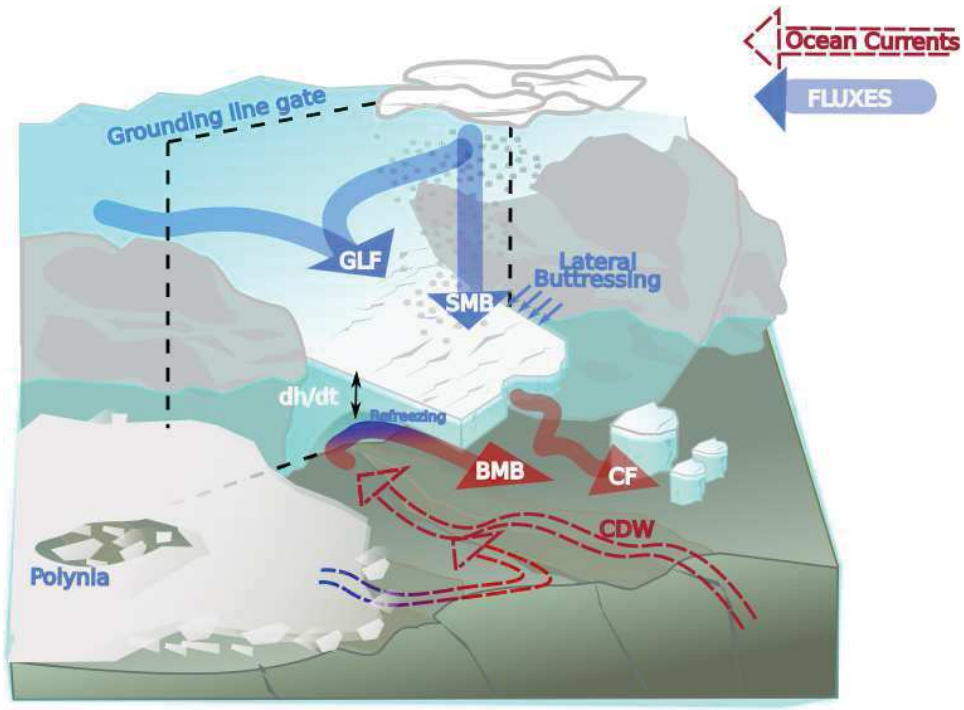


Figure 3.1: Schematic diagram of idealized Antarctic ice shelf, showing major fluxes and currents: Grounding Line Flux (GLF), Surface Mass Balance (SMB), Calving Flux (CF), Basal Mass Balance (BMB), Circumpolar Deep Waters (CDW)

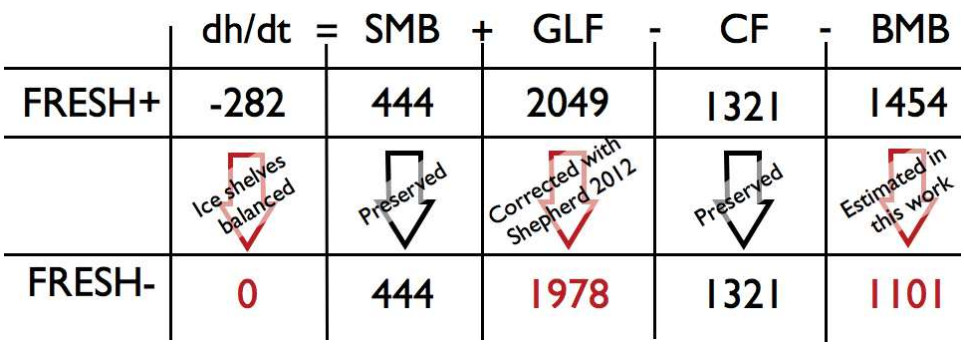


Figure 3.2: *FRESH+* and *FRESH-* full Antarctica integrated terms of the ice-shelf mass balance equation 1. Red numbers correspond to the terms having been modified in the *FRESH-* scenario with respect to the *FRESH-* scenario. Black numbers correspond to quantities that remain the same in both scenarios.

rate (dh/dt), or ice shelf mass convergence. This may be described by the following equation (Rignot et al., 2013; Depoorter et al., 2013).

$$dh/dt = SMB + GLF - CF - BMB \tag{3.1}$$

In the following paragraphs, we describe the two different glacial freshwater scenarios to be applied in the ocean model. Basically, this consists of determining a pair of CF and BMB values for: (i) a scenario corresponding to the current mass exchange between the Antarctic ice shelves and the ocean (*FRESH+*) and (ii) a scenario representative of the situation at the end of the 80s/beginning of the 90s (*FRESH-*). This latter scenario, built from FRESH+, is based on assumptions on the various terms of the ice shelf mass (equation 3.1) and computed for each ice shelf larger than 100km2. Details of the construction of both scenarios, *FRESH+* and *FRESH-* are given in sections 2 and 2 respectively. A summary of the two glacial freshwater scenarios with the full Antarctica integrated terms of equation 3.1 is presented in Figure 3.2. For each ice shelf, a detailed comparison of the BMBs corresponding to each glacial freshwater scenario is shown in Figure 3.3.

### 2.2.2 Scenario Fresh +

The aim of the scenario *FRESH+* is to represent the Antarctica-Southern Ocean freshwater exchanges of the decade 2000-2010. With this aim in mind, we consider the CF and the BMB fluxes directly from Depoorter et al. (2013). in which estimates were computed using data from the ICESat period (2003-2009) and previous satellite capaigns (ERS-1 and ERS-2 and others), covering almost entirely the decade 1990-2000 in many regions. In addition, the scenario takes into consideration ice ice-shelf thinning rates consistent with the observed enhancement of Antarctic mass discharge. All the data collected have been corrected so as to be representative of the decade 2000-2010. This means that the estimates of Depoorter et al. (2013) provide a reasonable representation of the annual glacial freshwater fluxes that were

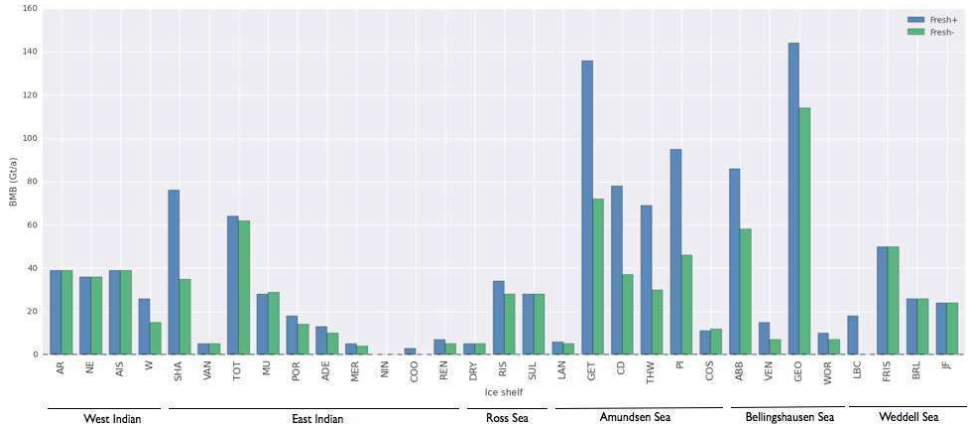


Figure 3.3: Basal Mass Balance (BMB) in Gigatonnes per year considered in the *FRESH+* (blue bars) and *FRESH-* (green bars) glacial freshwater scenarios per ice shelf. Ice shelf names and the oceanic sectors are based on the definitions of Depoorter et al. (2013).

released into the Southern Ocean at that time, and are consistent with other recent estimates (Rignot et al., 2013).

All the ice shelves locations considered in Depoorter et al. (2013) have been identified in our ORCA025 model grid following Merino et al. (2016). For a given ice shelf, the BMB flux is homogeneously distributed over all grid points along the ice shelf front in question. In addition, Depoorter et al. (2013) provides an upscaling mass flux term per oceanic basin so that the total estimated Antarctic mass loss can be matched. This is homogeneously distributed between the coastal surface grid points of the corresponding oceanic basin. All the BMB fluxes are kept constant over time since, to our knowledge, there is no evidence of any significant melt-rate seasonality inside the ice shelf cavity. The CF estimates are plugged into our iceberg model. CF values are kept constant over time with the same calving rates and locations as provided in Merino et al. (2016).

### 2.2.3 Scenario Fresh -

*FRESH-* scenario is designed with a view to estimating the glacial freshwater input into the ocean before the observed Antarctic mass imbalance (end of the 80s, beginning of the 90s (Rignot et al., 2011; Shepherd et al., 2012)). Recent acceleration of grounded outlet glaciers is linked to the thinning of the ice shelves as a consequence of the enhancement of their basal melting (Pritchard et al., 2012b) or collapse (Scambos et al., 2004). The thinning of the ice shelves decreases their buttressing effect (Gagliardini et al., 2010) impacting the pressure exerted on the upstream grounded part of the outlet glaciers. This leads to glacier acceleration and, consequently, to an increase in the grounded Antarctic mass loss. Therefore, considering the annual contribution of Antarctica to SLR to be null in the late 1980s (and consequently grounded mass budget has to be considered in equilibrium) is

consistent with the assumption $dh/dt = 0$ in equation 3.1. It should to be noted that this assumption may not be entirely true at the regional scale, as it is known that some glaciers in the Amundsen sector were already retreating early in the 80s (Hughes, 1981). However the corresponding associated *FRESH-* scenario represents a reasonable global estimate of a lower boundary for the freshwater release into the ocean at that time.

In constructing the *FRESH-* scenario, we start from the estimates provided in Depoorter et al. (2013). In addition to setting dh/dt to zero, as described in the previous paragraph, further hypothesis regarding SMB, CF and GLF are needed to compute BMB according to equation 3.1. SMB in Depoorter et al. (2013) corresponds to the mean values of a regional atmospheric model simulation for the period 1979-2010. It is based on the assumption that there have been no significant SMB trend in the coastal ice shelves in Antarctica during recent decades (Monaghan et al., 2006; Lenaerts et al., 2012) We therefore keep the same SMB values as presented in Depoorter et al. (2013), as they are supposed to also be representative of our period of interest. We proceed similarly with the CF since, to our knowledge, there is no evidence of any trend in the calving fluxes. Of course, individual events of ice shelf collapses (Rott et al., 1996) may introduce large inter-annual variability in the CF, but they can roughly be linked to a significant trend in iceberg production (Liu et al., 2015) Indeed, to our knowledge, ice front position does not present any significant variation over the last two decades, which is consistent with our hypothesis that the CF are constant between both scenarios. GLF needs to be corrected to at least the beginning of the 90s. Estimations of Antarctic contributions to sea-level rise may be used to that end. The recent mass loss from drainage basins in West Antarctica have been strongly linked with changes in ice dynamics (Shepherd et al., 2012). Similarly, it has been suggested that other glaciers in the Antarctic Peninsula (like Larsen ice shelves), or in the East Indian sector of East Antarctica (Totten and Cook) have also undergone mass losses of dynamical origin (Shepherd et al., 2012). Ice dynamics changes imply perturbations in the ice mass fluxes at the grounding line gate. We correct the more recent grounding line fluxes provided in Depoorter et al. (2013) with the mass loss estimates proposed in Shepherd et al. (2012). These corrections are made for all the ice shelves corresponding to West Antarctica, the Antarctic Peninsula and the East Indian sector of East Antarctica. However, we maintain the same GLF for all the other glaciers, since mass changes have been attributed to regional trend in the inland SMB. The corrections applied here to the GLF corresponds to mass change estimates associated with the period 1992-2009, and are therefore consistent with our aims.

Our approach is new in the sense that previous studies analysing the impact of glacial freshwater perturbations on the Southern Ocean properties are simply based on sea-level rise estimates (Bintanja et al., 2013; Swart and Fyfe, 2013). This commonly used approach completely neglects ice shelf thinning or thickening, and the distinction between Antarctic basin mass changes of dynamical origin and those of SMB origin. The ice shelves are the Antarctic glacial freshwater exchangers with the ocean, and therefore the construction of glacial freshwater scenarios should

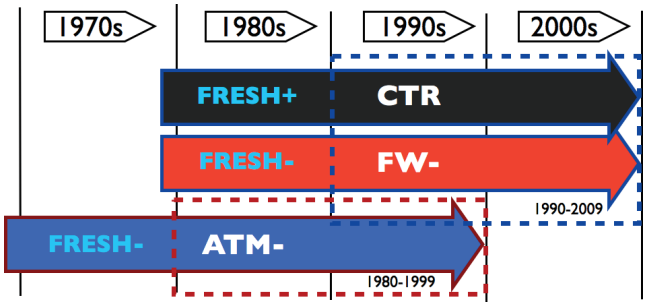


Figure 3.4: Schematic diagram showing the experiments conducted in this study. CTR considers the *FRESH+* glacial freshwater scenario and was run for a 31-year period starting in 1979. FW- uses the *FRESH-* scenario and covers the same time period as CTR. ATM- uses the *FRESH-* scenario and was run for a 31-year period starting in 1968.

always consider the ice shelves processes and mass balance equation 3.1.

## 2.3 Model experiments

Three model experiments were performed to study the sensitivity of the model to different forcing perturbations, as shown in Figure 3.4. The three runs use the same model set-up as described in section 2. They all consist of 31-year simulations with an 11-year spin up for the iceberg model in order to reach a stable iceberg meltwater distribution around the Southern Ocean (Merino et al., 2016). The comparison between experiments considers 20-year averages between the end of the iceberg spin up period and the last year of the simulation. Perturbations in forcing affect either the glacial freshwater scenario or the starting year of atmospheric forcing in the simulation in question.

The CTR run simulates the period 1979-2009 with the freshwater scenario *FRESH+* described in section 2. The FW- simulation considers the same period (1979-2009) as the CTR run, but with the freshwater scenario *FRESH-*. Finally, the ATM- run combines the application of the perturbed scenario *FRESH-* and an atmospheric forcing period starting and finishing 10 years earlier than for the other runs, thus covering the period 1969-1999. A schematic diagram of the three experiments is shown in 4. The comparison between CTR and FW- provides an estimate of the model response to our perturbation introduced in glacial freshwater forcing. This perturbation (scenario *FRESH+* versus *FRESH-* is considered in this study to be a reasonable estimate of the upper limit of the recent decadal change in the freshwater released by the Antarctic continent into the ocean. Accordingly, in the results and discussion sections, the CTR minus FW- comparison will be referred to as *freshwater-induced* changes due to perturbations in freshwater forcing. The FW- minus ATM- comparison provides an estimate of the impact of the recent decadal atmospheric trends considered by the ERA-Interim reanalysis. This comparison will hereafter be referred to *atmospheric-induced* changes due to perturbations in

atmospheric forcing. Finally, the CTR minus ATM- comparison accounts for both the perturbation in the glacial freshwater flux and for the time-lagged atmospheric forcing. It is suggested that this comparison indicates an upper limit of a reasonable estimate of a decadal change in the Southern Ocean. Hereafter, it will be referred to as *total* changes.

## 3 Evaluation of the experimental design

### 3.1 Sea-ice mean

Figure 3.5 compares model sea-ice results with observations. Model results correspond to the annual mean sea-ice concentration (SIC) over the last 20 years of simulation, averaged from the model solutions of CTR and ATM-. Observations are extracted from NSDIC monthly means for the period 1979-2010. Overall, the model set-up is able to reproduce the main spatial patterns and the order of magnitude of the observed SIC in both summer and winter. However, the model produces too much ice during the winter months, exhibiting a more concentrated ice pack at the sea ice margins. On the other hand, the model set-up melts too much ice during summer resulting in less concentrated sea ice in the West Pacific and the Amundsen sectors and a smaller sea-ice extent of the permanent sea-ice pack in the Weddell Sea.

### 3.2 Trend in the atmospheric forcing

Figure 3.6 shows the DFS5.2 mean anomalies between two different 20-year periods (1990-2010 minus 1980-2000) for air humidity, air temperature, and wind velocity. The anomalies represented in Figure 3.6 are an estimate of the mean atmospheric perturbations introduced between FW- and ATM- simulations. As shown in Figure 3.6, DFS5.2 proposes a dry mean decadal change with just two exceptions in the region between the Ross and Amundsen Seas, and in the western Weddell Sea. Air temperature tends to be warmer in the Amundsen and Bellingshaussen Seas, Amery, and the northern Weddell Sea, but it tends to be markedly colder ((by up to -1.5degC)) north of the Ross Sea and in the coastal Weddell Sea and West Pacific sector. Winds are stronger in the Atlantic and West Indian sectors and in some coastal regions of the Ross and Pacific sectors, and weaker from the Western coast of the Peninsula to the Amundsen Sea.

### 3.3 Sea ice trend

Figure 3.7-a and Figure 3.7-b show the sea-ice trends computed from experiments CTR and FW- respectively. As described in section 2, CTR and FW- consider the same period of analysis (1990 to 2010) with the only difference being in the glacial freshwater forcing. As expected, both simulations present a very similar trend in SIC as the atmospheric forcing applied is the same for both experiments. Overall, these results are consistent with the observations of the SIC trend during

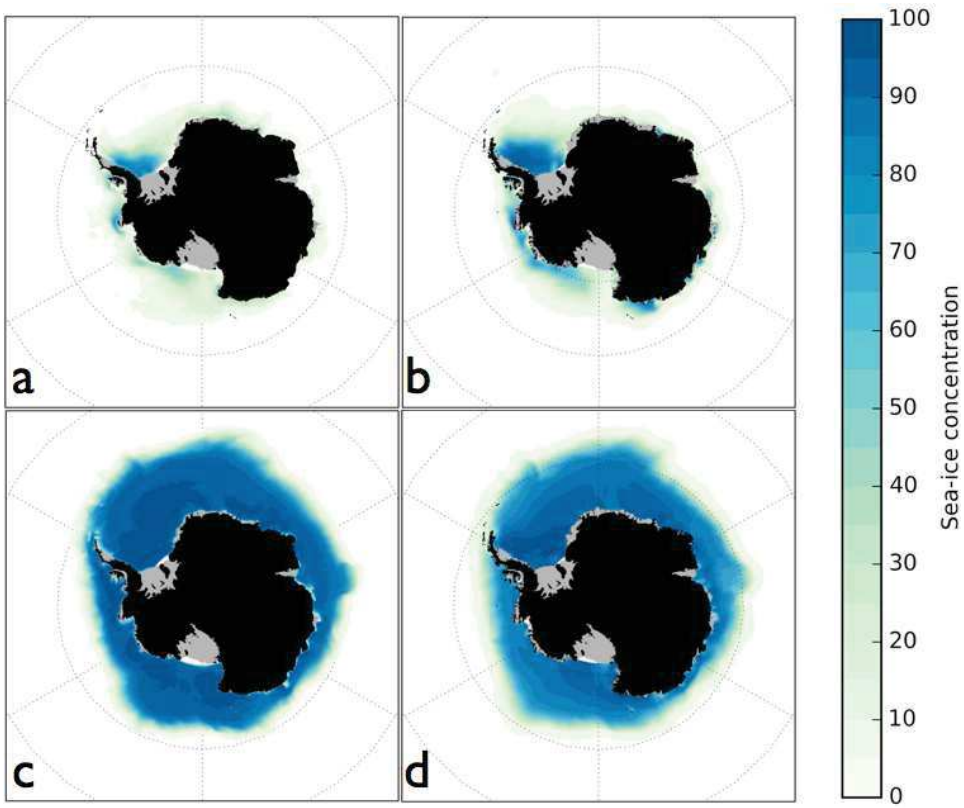


Figure 3.5: Sea-ice concentration (SIC) for: a) summer model results; b) summer observations; c) winter model results; d) winter observations. Summer months correspond to January, February and March. Winter months correspond to July, August and September. Model results are the annual means of SIC during the last 20 years of simulation averaged from the model solutions of CTR and ATM-experiments. Observations are extracted from NSDIC sea-ice concentration and averaged from the period 1979-2010.

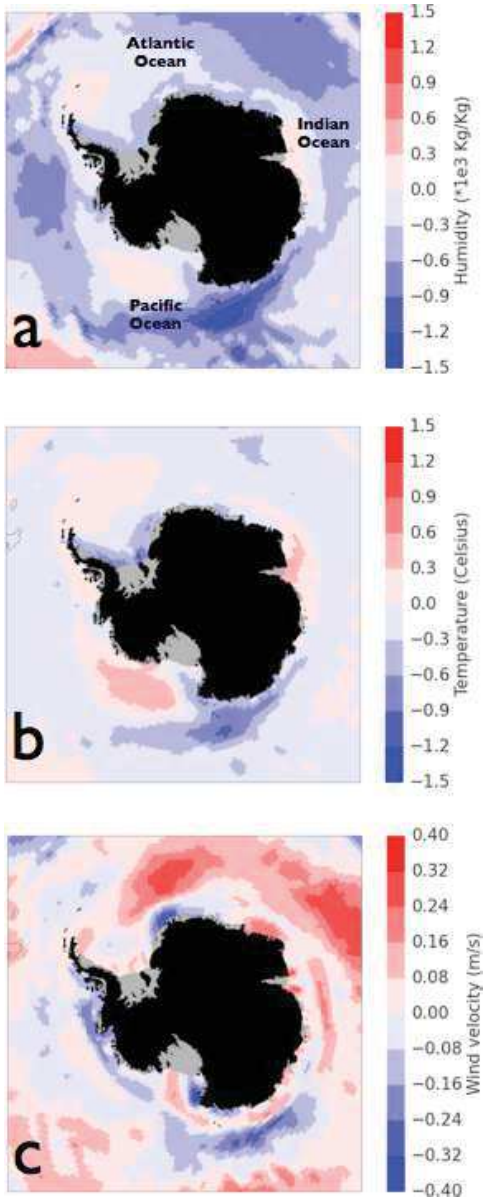


Figure 3.6: Atmospheric anomalies from DFS5.2 reanalysis for surface humidity (a), the surface temperature (b), and wind velocity (c). Anomalies consider 20-year averages for the period 1990-2010 minus 20-year averages for the period 1980-2000.

the same time period, as shown in Figure 3.7-c. Discrepancies between the modelled trend and the observations are mainly located in the coastal regions of the Amundsen, Bellingshausen and Ross Seas in the East Pacific sector. On the other hand, the trends in the Indian and Atlantic sectors are generally well reproduced by our simulations. As illustrated in Figure 3.3, the East Pacific sector (including the Bellinghausen and the Amundsen Seas) exhibits the largest change in glacial freshwater flux over the last two decades. However, as described in 2, glacial freshwater forcing has been kept constant over time in our experiments. The misrepresentation of the evolution of the freshwater fluxes in the East Pacific sector may be the reason for the discrepancies between the modelled trends and the observations in this sector in particular. Those discrepancies and their relation with the glacial freshwater trends are one of the motivations of the present study.

The choice of keeping glacial freshwater forcing constant during an experiment is based on the considerable uncertainties associated with the time series of freshwater flux variations. Thus, in this study we have analysed 20-year averaged solutions of a set of perturbed simulations to make our estimates. Figure 3.8-a shows a model estimate of the averaged *total* decadal SIC change for the period 1980-2010. As described in section 2, it is computed by comparing the model results of CTR and ATM- experiments. Our modelled estimate successfully reproduces the main spatial structure of the observed trend in the SIC for the same period of analysis (see Figure 3.8-b). According to this comparison, our experimental design is also able to reproduce the positive (respectively negative) SIC change in the Ross (respectively Amundsen-Bellingshausen) Sea sector, and the positive SIC change in the Atlantic sector. On the other hand, the observed negative SIC change in the Amery and in the Bellingshausen sectors is weaker in our model estimate. In addition, the model estimates a large positive SIC change north of the Amundsen-Bellingshausen Sea, which is not borne out by observations. However, the model results in the north of the Amundsen-Bellingshausen Sea are consistent with the averaged atmospheric trends in humidity, as shown in Figure 3.6. In order to make comparisons with observations, we define three regional sectors of analysis in the Ross, Amundsen, and West Pacific/East Indian sectors (see Figure 3.8-a). They are defined empirically and correspond to the sectors where the model set-up was better able to reproduce the observations in SIC and, as will be seen in the results section, the *freshwater-induced* changes are more significant.

## 4 Results: Role of the atmospheric and freshwater forcing perturbations in the model sea ice trend

### 4.1 Sea ice concentration and extent

Figure 3.8-c and Figure 3.8-d show respectively *freshwater-induced* and atmosphere-induced changes in SIC. Qualitatively, *total* modelled SIC trends are globally dominated by the signature of the atmospheric perturbations, especially in the Atlantic and West Indian sectors where freshwater perturbation barely impacts on the SIC.

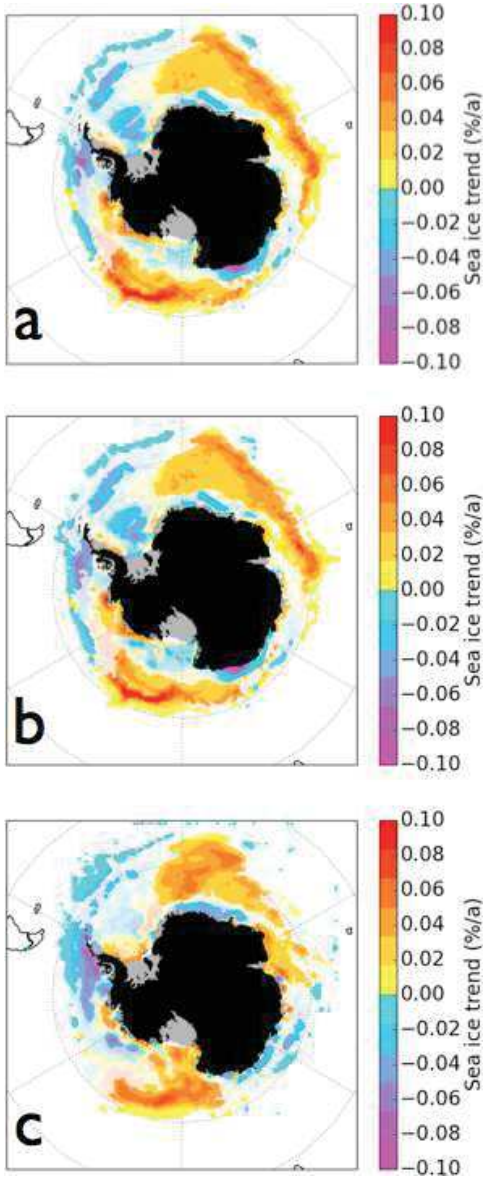


Figure 3.7: (a) Linear regression of the sea-ice concentration in the CTR experiment over 1990-2010, (b) linear regression of the sea-ice concentration in the FW-experiment over 1990-2010 (c) sea-ice concentration trend from NSDIC observations for the period 1990-2010. Colouring (bright to faint) indicates level of significance, with faint colours indicating non-significant trends (determined by two-sided test for $p<0.05$).

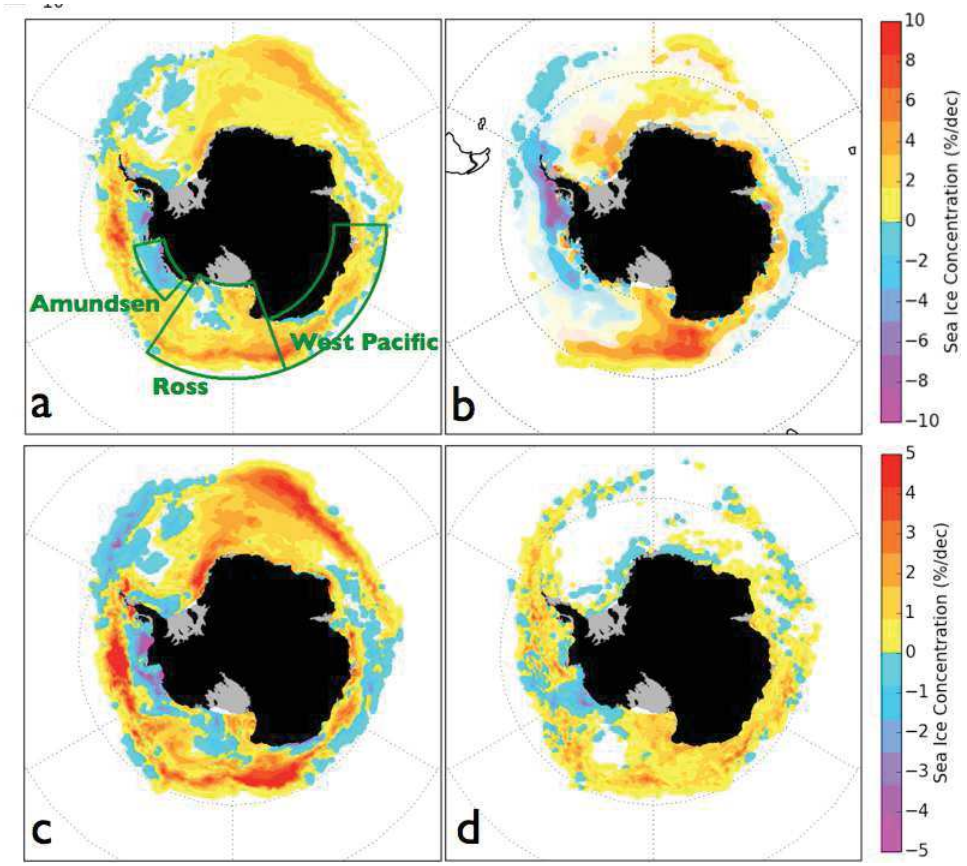


Figure 3.8: Sea-ice concentration changes in percentage per decade for: CTR minus ATM- model results (a), linear regression of observations for the period 1980-2009 (b), FW- minus ATM- model results (c), CTR minus FW- model results (d). Observations are extracted from NSDIC for the period 1980-2009. Colouring (bright to faint) indicates level of significance, with faint colours indicating non-significant points (determined by two-sided test for $p<0.05$). Model results consider annual means for the last 20 years of each simulation

However, there are other sectors where freshwater perturbation contributes to *total* changes, such as in the Ross, Amundsen Sea, and West Pacific sectors (see Figure 3.8-a for sector definitions) where the magnitude of *freshwater-induced* changes should not be neglected.

The quantitative comparison between CTR and ATM- indicates a *total* change in sea ice extent (SIE) of about 3.0%, which is larger than the 1.2% suggested by observations (Comiso, 2010). The *freshwater-induced* changes account for 0.75% of the *total* global SIE changes. This represents about 25% of the *total* modelled global change. In the Ross sector, the regional *freshwater-induced* changes in SIE account for about 1.4%, which represents 35% of the *total* change in the sector. In the Amundsen Sea, the model estimates a decrease of -2.7% in SIE. The freshwater perturbation contributes to 37% of the *total* SIE change in the sector. In the case of the West Pacific sector, *freshwater-induced* changes represent 52% of the *total* SIE change obtained in the sector

Figure 3.9-a shows the seasonality of *total* SIE changes, including the separate contributions of *atmosphere-induced* and *freshwater-induced* changes. Globally, *atmosphere-induced* changes mostly dominate the sea-ice cover changes during the sea-ice formation period (from March to May). The *freshwater-induced* changes are greater after winter, being dominant even during the last melting months (from December to February). *Freshwater-induced* changes dominate the global SIE changes in summer, compensating for the *atmosphere-induced* SIE decrease during late summer. This global pattern is more pronounced regionally in the Ross and West Pacific sectors. In the Amundsen sector, atmospheric perturbations control the SIE for most of the year.*Freshwater-induced* changes have a slight limiting effect on sea-ice formation during the early autumn, compensating for the *atmosphere-induced* increase in sea-ice formation. However, during the melting period, both the atmospheric and the glacial freshwater perturbations enhance sea-ice melt in the sector. Overall, *freshwater-induced* changes are increasingly important as summer advances

## 4.2 Sea ice thickness and volume

Figure 3.10 shows the response of sea-ice thickness (SIT) to perturbations in atmospheric and glacial freshwater forcing. *Freshwater-induced* changes are negligible in the Atlantic and West Indian sectors. However, SIT is srongly affected by the freshwater forcing perturbation in the rest of the ocean basins, as shown in Figure 3.10. Extra glacial freshwater considerably thickens sea ice in the Ross and West Pacific coastal sectors, and produces marked sea-ice thinning in the Amundsen Sea. The *total* annual global change (due to both *atmosphere-induced* and *freshwater-induced* changes) represents an increase in *total* integrated sea-ice volume (SIV) of 2.8%. 46% of this *total* global change is induced by the perturbation introduced in the glacial freshwater scenario. In the Ross sector, the integrated regional change in SIV is 3.6%, with up to 80% of this change being *freshwater-induced*. The West Pacific sector presents a *total* change in SIV of 10.0%, of which 61% is associated with the freshwater perturbation. In the Amundsen Sea, *total* change accounts for

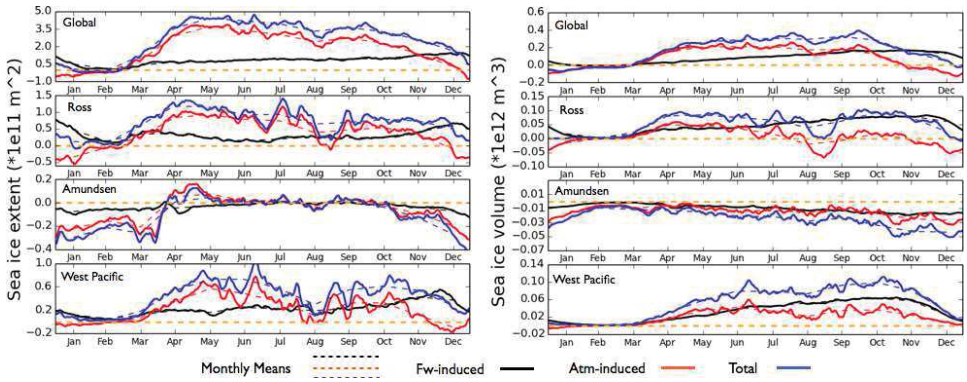


Figure 3.9: Time series of anomalies of sea-ice extent (left) and sea-ice volume (right), globally or regionally integrated over the Ross, Amundsen and West Pacific sectors. *Freshwater-induced* changes (black lines) consider/are obtained from CTR minus FW- model solutions. *Atmosphere-induced* changes (red lines) consider FW- minus ATM- model solutions. *Total* changes (blue lines) consider CTR minus ATM- model solutions. Dashed lines correspond to monthly averages. Orange dashed line provides the 0 reference line.

a decrease of -8.1% in SIV, the freshwater perturbation being responsible for about 40% of this.

Figure 3.9-b shows the seasonality of the changes in SIV induced by atmospheric and freshwater perturbations. Globally, *freshwater-induced* changes in SIV are not very significant during the late summer months (end of January, February, beginning of March). These changes become progressively larger from April to November. Regionally, in Amundsen, *freshwater-induced* changes contribute slightly to the sea-ice thinning induced by the atmospheric forcing perturbation over the late spring and summer months. Both the freshwater and atmospheric perturbations thicken the sea ice in the West Pacific sector throughout most of the year. In Ross, the *freshwater-induced* changes in SIV compensate for the thinning exerted by the atmospheric perturbations in summer (December and January). Overall, changes in freshwater forcing impact mainly on the SIV in regions other than the Atlantic and Indian sectors.

## 4.3 Sea ice cycle and ice season duration

As shown in section 4, the extra glacial freshwater added to the ocean globally increases the SIV and SIE. However, freshwater perturbation does not produce significant changes in the phase of the SIV cycle, but basically in its amplitude. As shown in Table 1 and Figure 3.9-b, the different glacial freshwater forcing applied in CTR with respect to ATM- and FW- simulations contributes to thicker sea-ice during the latter months of sea-ice formation, both globally and in the Ross and West Pacific sectors. This is not the case in the Amundsen sector, where *freshwater-induced* changes in SIV are negligible during the sea-ice formation months (see Figure 3.9).

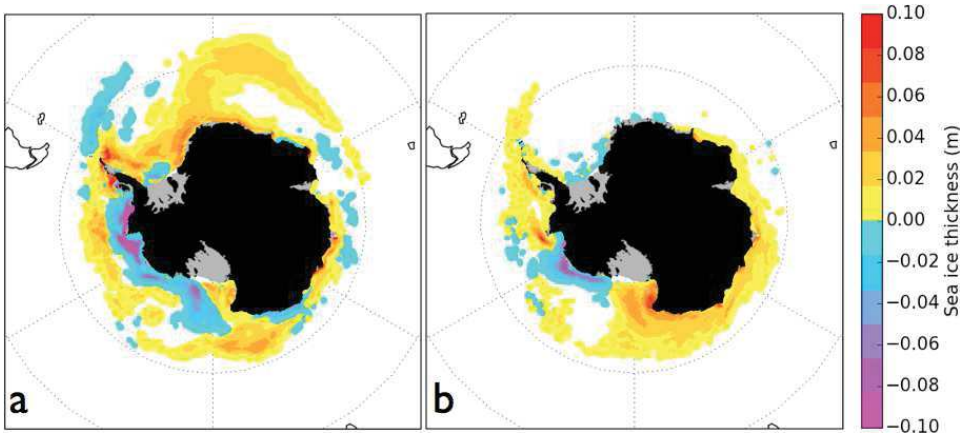


Figure 3.10: Sea-ice thickness changes (in meters) for: FW- minus ATM- model results (a), CTR minus FW- model results (d). Model results consider annual means for the last 20 years of simulations.

With the exception of the Amundsen sector, the FW- simulation presents its minima and its maxima at the same time of the year as the CTR simulation (just a negligible 1 day difference in the maximum of the global SIV cycle). Atmospheric forcing perturbations, however, mainly affect the sea-ice volume cycle, impacting both its amplitude and its phase. Despite the extra SIV produced in CTR, all the simulations, in general, present relatively small differences in the SIV minima, which implies that there is more sea-ice melting during the spring and early summer months

Even if, as a general rule, the perturbations in freshwater forcing do not produce significant changes in SIV seasonality, the *freshwater-induced* changes in SIV and SIE increase the Ice Season Duration (ISD) (as defined in Stammerjohn et al. (2008b)) in the Ross and West Pacific sectors, and decrease the ISD in the Amundsen sector. In the case of the Ross and West Pacific sectors, this is mostly related to the additional time needed to melt the extra SIV produced in winter. *Total* ISD changes for the combined atmosphere and *freshwater-induced* changes are illustrated in Figure 3.11. *Freshwater-induced* changes in ISD are relatively weak compared with the *total* modelled changes. Our model estimates of ISD (represented in Figure 3.11) are mainly produced by *atmosphere-induced* changes in the SIE and SIV. Overall, the spatial pattern is in good agreement with observations (Stammerjohn et al., 2008b), but the magnitude of the observed trend seems larger than that suggested by our model results. This may be related to the fact that our model experiments (ocean-forced simulations) does not account for coupling processes between the ocean surface and the atmosphere, which would arguably amplify the impact of *freshwater-induced* changes in sea-ice.

| Region | Run | Maximum | | Minimum | |
|---|---|---|---|---|---|
| | | Day | SIV ($\times 10^{11} m^3$) | Day | SIV ($\times 10^{11} m^3$) |
| Global | CTR | 264 | 147.5 | 49 | 2.97 |
| | FW- | 263 | 146.1 | 49 | 3.00 |
| | ATM- | 261 | 143.2 | 49 | 2.99 |
| Ross | CTR | 258 | 26.2 | 45 | 0.29 |
| | FW- | 258 | 25.9 | 44 | 0.26 |
| | ATM- | 243 | 25.8 | 44 | 0.26 |
| Amundsen | CTR | 216 | 5.55 | 53 | 0.16 |
| | FW- | 216 | 5.53 | 47 | 0.18 |
| | ATM- | 220 | 5.59 | 56 | 0.22 |
| West Pacific | CTR | 247 | 12.9 | 56 | 0.12 |
| | FW- | 247 | 12.7 | 56 | 0.12 |
| | ATM- | 237 | 12.4 | 59 | 0.12 |

Table 3.1: Regional and global averaged sea ice volume maxima and minima for the CTR, FW- and ATM- simulations, with the corresponding averaged day of the year when the maximum and minimum happen.

## 5 Discussion:Thermodynamics and dynamics freshwater-induced sea-ice changes

The freshening of the ocean surface may increase density differences between ocean surface and sub-surface water masses. This leads to a reinforcement of the density stratification on both sides of the pycnoclyne, affecting the convection regime and therefore the heat supply from the deeper and warmer ocean to the ocean surface. This process, suggested by Marsland and Wolff (2001), may affect thermodynamical sea-ice formation, resulting in more sea-ice with ocean surface freshening. The annual mean *freshwater-induced* change in the oceanic heat flux at the sea-ice base is shown in Figure 3.12-a, expressed as sea-ice volume equivalent. As expected, the freshening of the ocean surface in the model (see Figure 3.13-b) globally affects oceanic heat convection. As shown in Figure 3.12-b, the *freshwater-induced* changes in oceanic heat strongly affect the monthly thermodynamical sea-ice formation during the sea-ice production months (from March to September). The response of the sea-ice to freshwater perturbation in the Ross and West Pacific sectors seems to be largely consistent with the mechanism proposed in Marsland and Wolff (2001). However, other processes are at work in the reduction of sea-ice production in the Amundsen sector. The regional *freshwater-induced* changes in sea-ice for the Amundsen, Ross and West Pacific sectors are analysed separately in this section.

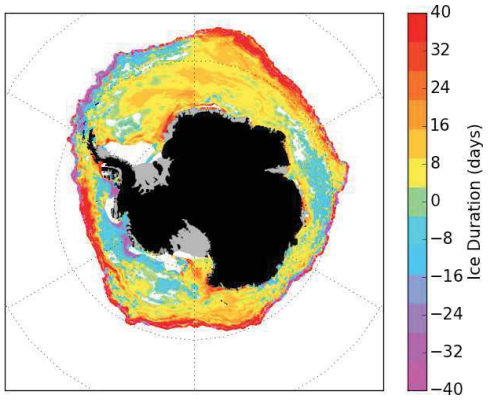


Figure 3.11: *Total* (CTR minus ATM-) modelled changes in Ice Season Duration as defined by Stammerjohn et al. (2012b).

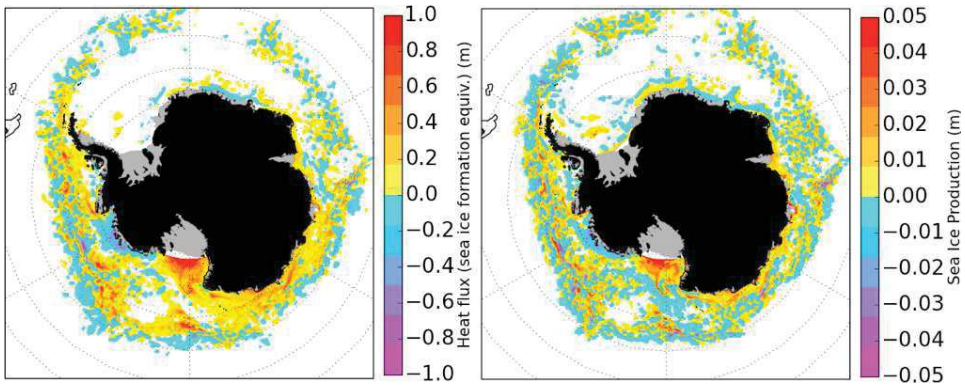


Figure 3.12: Mean *freshwater-induced* changes (CTR minus FW-) in: the annual mean oceanic heat flux at the sea-ice base (a), and the mean of sea-ice production during the sea-ice production months (from March to September) (b). Oceanic heat flux is expressed as sea-ice volume equivalent under the assumption that all the heat is used to form or melt sea-ice.

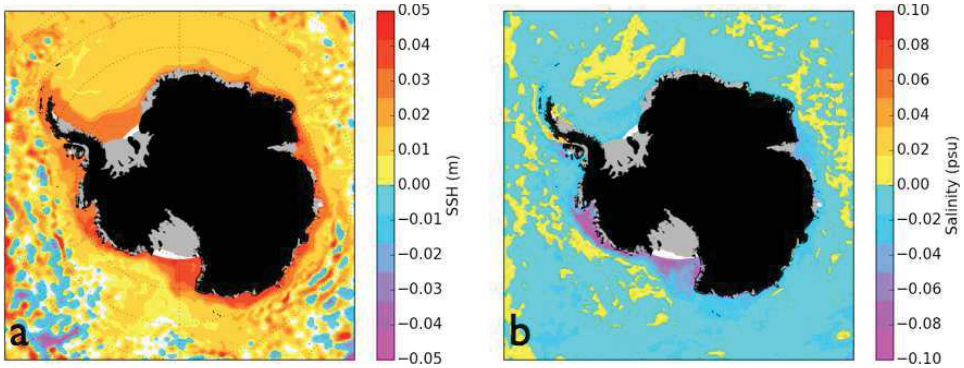


Figure 3.13: Annual averaged *freshwater-induced* changes (CTR minus FW-) in (a) sea surface height (SSH) and (b) surface salinity.

## 5.1 Ross Sea and West Pacific sector

As shown in Figure 3.12-b, the Ross and West Pacific sectors present an increase in thermodynamical sea-ice production at the coast where the ocean surface is much fresher (see Figure 3.13 b). In the Ross Sea sector, perturbations in glacial freshwater result in a SIV increase of $8.1 * 10^{10} m^3$ during the sea-ice production months (from March to September). The extra SIV produced in the CTR simulation (compared with the FW- simulation) occurs mostly along the coast and is advected, resulting in the increased SIC (see Figure 3.8) and SIT (see Figure 3.10). This northward export of sea-ice in the Ross sector is further helped by a strengthened Antarctic Coastal Current (ACoC). This is illustrated in Figure 3.13-a by a *freshwater-induced* rise in Sea Surface Height (SSH), which is consistent with (Marsh et al., 2015b). The stronger ACoC contributes to *freshwater-induced* changes in sea-ice divergence in the sector. These changes represent a mean SIV loss of $1.7 * 10^{10} m^3$ per year, which is relatively weak compared with the changes of thermodynamical origin in the sector.

As shown in Table 1, the SIV differences in minima between the CTR and FW-simulations are not significant compared with the SIV differences in maxima. Given the extra SIV produced by CTR, there is an excess of sea-ice that needs to be melted during the spring and summer months if both simulations are to show relatively similar sea-ice minima. According to Table 1, the sea-ice minimum obtained in the sector does not seem to be much affected by the freshwater or atmospheric perturbations introduced in our experiments. However, in the CTR simulation, the melting of sea-ice is amplified by summer *freshwater-induced* changes in the oceanic heat reaching the sea-ice base in summer (see Figure 3.14-a). In contrast to the annual integrated means (Figure 3.12-a), the oceanic heat supplied to the sea-ice base in summer is slightly greater in the CTR simulation than in the FW-simulation (represented by lower heat in sea-ice formation equivalent in Figure 3.14-a). This may be related to a sea-ice feedback, which helps to compensate for the extra sea-ice volume produced in winter. When the sea-ice retreats in late spring, the thicker sea-ice produced in CTR results in colder summer SST (as shown in Figure 3.14-b). The colder and denser sea surface affects buoyancy and therefore reduces the density stratification. Under these specific conditions, the oceanic heat convection in summer is facilitated in the sector as shown in Figure 3.14-a. However, this extra oceanic heat is not able to entirely explain the extra sea-ice melting in the Ross sector obtained in the CTR simulation.

## 5.2 Amundsen Sea sector

In the Amundsen Sea sector, the extra freshwater perturbation results in a mean increase in the oceanic heat flux at the sea-ice base (see Figure 3.12-a). This result explains the modelled decrease in SIC and SIT as shown in Figure 3.8 and Figure 3.10 respectively. Amundsen is the region of the Antarctic coast where the most rapid warming has been observed. This is due to a number of factors that include

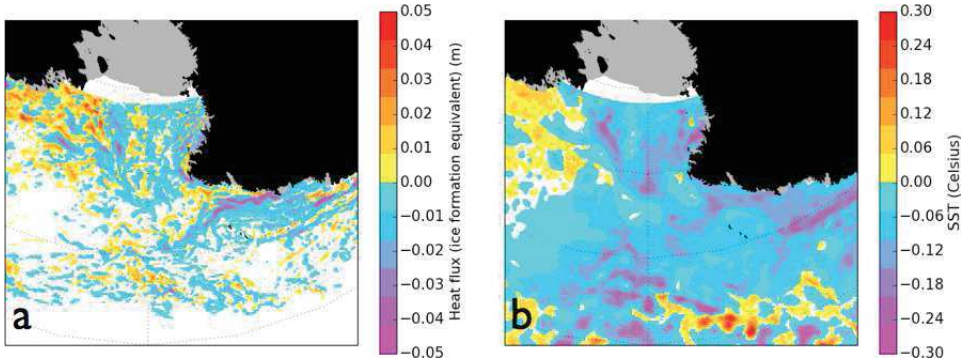


Figure 3.14: (a) Averages for December, January and February in the *freshwater-induced* changes (CTR minus FW-) in oceanic heat flux at the sea-ice base. Heat flux is expressed in sea-ice formation equivalent over the period. (b) December, January and February averages in *freshwater-induced* changes (CTR minus FW-) in sea surface temperature.

atmospheric features, the proximity of the region to the warm Antarctic Circumpolar Current (ACC) and topographic features (Walker et al., 2007), resulting in warm water intrusion into sub-surface waters (Jacobs et al., 2011; Thoma et al., 2008). In particular, observations have indicated intrusions of Circumpolar Deep Water (CDW) into ice-shelf cavities, with temperatures of 3 degrees above freezing point. This may be causing strong, grounded ice-mass losses in the Antarctic basins in the sector (Shepherd et al., 2012) due to the considerable ice-shelf thinning (Pritchard et al., 2012b) observed. These observations have been considered in our glacial freshwater scenario reconstruction (see Section 2). This makes the Amundsen Sea the region with the largest glacial freshwater forcing perturbation in our experimental set-up (see Figure 3.3).

As explained in section 2, the way glacial freshwater is added into our ocean model component is designed to emulate ice-shelf cavity recirculation. It is generated by the buoyancy fluxes introduced when distributing the ice-shelf freshwater flux along the vertical of the ocean model grid points adjacent to the ice-shelf. Therefore, the inclusion of more glacial freshwater strengthens coastal overturning, which may result in a stronger heat transport from deep layers to the surface.

The special conditions found in the Amundsen sector (i.e., very warm sub-surface water combined with the strongest glacial freshwater perturbation) would seem to explain the *freshwater-induced* anomaly in the oceanic heat flux reaching the ocean surface (see Figure 3.12-a). Indeed, as shown in Figure 15, the extra freshwater introduced in the CTR simulation in relation to the FW- simulation affects coastal stratification and promotes vertical heat transport. This leads to sub-surface cooling and surface warming in the model. However, in other sectors, like the Ross or Bellinghausen Seas, this feature is either not exhibited in the model at all or is not dominant compared with the impact of surface freshening on sub-surface heat convection (associated with the mechanism described in Marsland and Wolff

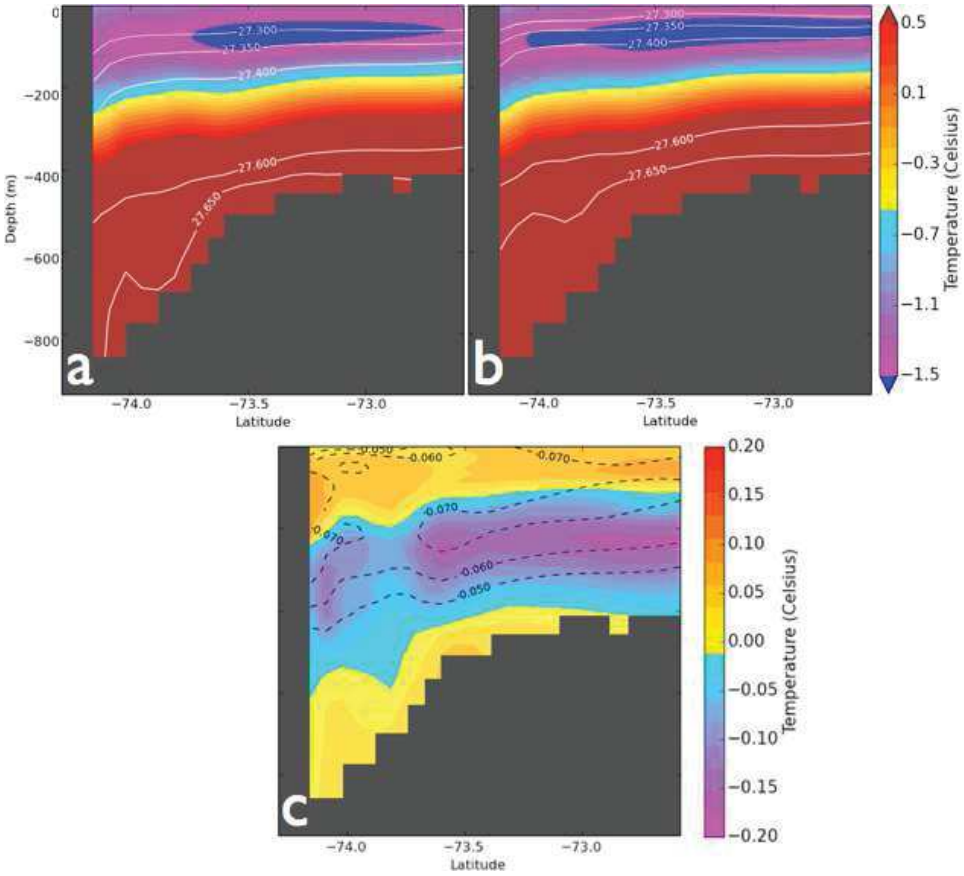


Figure 3.15: Temperature and density contour lines at a vertical section perpendicular to Dotson ice shelf (approximately at 112.54 degrees West) in the Amundsen Sea. They represent the annual mean ocean temperature at a given latitude and depth for CTR (a) and FW- (b) simulations, and the temperature anomalies (c) between both simulations (CTR minus FW-). Contour lines represent iso-density lines in plots a and b, and iso-density anomalies in plot c.

(2001)). This warming feature of the Amundsen Sea sector, which is the opposite to the response in the Ross and Pacific sectors, is consistent with observations (Jenkins, 1999). Indeed, it has been suggested that an increase in ice-shelf basal melt at the grounding line depth may enhance ice-shelf cavity overturning (Hellmer and Olbers, 1989) due to buoyancy changes in the interior of the ice-shelf cavity. However, the magnitude of an associated heat transfer between sub-surface and surface water masses is still unclear. The inclusion of the ice-shelf cavities in the ocean model should be considered, at least for this sector, in order to properly quantify the impact of ice-shelf basal melt in the special conditions of the Amundsen Sea sector.

## 6 Conclusions

The impact on sea-ice of recent changes in Antarctic glacial freshwater releases into the Southern Ocean has been investigated with a set of ocean/sea-ice/iceberg model experiments. The *freshwater-induced* changes in the global and regional sea-ice and ocean properties have been compared with the *atmosphere-induced* changes and observations. The model set-up considers an eddy-permitting ocean component (NEMO-ORCA025) coupled with a sea-ice model and a Lagrangian particle iceberg model and forced with DFS5.2 inter-annual atmospheric forcing. Model experiments consist of a control run and two perturbed simulations. The control run takes into account a recent glaciological estimate of the magnitude and spatial distribution of iceberg calving fluxes and ice-shelf basal melt fluxes. Perturbed simulations consider a decadal shift of the atmospheric variables and our own estimate of the pre-Antarctic-imbalance glacial freshwater released into the ocean. The perturbed freshwater scenario takes into account recent ice-shelf thinning and the dynamical mass change in the grounded Antarctic basins for the first time. It is based entirely on glaciological estimates and represents an improvement with respect to previous studies investigating the impact of recent glacial freshwater trends on ocean properties.

Results show that, overall, *freshwater-induced* changes in sea-ice extent (SIE) may potentially contribute 25% of the *total* trend in SIE. However, the regional impact in SIE differs markedly, accounting for 37% of the *total* decrease in SIE obtained in the Amundsen Sea sector, but 52% of the *total* modelled increase in SIE in the West Pacific sector. Perturbations in freshwater forcing produce a much greater impact on sea-ice thickness, and therefore on sea-ice volume (SIV). Globally, *freshwater-induced* changes in SIV represent almost 50% of *total* modelled changes, and are dominant with respect to *atmosphere-induced* changes in the Ross and West Pacific sectors.

The *freshwater-induced* changes in SIV and SIE during the sea-ice production months are shown to have only a slight effect on the maximum of the global SIV seasonal, but with important implications for the Ice Duration Season (IDS). In the Ross and West Pacific sectors, these changes are mostly produced by *freshwater-induced* changes in the oceanic heat convection related to ocean surface freshening. The changes in the oceanic heat reaching the sea-ice base are shown to produce significant thermodynamical changes in sea-ice production. In addition, the freshening of the ocean surface results in a strengthening of the Antarctic Coastal Current (ACoC), which may induce changes in sea-ice divergence. However, such changes remain relatively weak compared with the *freshwater-induced* thermodynamical changes in sea-ice production

In the Amundsen sector, the increased release of freshwater from the ice shelves results in an enhancement of coastal overturning. This leads to an increase in the oceanic heat supplied from the very warm sub-surface water mass to the ocean surface in the region. This observation suggests the need for explicitly considering ice-shelf cavities in models for this kind of study of sea-ice trends in the Amundsen

sector.

Most of the changes in glacial freshwater fluxes are believed to occur in the Pacific sector, especially in the Amundsen sector. The perturbations in freshwater forcing included in ocean models need to account for these regional changes instead of spreading the perturbation around the Antarctic continent in a homogeneous manner. In addition, the recently observed ice-shelf imbalance (Pritchard et al., 2012b; Paolo et al., 2015) is by no means negligible in relation to the Antarctic grounded mass loss. Consequently, both quantities need to be taken into account. These considerations may explain the differences in the results of our study with those of similar studies showing *freshwater-induced* changes in the Atlantic and East Indian sectors (Bintanja et al., 2013) or showing a very limited response of sea-ice to glacial freshwater perturbations (Pauling et al., 2016; Swart and Fyfe, 2013)

## Acknowledgments

We would like to thank Jean Marc Molines for his invaluable help with model configuration. The study was partially funded by the French National Research Agency (ANR) under the SUMER (Blanc SIMI 6) 2012 project, referenced as ANR-12-BS06-0018, and the TROIS-AS project referenced as ANR-15-CE01-0005-01. Numerical simulations were performed on IDRIS supercomputers (Saclay, France). NJ is an Associate Investigator of the ARC Centre of Excellence for Climate System Science.

Chapter 4

# Estimating model uncertainities to SLR projections with an idealized set up

Contents



## 1 Introduction

The investment of the ice sheet modeling community in marine-ice sheet problems has increased significantly in the recent years. Predicting the behavior of the marine ice-sheets has become a main challenge for computational glaciologists. Indeed, observations of West Antarctica imbalance in the beginning of 2000s revealed the inability of models to reproduce observed change. This has also been motivated by the potential contribution of this sector to SLR induced by the potential instability of the sector.

The largest marine ice-sheet is WAIS which has about 70% of its extent grounded below sea-level. As described in Chapter 1, since the 1970s this region has become a point of interest for glaciologists due to the theoretical finding of Weertman, Hugues and others about MISI (Hughes, 1973; Weertman, 1974). According to the initial MISI theory, and supported by further theoretical work (Schoof, 2007a) in an idealized case (flow-line glacier dynamics without lateral stresses), stable marine ice sheets with a grounding line resting on a upwards-sloping bed are mathematically impossible. These topographic conditions can be found as a result of isostatic

adjustment and are observed in WAIS and in the Amundsen sector in particular. However, recent works show that retrograde bed slope conditions is not a sufficient condition for MISI to occur, as marine ice sheet may find a stable position in such regions under the effect of lateral buttressing exerted by the ice shelves (Gudmundsson et al., 2012b), not considered in the previous MISI works. When ice shelves and ice streams interact with the topography in an embayment, ice rises or pinning points, like in Pine Island Glacier (PIG), the lateral stresses affect the upstream dynamics of the ice flow and contribute to the stabilization of the grounding line over upward-sloping beds. Therefore, marine ice sheet glaciers are extremely sensitive to ice shelf perturbations due to ice-ocean interactions. For instance, a thinning or a collapse of an ice shelf, because it leads to a loss of buttressing, may induce a retreat of the grounding line and increase the ice discharge and therefore impacts the sea level. This mechanism is suggested to explain the observed glacier acceleration of the Amundsen sector driven by the warming of the ocean and the subsequent increase in basal melting of the ice shelves (Pritchard et al., 2012a).

The ability of ice sheet models to correctly represent the impact of the ice-ocean interactions on the grounding line dynamics remains still unclear. Modeling the grounding line migration of marine ice sheets has become the key factor in AIS SLR projections (Durand and Pattyn, 2015). Of particular note in the last IPCC report (Stocker et al., 2014) were "the problems in modeling the dynamical response of marine ice sheet due to capture the large-scale grounding line instabilities". Motivated by this issue and the potentially critical contribution of Antarctic outlet glaciers to future SLR, community efforts have been undertaken in order to improve the modeling of the grounding line dynamics. The first Marine Ice Sheet Model Inter Comparison Project (MISMIP) was launched in 2009 (Pattyn et al., 2012). This first exercise was mostly focused on the stability of the grounding line and on the ability of different models to reproduce steady states in response to different perturbations in a highly idealized two-dimensional geometry. This first exercise concluded that extensional stresses can not be neglected (as for instance within the Shallow Shelf Approximation (SSA)) in order to reproduce the expected steady states in agreement with boundary layer theory (Schoof, 2007a). In addition, it was found that the accuracy of the models depended strongly in the spatial discretization. A second model intercomparison exercise, MISMIP3D (Pattyn et al., 2013), proposed a configuration with 3-dimensional geometry, in order to study the effect of lateral stresses in the grounding line stabilization. Main conclusions were about the need for at least 500 m resolution at the grounding line (without any flux parametrization at the grounding line) in order to accurately reproduce the grounding line migration under perturbations in basal sliding. In addition, models using SSA, and therefore neglecting vertical shearing, overestimate the ice viscosity and produce larger ice sheets when compared to models that explicitly incorporate the vertical shearing (full Stokes) or parametrized its effect (SSA*). SSA models also predict faster retreat on the downwards-sloping bed of MISMIP3D setup when compared to SSA* or full Stokes (Pattyn and Durand, 2013).

After desintangling physical and numerical aspects required to confidently model

marine ice sheet dynamics, community efforts are now more concentrated on the response of marine ice-sheet to oceanic perturbations. For instance, various studies have shown the evolution of glaciers in response to ocean melting at the interior of the ice shelf cavity (Favier et al., 2014; Joughin et al., 2014). In both of these studies, melting rates are prescribed based on different ad-hoc parametrizations applied at the ocean/ice shelf interface, which are not well constrained by the limited available observations. In addition, this widely used practice neglects the impact that changes in the ice cavity may have on the ocean circulation and therefore on melting rates. The related potential feedback needs further investigation and a new generation of ice sheet-ocean coupled models is appearing.

Motivated by the development of new ice sheet-ocean coupled models, a third model inter comparison exercise has recently been proposed, MISMIP+, as a part of the Marine Ice Sheet Ocean Model Inter Comparison Project (MISOMIP) (Asay-Davis et al., 2016). The main goal of MISOMIP is to provide a framework for better exploring and understanding model differences, and to aid in model development of ice sheet-ocean models. A set of intercomparison problems is proposed for standalone ocean (ISOMIP+) standalone ice sheet models (MISMIP+), and coupled models, in an idealized setup emulating the geometry of PIG. In particular exercise MISMIP+ simulates grounding line migrations in a retrograde slope induced by perturbations in the ice shelf buttressing, either forced by a prescribed basal melting, or by an ice shelf collapse. The objective is to better understand the response of the different models, approximations and parametrizations to grounding line retreats forced by interactions with the ocean in confined ice-shelf glaciers like PIG.

Among the modeling choices to which the grounding line position and migration in the MISMIP+ context are expected to be most sensitive, are the stress approximation of the Stokes equations and the basal friction law applied at the basal boundary condition. The model response to different stress approximations was already studied in MISMIP3D. As mentioned for MISMIP3D exercise, in the case of an unconfined ice shelf on a downwards-sloping topography, differences between the most common approximations (SSA and SSA*) were found to be relatively important. In the case of the friction laws, the most common choices are Weertman non-linear power law, or an effective-pressure-dependent basal friction laws (Schoof, 2007b; Tsai et al., 2015). Effective-pressure-dependent basal friction laws produce a continuous transition of the sliding coefficient between the grounded and the floating parts of the glacier. There are some voices in the community, not confirmed yet by observations, suggesting that this representation of the friction across the grounding line is more appropriated for marine ice sheet models instead of a discontinuous transition. However, effective-pressure-dependent basal friction laws have not been tested in any of the previous model intercomparisons, and in addition, power law have been widely applied in SLR estimates in the region of Amundsen (Favier et al., 2014; Joughin et al., 2014). The validity of using, for instance, the simpler SSA or a power friction law with respect to the more physical SSA* and effective-pressure-dependent friction laws, still needs to be tested in confined-ice shelf-type glaciers.

In this chapter we will use the set up proposed for MISMIP+ (Asay-Davis et al., 2016) in order to study the sensitivity of the confined-ice shelf glacier to two stress approximations of the Stokes equations and to the two main families of basal friction laws. Our objective is to estimate and better understand the uncertainity associated with those model parametrisations when producing model SLR projections of Pine-Island-like glaciers.

## 2 Equations and experimental set up.

This section introduces the two types of englacial stresses approximations and friction laws that will be studied by comparing three different experiments. We will also describe briefly the experimental set up, similar to MISMIP+ set up, that will be used to carry out our model experiments. Finally, the details of those experiments will be described in section 2.4.

### 2.1 Englacial stress approximations

The ice flow is governed by the Stokes equations. The Stokes equations are simplifications of the general Navier-Stokes equations where the acceleration terms are neglected. If ice is assumed to be incompressible, the mass and momentum balances yield:

$$\nabla \cdot \sigma = -\rho \vec{g} \tag{4.1}$$

$$\nabla \cdot \vec{u} = 0 \tag{4.2}$$

where $\sigma$ is the Cauchy stress tensor, $\vec{g}$ is the acceleration of the gravity and $\vec{u}$ is the ice velocity.

Components of Cauchy stress tensor ($\sigma_{ij}$) can be defined as a function of the deviatoric stress tensor components ($\tau_{ij}$) and the pressure as follows:

$$\sigma_{ij} = \tau_{ij} - p\delta_{ij} \tag{4.3}$$

where $\delta_{ij}$ is the Kronecker delta function.

In glaciology, the most common ice rheology used for ice flows is a Norton-Hoff power law, namely Glen's law (Glen, 1955), which relates the deviatoric stresses to the strain rate tensor ($D_{ij}$):

$$\tau_{ij} = A^{-1/n} D_e^{1/n-1} D_{ij} \tag{4.4}$$

$$2D_e^2 = D_{ij} D_{ji} \tag{4.5}$$

where $D_e$ is the second scalar invariant of the strain rate, $A$ is a rate factor and $n$ is the Glen's exponent, which in glaciology is commonly assumed to be $n = 3$. The resulting effective viscosity is $\eta = 1/2\, A^{-1/n} D_e^{1/n-1}$ making the governing equations of the fluid non-linear due to the dependence of the viscosity on the ice velocity.

The non-linear problem described above, without any approximation of the stress tensor expression, is usually referred as the full-Stokes model. It has been used even at the ice sheet scale (Gillet-Chaulet et al., 2012). However, the use of a full-Stokes model has a high computational cost and several approximations in the stress tensor have been proposed in order to solve the ice dynamics in some particular situations. In the present study, with a fast-sliding glacier with a confined ice shelf like PIG, the most common approximations relate to the vertical shear. When the basal sliding is significant, the driving stresses are primarily balanced by the horizontal stresses ($\tau_{xx}, \tau_{yy}$ and $\tau_{xy}$), and the vertical shearing terms have a reduced impact on the ice dynamics. Indeed, the consideration of the horizontal stresses across the grounding line in ice sheet models is suggested to be a minimum requirement to cope with grounding line migrations (Pattyn and Durand, 2013). In this chapter we will use two of those "membrane models", the SSA (MacAyeal et al., 1996), and the Schoof-Hindmarsh model as implemented in Cornford et al. (2013) (commonly known as SSA*).

SSA assumes that vertical shearing terms are negligible in comparison with the longitudinal and lateral stresses, which are, in addition, assumed to be depth-independent. There can be basal traction at the glacier base but its impact on the vertical profile of the ice velocity is assumed to be negligible in order to simplify the Stokes equations. This leads to a depth-independent horizontal ice velocity which simply takes the computed value of the basal velocity of the glacier. This is a good approximation for fast sliding glaciers with small aspect-ratio, but it may lead to a significant overestimation of the effective viscosity when basal drag becomes significant, and therefore it may produce larger and slower ice sheets (Pattyn et al., 2013).

SSA* is based on the same principle as SSA, in which membrane stresses dominate the force balance. However, SSA* includes vertical shearing terms in the calculation of the effective viscosity, providing a better approximation of the Stokes stress. In practice, SSA* computes the basal velocity with the same equations as SSA, but applies a Stokes-model-derived expression to estimate the vertical profile of the ice velocity. This fully 3-dimensional stress field is used for the computation of the depth-integrated effective viscosity, which is applied into a 2D vertically-integrated system of equations of the same form as the SSA. However, following Cornford et al. (2013), vertical variations of the horizontal velocities due to the vertical shear stresses are neglected in the mass transport equation due to numerical disadvantages.

The introduction of a vertically integrated effective viscosity has been shown to notably increase the accuracy of the SSA equations in three dimensional problems with respect to full-Stokes model on the MISMIP3D set-up (Pattyn et al., 2013). However, both SSA and SSA* assume normal stresses at the basal boundary ($\sigma_{nn}$) to be hydrostatic, i.e, there is an exact balance between the vertical pressure gradient and the gravitational force. This may result in differences with respect to full-Stokes solutions, in which the $\sigma_{nn}$ term is explicitly solved and it is used for evaluating the ice/bedrock contact (therefore the grounding line location). The hydrostatic

approximation of the normal devioatoric stresses may not be valid in some glacier configurations presenting non-negligible vertical deviatoric stresses, and therefore, "membrane stresses" models may not give accurate grounding lines migrations.

## 2.2 Friction laws

In glaciology, friction laws are difficult to formulate and validate due to the unknown basal conditions which may strongly depend on subglacial hydrology, and thus can be highly variable both temporally and spatially. The choice of a friction law should depend on the type of glacier that we have to simulate. Here we introduce three common friction laws which are widely used in glaciology problems, two of which are then applied in our numerical simulations.

A friction law basically relates the basal shear stress $\tau_b = (\sigma_{n,t1}, \sigma_{n,t2})$ (n means normal to the bedrock and t1 and t2 are the two associated tangent directions) with the sliding velocity $\vec{u_b} = (u_{t1}, u_{t2})$. A general form for the friction laws typically follows:

$$\vec{\tau_b} + f(\vec{u_b}, ...) = 0 \tag{4.6}$$

The simplest relationship follows a linear expression of the form :

$$\vec{\tau_b} + \beta \vec{u_b} = 0 \tag{4.7}$$

where $\beta$, the basal friction parameter, is a control field commonly used in inverse methods or data assimilation.

The most widely used friction law is the Weertman friction law, where the friction parameter, seen before for the linear expression, depends on the sliding velocity itself in the form:

$$\vec{\tau_b} + \beta_m |\vec{u_b}|^{m-1} \vec{u_b} = 0 \tag{4.8}$$

where m is the friction exponent and $\beta_m$ is a friction parameter, equivalent to the basal friction parameter $\beta$ when $m = 1$. This friction law is particularly appropriate for flows over undulating beds without cavitation. In such cases, it is theoretically demonstrated that $m$ is equivalent to $1/n$, where $n$ is the Glen's law exponent commonly set to $n = 3$ (Lliboutry, 1968).

The third friction law, the "Coulomb-like" Schoof friction law, considers the role of the effective pressure and cavitation on sliding problems. In the vicinity of the grounding line of marine ice sheets, where the ice likely meets the ocean because channels and topographic features, it has been proposed that a Coulomb-type law may be more appropriate for those rough terrains (Schoof, 2005; Gagliardini et al., 2007; Leguy et al., 2014). Coulomb-type friction laws in glaciology are those which fulfill Iken's bound (Iken, 1981)

$$0 < \frac{|\vec{\tau_b}|}{N} < m_{max} \tag{4.9}$$

where $m_{max}$ is the maximum slope of the topographic features, and $N$, commonly expressed as $N = -\sigma_{nn} - P_{water}$, is the effective pressure, where $P_{water}$ is the

seawater pressure. Coulomb-type friction laws consider that eq. 4.9 should present a maximal bound for $\tau_b$, depending on the effective pressure but independent on the sliding velocity $\vec{u_b}$. This represents the impact on the basal sliding of the cavities, produced at the base of the glaciers by interacting with the topography which are filled up with melt water or sea water. This limits the traction exerted by the bedrock at high glacier velocities, contrary to what is proposed in the Weertman friction law, where $\tau_b$ is unbounded.

Coulomb-type friction laws model the transition between a power law behavior at relatively low velocities, to an Iken's bound limit at relatively high velocities. This transition can be produced abruptly like in the case of Tsai friction law (Tsai et al., 2015) or smoothly like, for instance, the relationship proposed in (Schoof, 2010). The latter gives a basal traction continuous and differentiable everywhere except across the grounding line, which is preferable for numerical simulations. In both Tsai and Schoof cases, contrary to the power friction law, $\tau_b = 0$ independently of the value of $\beta_m$ at the grounding line. This is because at the grounding line, the effective pressure is considered $N = 0$ because the ice is assumed to be in exact flotation balance, and therefore the friction law predicts perfect sliding.

The Coulomb-type Schoof friction law is expressed following Gagliardini et al. (2007):

$$\tau_b + CN \left( \frac{\chi |\vec{u_b}|^{1-n}}{1 + \alpha_q (\chi |\vec{u_b}|)^q} \right)^{1/n} \vec{u_b} = 0 \tag{4.10}$$

with $\chi = 1/(C^n N^n A_s)$, $\alpha_q = (q-1)^{q-1}/q^q$, $A_s = \beta_m^{-1/n}$ the sliding parameter in absence of basal water, $n = 3$ the Glen's law exponent, and C the bound of the Coulomb-law given as $m_{max}$ in equation 4.9 (commonly $C = 0.5$). The value of $q \geq 1$, the post-peak exponent, controls the post-peak decrease.

Figure 4.1 represents for typical values of the effective pressure in the vicinity of the grounding line ($N = 0.1$ MPa and $N = 0.2$ MPa) the value of $\tau_b$ computed with the Weertman, and the Schoof friction laws for different values of q. As we can see, the closer we are to flotation criterion (i.e. lower values of N) the lower the ice velocity needed to reach the Iken regime. Most applications of the Schoof law use $q = 1$, for which there is no post-peak decrease and $\tau_b$ tends asymptotically to the Iken's bound value.

## 2.3 Experimental set up

The experimental set up used in this chapter corresponds strictly to the one proposed for the MISMIP+ experiment. Here we just summarize some details of the general set up, but a deeper description can be found in Asay-Davis et al. (2016), in particular the value of the model and equations parameters can be founded in Table 1 of Asay-Davis et al. (2016),.

Basically, the glacier domain is a rectangle of 640 km long in the main flow direction (hereafter the x-axis) and 80 km wide (the y-axis). An analytical bedrock topography, inspired by Gudmundsson (2012), is defined over the rectangular do-

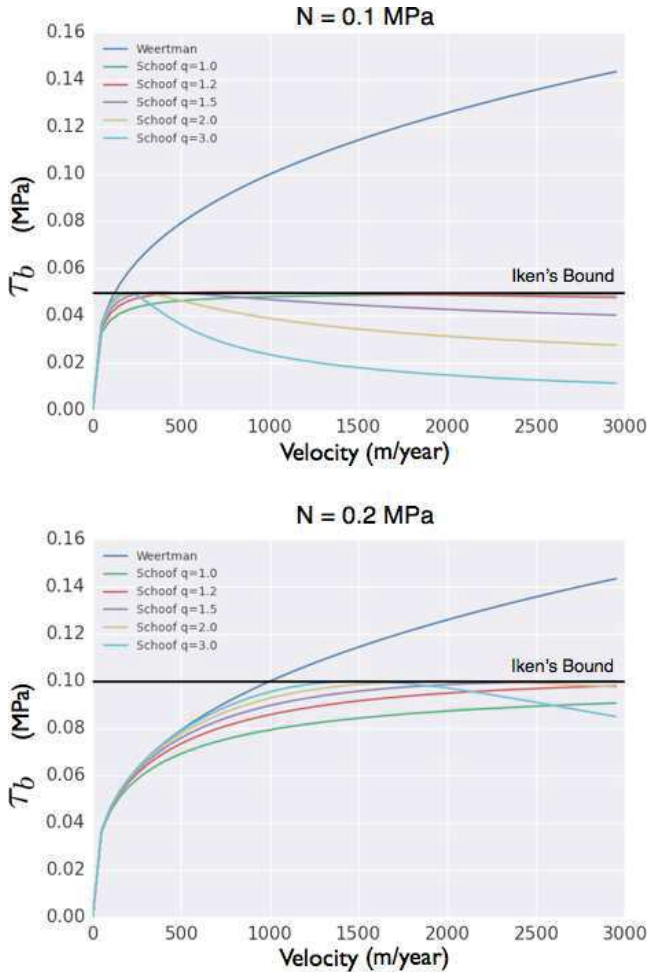


Figure 4.1: Basal shear stress $\tau_b$ versus glacier sliding velocities for different values of the post-peak exponent $q$ of Schoof friction law and Weertman friction law. Left plot considers the effective pressure $N = 0.1MPa$ and the right plot, the value $N = 0.2MPa$. $C = 0.5$ is considered in all cases.

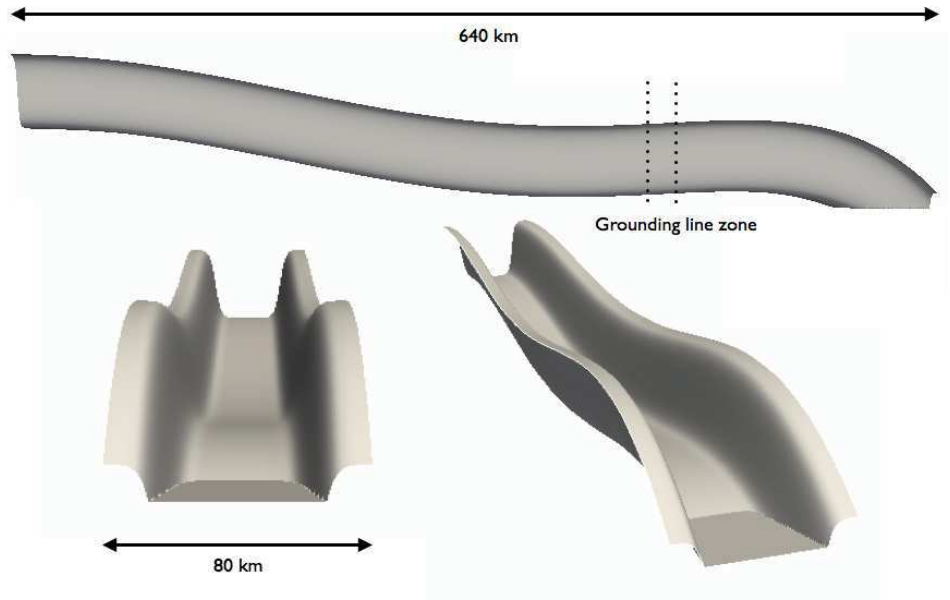


Figure 4.2: Bedrock geometry of the set up: lateral view with the grounding line zone for the steady state (top), frontal view from the ice front (bottom left), and perspective view (bottom right). Aspect-ratio is modified by multiplying z-coordinate by 100

main. It aims at providing an idealized representation of the main Pine Island central stream. The bedrock shows a central deep channel and an x-axis profile presenting a retrograde slope region as shown in figure 4.2. With the particular choices for the flow parameters, this bedrock leads to a stable curved grounding line resting on the retrograde slope at the center of the channel. MISMIP+ is the first model intercomparison exercise which includes a steady state with significant lateral stresses able to account for this particular grounding line configuration. This adds a bit of realism to the experimental set up in response to outcomes from the previous MISMIP3D. Indeed, these conditions have not been tested yet by either previous MISMIP, even though, most outlet glaciers in the Amundsen sector present confined ice streams and the lateral stresses strongly contribute to the stability of grounding lines in retrograde slopes.

At the lateral boundaries of the glacier (y=0 and y=80 km) and at the x=0 inland boundary, a free slip and a non-slip boundary condition are respectively applied. Ice is removed at the calving front boundary, x=640 km, with sea water external pressure imposed assuming a steady calving front position. A free stress boundary condition is applied to the upper surface and external water pressure condition is applied to the free surface in contact with the ocean. At the ice base in contact with the bedrock, we impose a no-flow-across-boundary boundary condition (normal velocities are set to zero) and tangential velocities are affected by a tangential basal traction computed from a friction law. A choice of non-linear friction laws is given to participants of MISMIP+. In this study we will use the

most common Weertman power law (n=3), and the effective-pressure-dependent Schoof friction law, described in detail in section 2.2, both with friction parameter $\beta_m = 1 \times 10^4$ Pa m$^{-1/3}$ a$^{1/3}$. In particular, we apply a Schoof friction law with values $q = 1$, $C = 0.5$ (see Figure 4.1). In addition, a simplistic hydrological model is considered in order to approximate the $\sigma_{nn}$ by the following expression:

$$N = \rho_i g(h - max(0, -\frac{\rho_w}{\rho_i} z_b) \tag{4.11}$$

where $h$ is the ice thickness, $g$ the gravity acceleration, $z_b$ is the bedrock elevation, $\rho_w$ is the sea water density and $\rho_i$ is the ice density

The ice rheology is given by Glen's flow law as described in equation 4.4. Ice is assumed to be isothermal and the ice-viscosity parameter $A$ in equation 4.4 is kept constant at $A = 2.0 \times 10^{-17}$ Pa$^{-3}$a$^{-1}$ in time and space

Participants of the MISMIP+ exercise are expected to initialize a steady state with the grounding line crossing the center of the channel (the line $y = 40$ km) at a position in between $x = 440$ km and $x = 460$ km (see Figure 4.2). To this aim, the ice viscosity parameter $A$ in equation 4.4 and/or basal friction parameter $C$ in equations 4.8 for Weertman or 4.10 for Schoof laws, can be modified by participants in case the default parameters provided in Asay-Davis et al. (2016) does not produce the required steady state. Contrary to previous MISMIP exercise where all the participants used the same physical parameters, in MISMIP+ all participants are invited to initialize to the same geometry with the physical parameters chosen as close as possible to the ones proposed by the exercise. This new approach, more in the line with the way that realistic glacier geometries are modeled, is in response to the outcomes of previous MISMIPs. In the model simulations shown in this chapter, none of those parameters have needed to be modified with respect to the values proposed in Asay-Davis et al. (2016).

In the previous MISMIP3D (Pattyn et al., 2013), grounding line migration was induced by changes in the basal traction coefficient. In the case of the Amundsen sector, however, the observed grounding lines changes are though to be driven by the ice shelf melting. In MISMIP+ and in our model simulations, the ice shelf is perturbed by the following simplified parametrization for melting rates to be applied at the ice shelf/ocean interface. This parametrization for the melt rates $m_i$ consists in an "ad-hoc" analitical expression calibrated with Parallel Ocean Program (POP) simulations using ice shelf draft from preliminar MISMIP+ simulations.

$$m_i = \Omega \tanh\left(\frac{H_c}{H_{c0}}\right) \max(z_0 - z_d, 0) \tag{4.12}$$

$$\Omega = u_{*,0} \frac{T_{*,0}}{z_{ref}} \frac{\rho_i c_w \Gamma_T}{\rho_{fw} L} \tag{4.13}$$

where $z_d$ is the elevation of the ice/ocean interface, $H_c = z_d - z_b$ is the water column thickness, $H_{c0} = 75$ m, $z_b$ the elevation of the bedrock, and $T_{*,0}$, $u_{*,0}$, $H_{c0}$ and $z_{ref}$ are fitting constants that together resulted in a value $\Omega = 0.2a^{-1}$

This expression accounts for the linear dependency of the sea water friction velocities on distance from the grounding line as suggested in some studies (Galton-Fenzi, 2010; De Rydt et al., 2014). In the POP simulations used in the calibration, melting reached zero at -100 m depth. From there to the surface some refreezing may occur, but the parametrization considers that there is neither melting nor refreezing between -100 m and the surface. Asay-Davis et al. (2016) emphasizes the fact that this is an ad-hoc expression only appropiate for the purpose of the model intercomparison, and adapted for the ice cavity geometry of the set up. There are missing physics such as the dependence on the slope of the ice/ocean interface (Goldberg et al., 2012) and the quadratic dependence on the ambient temperature (Holland et al., 2008).

### 2.4 Model Experiments

In this chapter, three simulations have been performed with the ice sheet model Elmer/Ice, described in Appendix A, based on the setup described in section 2.3 of this chapter. Simulation SSA-WEER computes the SSA equations with a Weertman friction law, SSA-SCH combines the SSA equations with the Schoof friction law and STAR-SCH solve the SSA* equations with a Schoof friction law.

Experiments start with an individual spin-up run (without any melting) until reaching: (i) a stable grounding line position resting in the MISMIP+ defined bounds, and (ii) a mean volume change criteria of $\frac{\Delta V}{V} < 10^{-5}a^{-1}$. Once the simulations are spun-up, we switch on the melting parametrization described in equations 4.12 and 4.13 and simulate 100 years of grounding line retreat. Sensitivity analyzes are made by comparing the solutions provided by the three experiments.

All the simulations in this chapter use the same fixed triangular mesh (see Figure 4.3) and a constant time step. The mesh domain consists of three box sub-domains with smooth transition of the element size. In particular, the central box of the domain (see Figure 4.3), is a structured triangular mesh with constant mesh-element size. This box is delimited by 320 km $\leqslant x \leqslant$ 520 km in order to have the grounding line contained in the box during at least 100 years of retreat. Convergence studies have been carried out for SSA-WEER during 80 years of simulation (see Figure 4.4). After those test, we have chosen the use of a resolution of 500 m of resolution at the grounding line (consistent with other finite element model participants in MISMIP+) and a time step of 0.1 years for our experiments. As shown in Figure 4.4, there are not significant differences in the center channel grounding line position and changes in glacier volume between our choice and the most accurate simulation tested (250 m of resolution and 0.025 years of time step).

## 3 Results

Figures 4.5 and 4.7 show the comparison of the glacier surfaces for the three experiments at the center of the bedrock channel (y=40 km) and the grounding line position at various time steps respectively. We observe that, differences in the

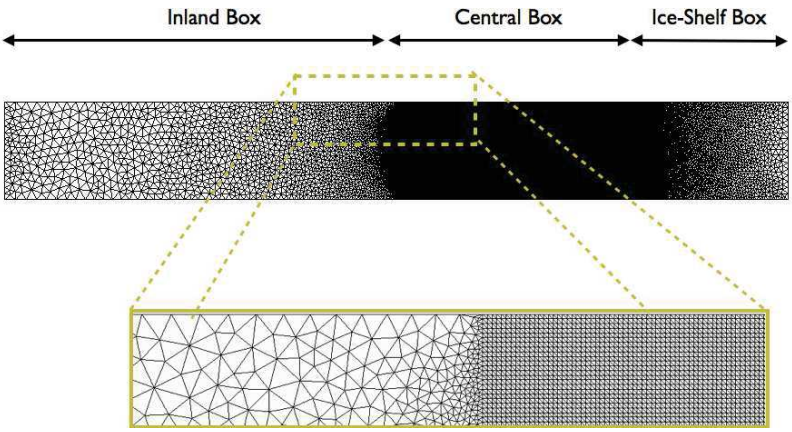


Figure 4.3: Experimental mesh, approximate positions of the three domain boxes and a zoom to the transition between inland and central boxes

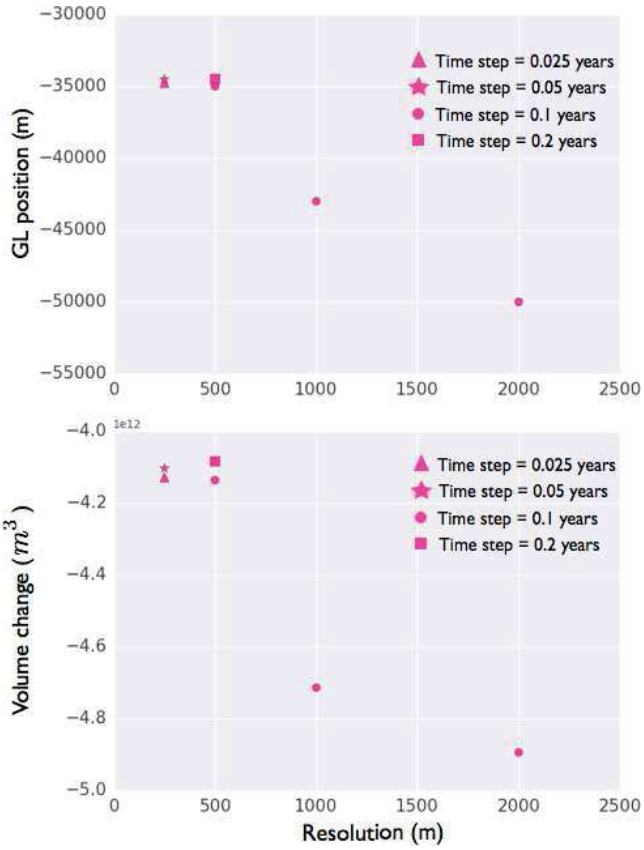


Figure 4.4: Results of the sensitivity tests for different mesh resolution and time steps after 80 years of simulation SSA-WEER of the grounding line position at the center of the channel (top) and glacier volume change (bottom).

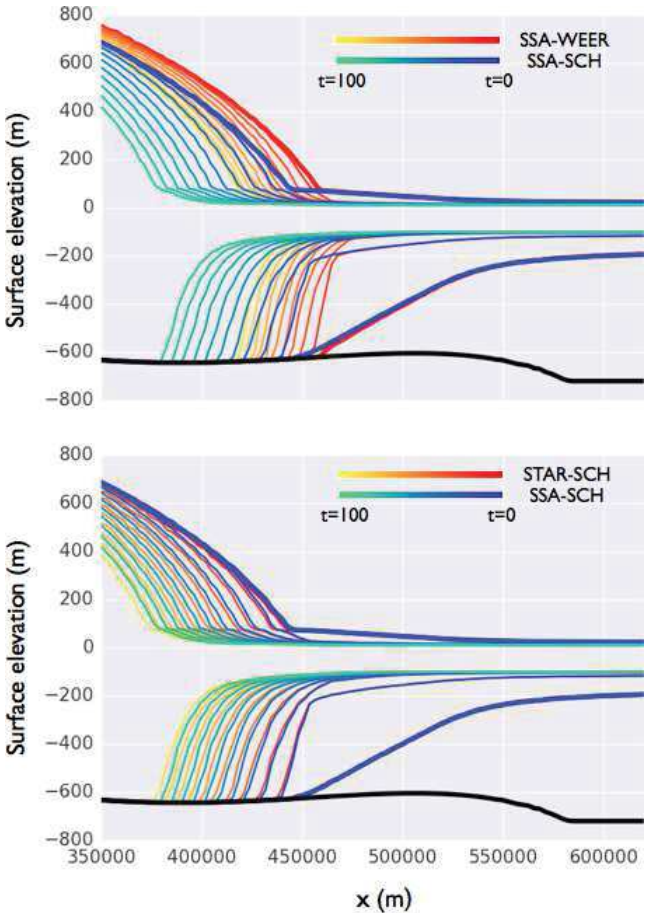


Figure 4.5: Comparison in the vicinity of the grounding line of the ice sheet surfaces at $y = 40km$ at different time steps for: (top) SSA-WEER (red to yellow color scale) and SSA-SCH (blue to green color scale) simulations, and (bottom) for STAR-SCH (red to yellow colors scale) and SSA-SCH (blue to green color scale) simulations.

grounding line at the steady state ($t = 0$) are relatively significant in between simulations SSA-SCH and SSA-WEER. At the center of the channel, SSA-SCH converge to a grounding line position located 14 km upstream from the one obtained by SSA-WEER. The difference is smaller close to the lateral boundaries of the domain where the grounding line is located only 5 km upstream. In contrast, differences between the spin up geometries of SSA-SCH and STAR-SCH simulations are much smaller. The steady state grounding line position at the center of the channel obtained by STAR-SCH is just 1 km upstream than the grounding line obtained by SSA-SCH, this is only two grid cells of difference. The upstream position of SSA*-based simulation is consistent with results of MISMIP3D (Pattyn et al., 2013). However, differences obtained on the MISMIP+ setup are of much less significant than the difference of about 70 km that is observed between steady state grounding line positions in MSIMP3D.

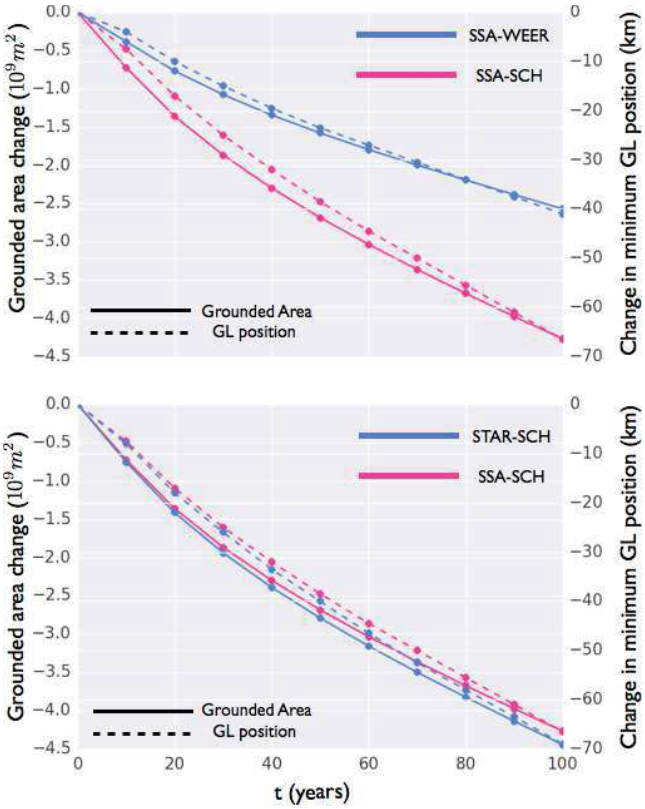


Figure 4.6: Comparison of grounded area change (left vertical axes with solid lines) and the grounding line position at the center of the channel (right vertical axes and dashed lines) during 100 years of simulations: (top) SSA-WEER in blue and SSA-SCH in magenta, and (bottom) STAR-SCH in blue and SSA-SCH in magenta.

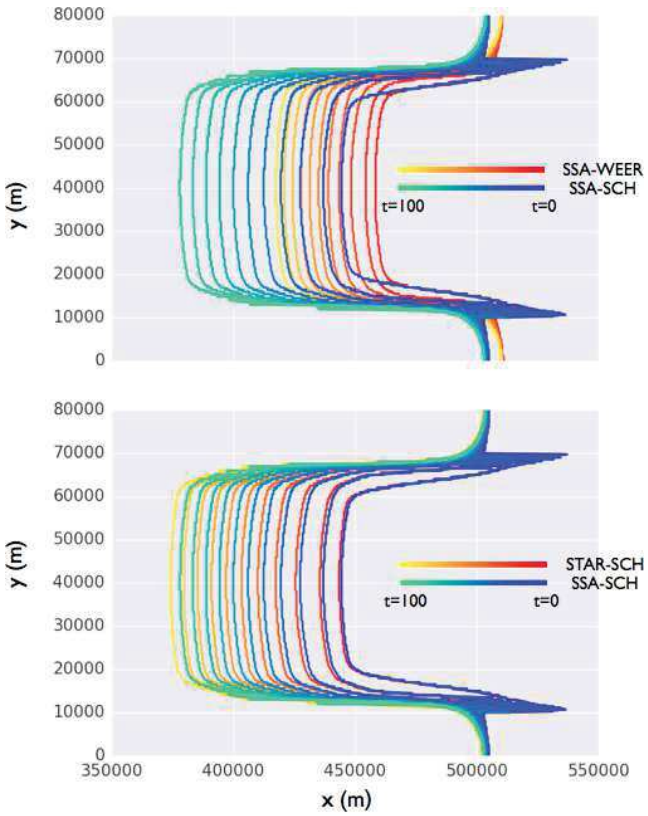


Figure 4.7: Comparison of the grounding line shape at different time steps for: (up) SSA-WEER (red to yellow color scale) and SSA-SCH (blue to green color scale) simulations, and (bottom) for STAR-SCH (red to yellow colors scale) and SSA-SCH (blue to green color scale) simulations.

Once the melting parametrization is activated, the grounding line starts to retreat in all simulations. During the retreat, the differences in the upper glacier surface elevation (Figure 4.5), the change in grounded area (Figure 4.6) and grounding line position (Figure 4.7 and Figure 4.6) becomes more significant, in particular between the SSA-SCH and the SSA-WEER simulations. At the end of the 100 years of retreat, the grounding line at the center of the channel in SSA-SCH is found 40 km upstream than in SSA-WEER simulation. Taking the differences with the initial position, there is a difference of 26 km in the total modeled grounding line retreat depending on the chosen friction law. This different grounding line retreat is also associated with differences of about 40% in the total change in grounded area between the simulations. Comparing the different englacial stress approximations, STAR-SCH gives a retreat of the grounding line at the center of the channel that is only 2.5 km larger than SSA-SCH and a slightly larger decrease in the grounded area of the glacier by about 4%.

Figure 4.8 shows the comparison of the changes in volume, Volume Above Flotation (VAF) and their difference during the 100 years of modeled glacier retreat. Overall, all the simulations present a similar pattern: a rapid volume loss acceleration during the first years followed by a quasi-linear decrease until the end of the simulation (see also Figure 4.9), and increasing differences between VAF changes and total volume changes as the simulation advances. More significant differences in total volume loss are found again between SSA-SCH and SSA-WEER simulations (top pf Figure 4.8). In 100 years, simulation SSA-SCH loses $2.32\,10^{12}$ m$^3$ more ice than SSA-WEER. This difference represents about 50% of the total volume loss estimated by SSA-WEER for the same period. Volume changes are much less sensitive of the choice between SSA or SSA*. STAR-SCH produces a 3.4% higher volume loss than SSA-SCH.

As the grounding line retreats, the previously grounded parts of the glacier progressively become afloat and contribute to the change in VAF, which is the contribution of the glacier to sea level rise. VAF is estimated by the following equation:

$$VAF = V - V_{submerged} * \frac{\rho_w}{\rho_i} \tag{4.14}$$

where $V$ is the total glacier volume, $V_{submerged}$ is the volume below sea level, $\rho_w$ is the sea water density and $\rho_i$ is the ice density. There is a significant VAF loss in our simulations controlled by the strong grounding line retreat and glacier acceleration As with other metrics of retreat, VAF changes seems more sensitive to the friction law chosen than to the englacial stress approximation chosen. SSA-SCH estimates a total VAF loss of $4.49 \times 10^{12} m^3$, which is $1.32 \times 10^{12} m^3$, or 42%, more VAF loss than SSA-WEER simulation during the same period of 100 years. Regarding the choice of englacial stress approximation, SSA* results in only a 2.8% more VAF loss than SSA equations.

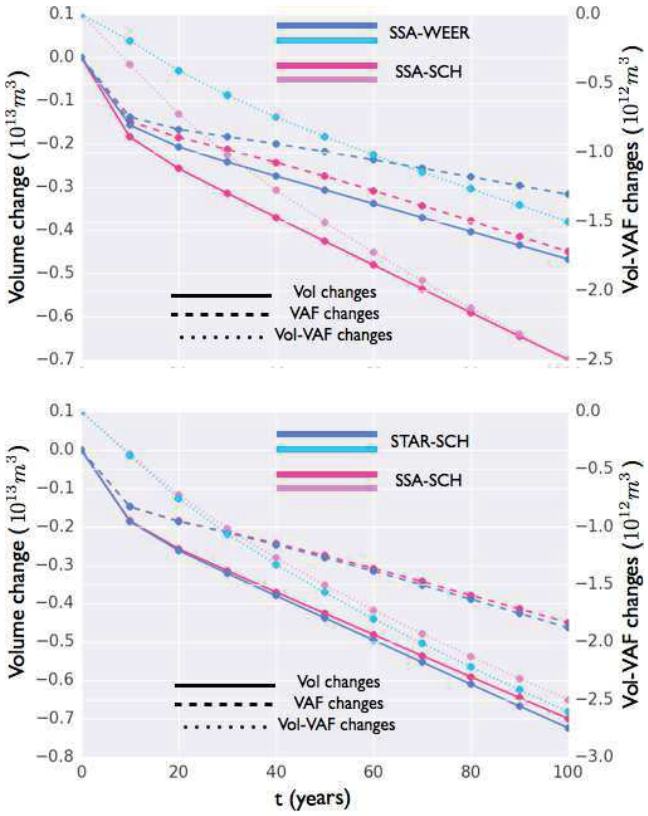


Figure 4.8: Comparison of total cumulative glacier volume change (left vertical axes with continuous lines), volume above flotation (VAF) cumulative changes (left vertical axes and discontinuous lines) and the difference between the total volume change and the VAF change (right vertical axis and dotted lines) during 100 years of simulations: (up) SSA-WEER in blue and SSA-SCH in magenta, and (bottom) STAR-SCH in blue and SSA-SCH in magenta.

# 4 Discussion

The differences in the grounding line position showed in Figures 4.5 and 4.7 for the steady state of different simulations are not unexpected.

Concerning the differences between SSA-WEER and SSA-SCH, we may expect that the Schoof friction law, for the same rheology and geometry, may produce a faster flow at the grounding line, leading to a greater ice flux and therefore upstream migration of the steady state grounding line position. This is mainly due to two reasons: First, in contrast to the Weertman friction law, the Schoof friction law fulfills Iken's bound, so the traction exerted by the bedrock is bounded, constrained by the local effective pressure, independently of the local basal velocity. Second, even at low velocities, the hydrology model used with the Schoof friction law considers that the effective pressure at the grounding line should be zero and therefore there should be perfect sliding. This leads again to a reduction of friction in the vicinity of the grounding line.

Concerning the differences between SSA-SCH and STAR-SCH, in agreement with conclusions of previous MISMIP3D, we may expect that SSA* produce a faster flow to the grounded parts of the glacier than SSA. This is because SSA* takes into consideration the vertical stresses in the computation of the effective viscosity, leading to a less viscous ice than with SSA where vertical stresses are neglected. For a given geometry, the lower viscosity in SSA* predicts a faster ice flow just upstream the grounding line (therefore a larger ice flux considering that we are on upward-sloping bedrock) and therefore it will converge to more upstream steady grounding line position than the SSA. However, those differences for the MISMIP+ setup appears to be much smaller than for the setup of MISMIP3D. In that case, SSA models and SSA* models where found to differ by more than 50 km in the grounding line position at the steady state. This indicates that the steady state in MSIMIP+ is mostly controlled by the effect of buttressing in the membrane stresses, and vertical shearing is less important than in laterally uniform geometries like in MISMIP3D.

Once the melting parametrization is activated (at $t = 0$), the perturbation induces a decrease of the total glacier volume and the grounding line starts to retreat. As shown in Figure 4.9, total volume of the glacier decreases rapidly from the beginning until the 30th year of simulation, after which, the total volume decreases at a constant rate. As illustrated in Figure 4.5, this initial phase of strong volume decrease is related to a strong change in the ice draft, and ice shelf thinning. This leads to a strong initial decrease in the grounded area close to the lateral walls of the channel as observed in the differences of grounding line shape between the steady state and the first 10 years of retreat in figure 4.7 for all the simulations. This reduction of the grounded area produces a loss of buttressing and a subsequent glacier retreat as observed for all simulations.

There are three contributors to the glacier volume changes in our particular setup (no glacier surface melting): the accumulation rate at the surface, the calving flux at the calving front ($x = 640$ km), and the melt volume flux of ice at the

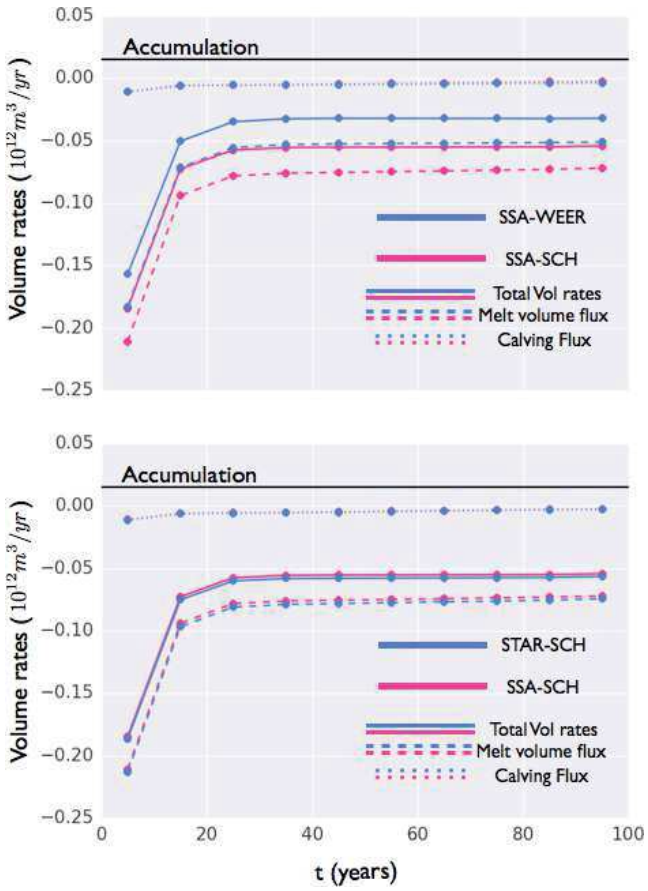


Figure 4.9: Average estimates of contributors to glacier's net rate of volume change during 100 years of simulations for: (top) SSA-WEER in blue and SSA-SCH in magenta, and (bottom) STAR-SCH in blue and SSA-SCH in magenta.

ocean/ice interface. At the steady state with no basal melting, the accumulation gain is compensated by mass loss at the calving front. Once the melting is activated, apart from the volume losses directly attributable to melting, the melting also induces dynamic volume changes related to the subsequent ice acceleration and thinning, which alter the ice flux at the calving front. Figure 4.9 shows the volume fluxes associated to each volume change contributor. As shown for each of our three simulations, net glacier volume losses are almost entirely controlled by melting as calving fluxes are almost negligible. Even if the grounding line retreat leads to glacier acceleration (which might indicate further volume losses), the volume fluxes at the calving front are strongly affected by the large ice shelf thinning, resulting in relatively small negative volume flux changes at the calving front. Therefore, the melting of ice decrease the dynamical volume losses due to calving fluxes, resulting in net volume gain associated to the ice outflow. However, this volume gain is negligible compared to the strong volume losses associated to ice melting. In conclusion, in our particular set up, the ice melting reduce the calving fluxes, which becomes a negligible contributor to the volume changes of the glacier.

Differences in melting rates between the three simulations are shown in Figure 4.9. Simulation SSA-WEER shows significantly lower melt rates than the other two simulations. This is caused by differences in its ice cavity draft since the melting parametrization only depends on the geometry of the ice cavity. Basically, the bigger the cavity is the more the ice surface is in contact with the ocean, which means larger integrated melt rates. In addition, according to equation 4.12, deeper ice leads to higher melting rates, either because the grounding line is found deeper, or because the basal ice surface elevation slope in contact with the ocean is softer. This is the case of simulation SSA-SCH and STAR-SCH, which have more and deeper ice surface in contact with the ocean than SSA-WEER at a similar time step. This is because: (i) the faster grounding line retreat means a bigger ice shelf cavity, (ii) the faster grounding line retreat in a retrograde slope leads to having deeper ice in contact with the ocean. Accordingly, the larger the melting rates are, the larger the grounding line retreat will be, leading to further increase in the melt rates. This positive feedback of the melt rates, hereafter *ice-draft-melting feedback*, contributes to producing and sustaining the increasing grounding line differences between the three simulations as the grounding line retreats.

As shown in Figures 4.5 and 4.7, at the initial steady state, SSA-WEER presents a slightly smaller ice shelf cavity and a downstream grounding line position with respect to both Schoof-based simulations SSA-SCH and STAR-SCH. Due to these differences of the ice draft at the initial state, SSA-WEER initial melting rates are 8% smaller than SSA-SCH or STAR-SCH simulations (both schoof-based simulations present melt rates almost similar). One may wonder if the *ice-draft-melting feedback* could entirely explain all the obtained grounding line retreat differences between Schoof-based and Weertman-based simulations triggered by the initial differences in the melt rates. As the simulations advance in time, the relative difference in melting rates between SSA-WEER and SSA-SCH grow significant and converge from the 20th year to a value around 30% (see Figure 4.9). This suggests that

the initial trigger of the strong acceleration of the differences in the grounding line retreat between the three simulations, might not be only controlled by the *ice-draft-melting feedback*. We propose in the following paragraphs a mechanism, apart of the *ice-draft-melting feedback*, contributing to explain the obtained results.

The different sensitivity that Weertman-based simulations and Schoof-based simulations have in response to melt perturbations is illustrated by Figure 4.10. This sensitivity can be quantified by the melting efficiency coefficient $\gamma_{melt}$ defined here as:

$$\gamma_{melt} = \frac{\Delta(VAF)/\Delta t}{V_{melted}} \tag{4.15}$$

where $V_{melted}$ is the total melt volume flux. The coefficient $\gamma_{melt}$ provides and estimate of how efficient a melting perturbation is in producing VAF losses in a glacier. That is, given a melted-volume loss and the subsequent loss in buttressing of the glacier, how strong will the dynamic transfer of VAF in flotation volume ($V_f$) (total glacier volume = $VAF + V_f$ ) be. We note that the melting only reduces the volume of the ice shelf, therefore melted ice volume is always removed from $V_f$. Since the calving fluxes are negligible (see Figure 4.9), the difference in $V_f$ between two consecutive glacier states during a glacier retreat will be the balance between the melted volume and the VAF transformed in $V_f$ due to a dynamical response of the glacier. For instance, hypothetical values of $\gamma_{melt} > 1$, would mean a $V_f$ net gain (here neglecting changes by the calving front fluxes). Another limit can be attributed to $\gamma_{melt} = 0.5$, which implies that the glacier looses VBF and VAF at the same rate. As shown in Figure 4.10, the two simulations using a Schoof friction law present a very similar VAF rate and $\gamma_{melt}$ during the grounding line retreat. From the beginning of the simulation, STAR-SCH and SSA-SCH simulations present values of $\gamma_{melt} < 1$ peaking at the beginning of the simulation at relatively high values of about $\gamma_{melt} = 0.7$. As the simulation advances, $\gamma_{melt}$ of STAR-SCH and SSA-SCH both decrease during the first 30 years. After that, $\gamma_{melt}$ starts to increase and converge to the balanced limit $\gamma_{melt} = 0.5$, this is presenting almost similar VAF and $V_f$ losses in response to melting perturbations. Similarly to STAR-SCH and SSA-SCH, SSA-WEER shows values of $\gamma_{melt} < 1$. However, from the 20th year, SSA-WEER experiment shows lower values of $\gamma_{melt}$ converging at the end through values of about $\gamma_{melt} = 0.40$. This result indicates that for the particular geometry tested in this study, Weertman-based simulations are less sensitive to the melting perturbations than Schoof-based ones.

The reason for this extra sensitivity of Schoof-based simulations, at least at the beginning of the retreat, might be related to the strong impact that the glacier parts grounded on the lateral walls of the channel may have in the grounding line stability in this particular set up for those particular simulations. As discussed before, when applying a Schoof friction law, the bedrock in contact with the fastest parts of the glacier in the center of the channel exerts a limited traction (bounded by the Iken's bound), strictly smaller (for a given ice thickness and ice velocity) than in the simulations using a Weertman friction law. Therefore, for the grounding line position and stability, we can expect that the traction and lateral buttressing

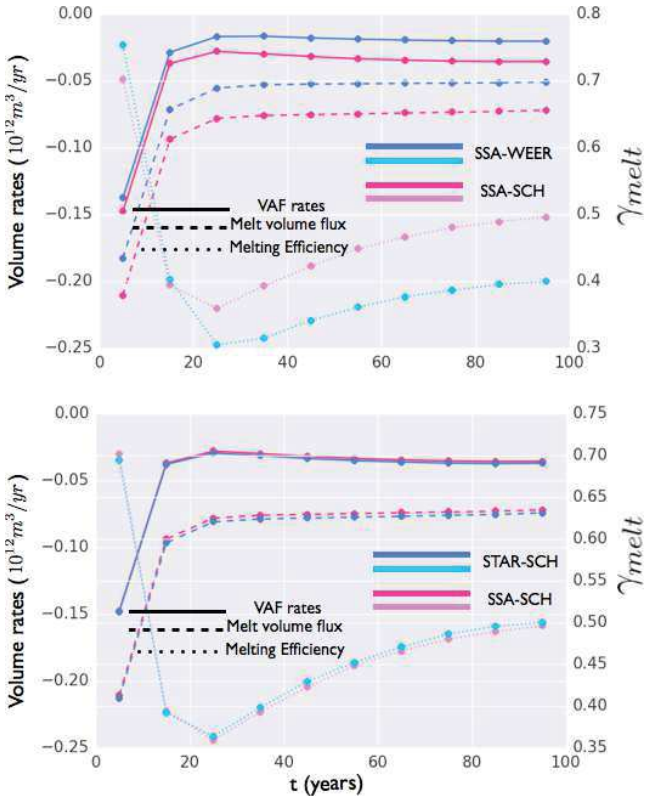


Figure 4.10: Average estimates of the melt rates, volume above flotation rates and melting efficiency $\gamma_{melt}$ for (top) SSA-WEER in blue and SSA-SCH in magenta, and (bottom) SSA-SCH in blue and STAR-SCH in magenta.

exerted by the grounded parts on both sides of the ice shelf have a larger relative importance in Schoof-based simulations than in Weertman-based simulations. As we can see in Figure 4.11, at the steady state, SSA-SCH simulation shows higher values of the shear stress $\tau_b$ (computed normal to the flow direction) in the vicinity of the grounding line on both sides of the channel. The rapid ice shelf thinning during the first 10 years showed in Figure 4.5 may explain the stronger impact on the stability of the grounding line of Schoof-based simulations. Therefore, this stronger loss of related buttressing may contribute to the initial faster glacier acceleration showed by Schoof-based simulations, in addition to the difference in the initial melt rates previously discussed,.

# 5 Conclusion

A set of model experiments have been performed with Elmer/Ice model in order to study the response of a confined marine ice sheet outlet glacier to different friction laws and englacial stress approximations. In particular, the solution computed with a Weertman friction law has been compared to the solution computed with a more

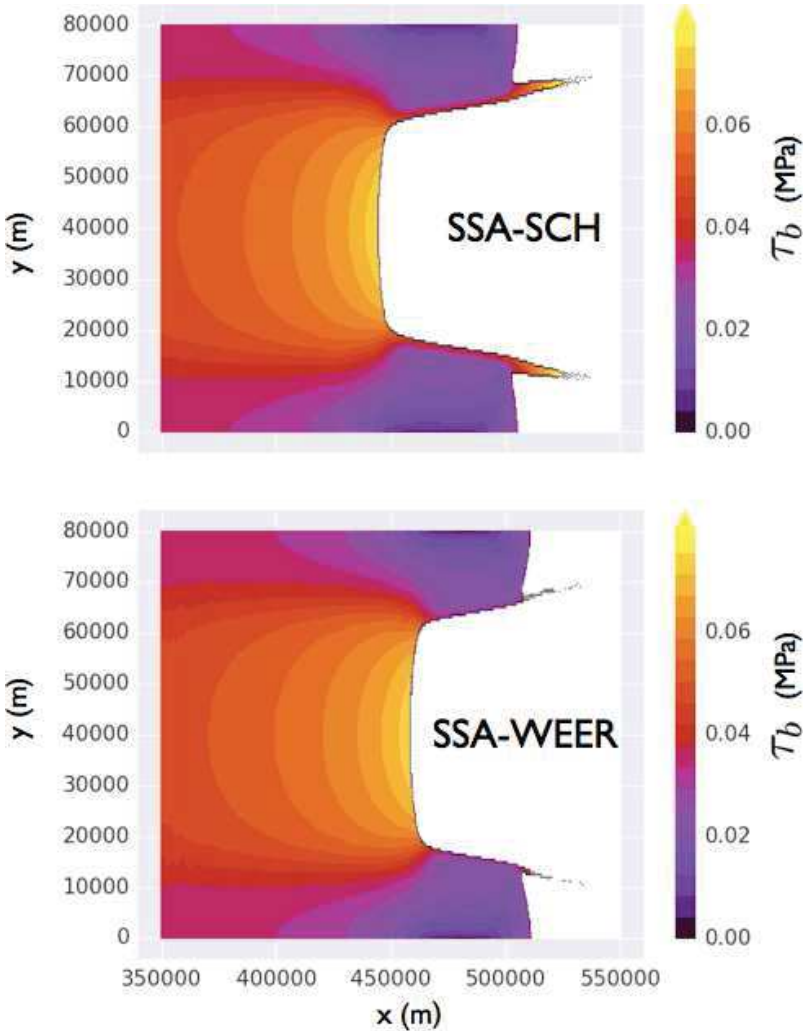


Figure 4.11: Estimates of the basal shear stress $\tau_b$ normal to the flow direction for the steady states of (top) SSA-SCH simulation and (bottom) SSA-WEER simulations.

physical Coulomb-type Schoof power law, and the solution of SSA equations has been compared to the solution of SSA* equations in a idealized PIG-like glacier set up. Model experiments are based on the MISMIP+ setup (Asay-Davis et al., 2016), which produces 100 year of grounding line retreat from a steady state induced by a basal melting parametrization to be applied at the subsurface of the ice shelf cavity.

At the steady state, Weertman-based simulation predicts a larger ice sheet with a grounding line position 14 km downstream then Schoof-based simulation with SSA. For a similar friction law, SSA*-based simulation predicts a one-kilometer upstream position with respect to SSA-based simulation. This is in agreement with conclusions of the previous MISMIP3D experiments (Pattyn et al., 2013), although in MISMIP3D differences between SSA and SSA* were much larger. This might be related to the particular bedrock applied in our set up, as the grounding line position is expected to be more impacted by the lateral buttressing exerted by the confined ice shelf than in the case of laterally uniform geometries as used in MISMIP3D experiments.

At the steady state, the calving flux at the calving front balances the volume flux due to snow accumulation. Once the melting parametrization is activated, all the simulations present strong total volume losses, which are almost entirely controlled by the melting rates. Melt losses more than the volume gain due to the snow accumulation and the decrease in volume flux due to dynamical decreases in the calving flux. Indeed, the melting beneath the ice shelf produces ice shelf thinning, which reduces the flux of ice flowing through the calving front. Anyway, those changes are negligible compared to the melting rates. In all the simulations, the melting of the ice shelf induces strong grounding line retreat, associated to the loss of grounded area and the subsequent loss of buttressing. As the simulation advances in time, the Schoof-based simulation retreats faster than the Weertman-based simulation, with 26 km of further retreat and a 40% of grounded area difference at the end of the 100 years. The SSA*-based simulation only predicts a 2.5 km larger retreat than SSA-based simulation with only a 4% of grounded area differences between the simulations. According to these results, grounding line migration in the particular setup of this work is very sensitive to the choice of the friction law, and relatively unaffected by the choice between the two englacial approximations tested.

Grounding line retreat produces a significant loss in volume above flotation (VAF), which is directly associated with the glacier contribution to sea level rise. As for the rest of the quantities explored, relative differences associated with the englacial stress approximations applied are not significant. However, according to our results, after 100 years of glacier retreat, the Schoof-based simulations predict 42% larger contribution to sea level rise than Weertman-based simulations. This result is comparable to a recent estimate of the impact of coupling the ice sheet model with an ocean model in a similar geometry (De Rydt and Gudmundsson, 2016). However, most of estimates of PIG sea level contribution does not consider a Coulomb-type friction law (Joughin et al., 2010; Favier et al., 2014; Joughin et al., 2014), which is expected to better reproduce the friction transition in the vicinity of the grounding line, and therefore preferable in modeling grounding line migrations.

The robustness of our conclusions is subjected to further work regarding the melting perturbations and their impact on the dynamics of the glacier. As discussed, the melting parametrization applied in this work depends strongly on small differences in the ice cavity draft. Even if the MISMIP+ set up invites the participants to converge to a relatively similar initial steady state, the range of possible geometries admitted by the set up leads to significant differences in the magnitude of the melting perturbation. In our experiments, differences in the initial melting rate are as large as 8% between Weertman-based simulation and Schoof-based simulations. It is not clear if the *ice-draft-melting feedback* is able to explain all the obtained VAF losses differences between our simulations. If so, our conclusions would not be valid as the results are dependent on the experiment set up design and therefore not dependent on the friction law or the englacial approximation applied. In any case, the analyze of the melting perturbation efficiency through the melting efficiency coefficient $\gamma_{melt}$, indicates the higher sensitivity that the Schoof-based simulations to the melting perturbations. This result confirms our expectations of Schoof-based simulations should produce more VAF losses than Weertman-based simulations. However, the quantification of the differences in VAF losses depending on the friction law applied would require further modifications in the melting parametrization, in order to reduce the impact of the *ice-draft-melting feedback* in the sensitivity experiments.

Chapter 5

# Conclusions and perspectives

Contents



## 1 Context

In the upcoming years, the way how climate models will predict the evolution of the Antarctic Polar Region in the context of climate change will be different from today. From recent years, we are attending to the birth of new ice-sheet/ocean coupled systems, which will frequently be used, at least for Greenland and the Arctic Ocean, in the next generation of climate models and Earth System Models. This new step of complexity mainly consists in the inclusion of an ice dynamics component for the polar ice sheets and therefore improve the representation of the impact of the cryosphere on future climate. Historically, in Earth System Models, the cryosphere has been treated as part of the land component, and the mass balance of continental glaciers, ice caps, and ice sheets have been computed in association with the atmospheric component of the model, without solving the flow of ice and without interacting with the ocean. This practice assumes that the mass balance of the cryophere only depends on the ice surface melting and snow precipitation, neglecting the mass losses related to the ice flow acceleration or the warming of the oceans. This approximation is suitable for the continental glaciers and ice caps, indeed, the larger contributors to the sea level rise so far. However, this is not valid for computing the mass balance of the polar ice sheets. For instance, in the case of the Antarctic Ice Sheet, the mass output is almost entirely controlled by the ice dynamics since the annual mean of the surface melting of ice only correspond to 1% of the total snow accumulation.

Up to the last two decades, the Antarctic Ice Sheet was believed to be more or less stable and to present a marginal contribution to the rise of the sea level and the climate change. This is why the representation of AIS in climate models has not been a priority so far and a number of processes are misrepresented. During the last decade, rapid changes in the ice thickness and glacier velocities widely associated with the interaction of the outlet glaciers with the Southern Ocean, have been

observed. These changes are expected to become more important over the XXIth century, motivating the necessity of including a proper representation of the AIS mass balance in the next generation of climate models. This means to explicitly include the ice-ocean interactions impacting the AIS dynamical mass imbalance, in order to account for the different ice-ocean interactions affecting the Southern Ocean, consequences of the AIS imbalance.

As mentioned above, causes of the AIS imbalance have been strongly associated to the interaction of the outlet glaciers with the Southern Ocean. This is particularly true in the Amundsen Sea, where the intrusion of warm Circumpolar Deep Waters into the Antarctic Continental Shelf is suggested to increase the ice shelf melting, reducing the buttresing effect of the ice shelves and inducing upstream glacier acceleration. Accounting for ice sheet dynamics is crucial in order to capture the evolution of the outlet glaciers in response to oceanic perturbations at the interior of the ice shelf cavity. In addition, an accurate representation of this ice-ocean interaction would require the computation of the ocean circulation at the interior of the ice shelf cavity. As the ocean properties change and the ice cavity draft varies due the retreat of the glaciers, the ocean circulation in contact with the ice shelf evolves, impacting the melting of ice.

Among the consequences of the AIS imbalance in the ocean properties and climate, the larger concern is mainly associated to the sea level rise. Even if AIS contributes with only 10% to the ongoing sea level rising rate, the rapid acceleration of the Amundsen sector and its strong potential contribution of about 1 meter by the end of the current century make necessary a better representation of AIS changes in climate projections. However, concerns about AIS imbalance are not restricted to sea level rise. Consequences of the AIS imbalance in forthcoming future climate might potentially include significant changes in the sea ice cover and the bottom water production due to salinity changes induced by the increasing glacier freshwater fluxes. The potential role of AIS in the future properties of the Southern Ocean, and the ability of future ice-sheet/ocean coupled models to capture the ice-ocean interactions needs however further investigations.

In this thesis, a number of modeling studies have been performed in the context of upcoming ice-sheet/ocean coupled models. These studies aim at better understanding the causes and the consequences of the AIS imbalance in standalone components of future coupled systems. Before studying the technical issues related to the oncoming coupling of both models, this thesis identifies the axes of developments and the capacities of the future set up of both standalone models. In particular, ocean simulations have been used to investigate the response of a global ocean/sea-ice model at quarter degree of resolution (set up of NEMO ocean model in some of the future CMIP6 models) to realistic changes in the glacial freshwater forcing from Antarctica. To this end, further technical work has been needed in order to force the ocean model with a realistic representation and distribution (both seasonal and spatial) of the glacial freshwater fluxes. In addition, ice-sheet simulations have been used to study the sensitivity of the ocean-driven grounding line retreats to different friction laws or englacial stress approximations to be considered

in the ice-sheet models. This has been studied in the context of the MISMIP+ exercise for an idealized geometry corresponding to the characteristics of Pine Island Glacier.

# 2 Main conclusions and perspectives of the different studies

When this work started, two modeling studies had investigated the sensitivity of the Antarctic sea ice to changes in the glacial freshwater fluxes (Bintanja et al., 2013; Swart and Fyfe, 2013). Both of these studies, together with a more recent similar one (Pauling et al., 2016), show limitations as to their distribution of glacial freshwater fluxes and perturbations, which are weakly constrained by observations. Motivated by similar questions, we have here paid a great attention to use the more realistic representation of the freshwater fluxes as possible, as close as it would be in the future ice-sheet/ocean coupled system. This is the work described in Chapter 2

Based on the state-of-the art of glaciological estimates of ice volume discharge (Depoorter et al., 2013) a set of improvements have been proposed in this work in order to improve the glacial freshwater forcing. Firstly, larger ice shelves have been identified in the global ORCA025 grid of NEMO, where the corresponding estimates of basal ice shelf meltwater have been applied. This is expected to improve the spatial distribution of the freshwater fluxes corresponding to the basal melting of the ice shelves. The improvements in the distribution of the ice shelf basal melting is combined with the inclusion of an iceberg model in order to distribute the meltwater produced by the drift of icebergs around the Southern Ocean. The calving rates extracted from Depoorter et al. (2013) are applied into a reviewed version of the NEMO/ICB iceberg model (Marsh et al., 2015a). This reviewed version firstly introduced in this study consists in considering the vertically average ocean velocity in the computation of the iceberg dynamics, the vertical integration of the melt rates along the iceberg thickness, and a simple interaction with a shallow bathymetry. Chapter 2 shows the sensitivity of the modeled icebergs to the inclusion of theses modifications, in particular to the consideration of the averaged ocean velocity onto the computation of the ocean drag in the icebergs. This practice, instead of only considering ocean surface velocities as it was globally applied in iceberg models, improves the representation of iceberg trajectories in the sub-polar gyres, as supported by satellite observations of small icebergs from Tournadre and Accensi (2015).

Our study confirms the strong seasonality of the meltwater fluxes from the Antarctic icebergs and the particular spatial pattern of those fluxes around the Southern Ocean. Indeed, almost half of the freshwater released by icebergs in the Ross and the Amundsen sector occurs between January and February. However, the seasonality of the Indian sector seems to be slightly shifted with respect to other oceanic sectors. In general, Antarctic sea ice seems particularly sensitive to the freshwater fluxes from icebergs, globally increasing in concentration and thickness.

This may be the effect of the extra freshwater released in the ocean surface, which contributes to limit the convective heat supply from the warmer sub-surface ocean to the ocean surface, therefore resulting in more sea ice volume. Surprisingly, the inclusion of icebergs results in thinner sea ice in the Bellinghaussen Sea, probably due to the surface advection of warm waters along the Antarctic Coastal Current from the Antarctic Peninsula.

These results illustrate the importance of including iceberg meltwater in the study of the Antarctic sea ice, and therefore should be considered in the upcoming ice-sheet/ocean coupled models. The explicit representation of icebergs in ocean simulations should consider our proposed modifications relative to the inclusion of more vertical physics in the computation of the thermodynamics and the dynamics of icebergs. The extra computation cost of running an iceberg model can be drastically reduced by forcing the ocean surface with the monthly climatology of iceberg meltwater proposed in Chapter 2. It has been shown that almost similar results can be achieved by using this forcing strategy instead of explicitly coupling with the iceberg model, however, further work is needed in order to adapt this forcing strategy to climate simulations. For instance, in absence of an iceberg model, the estimates of calving rates produced by an ice-sheet model could be used in order to modify interactively a normalized distribution of icebergs meltwater fluxes. At a given ocean grid point, the fraction of meltwater melted from icebergs released from a particular region of AIS can be adapted accordingly to the changes in the iceberg production of this particular region of AIS. This set up requires a preliminary estimate of the fraction of meltwater flux coming from each individual Antarctic sector. This information, having already been produced, will be used in a study in the forthcoming months.

Based on the technical work concerning the construction of a realistic glacial freshwater forcing for ocean models (see Chapter 2), a set of NEMO ocean model sensitivity experiments have been carried out in Chapter 3 in order to study the impact of the AIS imbalance on the Antarctic sea ice. Based on estimates of the Antarctic ice shelf volume losses of the 2000s decade (Depoorter et al., 2013) and average estimates of the dynamical mass losses by the Antarctic glaciers during the last two decades (Shepherd et al., 2012), we propose a reconstructed scenario of the Antarctic ice shelf volume losses corresponding to a stable interaction of mass exchanges between AIS and the Southern Ocean. This scenario is a reasonable estimate of the lower boundary of the ice shelf-ocean exchanges. In most of ice shelves it is likely corresponding to the situation of ice shelves at the beginning of the 90s, when the AIS was believed to be more or less in mass equilibrium. The comparison between the Antarctic ice shelf volume losses of the 2000s decade and our resconstructed scenario based on our hypothesis, correspond therefore to a maximal but reasonable boundary for a decadal perturbation of the glacial freshwater fluxes released into the Southern Ocean. We conclude that the comparison between these two scenarios is appropriate for estimating the potential role of the increasing glacial freshwater release in the ongoing changes of the Antarctic sea ice.

The two scenarios of Antarctic ice mass release to the ocean have been tested

with 30-year long ocean/sea-ice/iceberg coupled model simulation forced with the inter annual atmospheric forcing DFS5.2 for the period (1979-2010). A third simulation has been performed with a ten years shift (1969-2000) in the atmospheric conditions in order to compare the sea ice sensitivity to glacial freshwater perturbations with the sea ice sensitivity to perturbations in the atmospheric properties. The three simulations have been used to construct the three corresponding sea ice climatologies over the modeled period and have been used in order to produce the quantification of model sensitivities. Our results confirm a significant potential response of the sea ice to the perturbations in glacial freshwater fluxes as it was discussed in Bintanja et al. (2013) but in larger agreement with the observed spatial distribution of the sea ice trends. Perturbations in glacial freshwater fluxes may potentially impact positively the global sea ice extent by a 25%, and the global annual sea ice volume up to a 50% of the total changes. However, a robust quantification might require the future inclusion of the atmospheric retroactions with the ocean surface, either parametrizing them, or via the coupling with an atmospheric model. The sea-ice/atmospheric surface retroaction, not represented in our atmospheric-forced modeling study, are expected to produced larger sea ice differences between the two perturbed simulations.

In addition, model results present a very distinctive regional response. Glacial freshwater perturbations does not impact significantly the sea ice in the Atlantic sector, but are a potential dominant contributor to sea ice volume changes in the Ross and the West Pacific sectors. This is mostly related to sea ice production changes induced by a reduction in the convective heat supplied from the sub-surface waters reaching the sea ice base as proposed in (Marsland and Wolff, 2001). On the contrary, in Amundsen Sea the glacial freshwater perturbation affects negatively the sea ice production due to a an enhancement of the coastal overturning. This mechanism, proposed previously in the literature (Jacobs et al., 1996) leads to an increase in the oceanic heat from the very warm sub-surface water mass to the ocean surface in the region. This is likely the result of the combination in the Amundsen region of a very warm sub surface due to the intrusion of warm Circumpolar Deep Waters and the strong perturbation introduced in the glacial freshwater fluxes at the coastal grid points.

The results obtained in the Amundsen sector suggest the needs for considering the inclusion of explicit ice shelf cavities in future climate models in order to correctly reproduce the coastal overturning, and the heat and freshwater exchanges at the interior of the ice shelf cavity. Our study has clearly shown the sensitivity of the sea ice model to glacial freshwater perturbation realistically distributed at a model resolution applicable in the future climate models. This sensitivity indicates the importance of an ice sheet model component in order to estimate reasonably the glacial freshwater fluxes to be applied into the ocean. Therefore, a correct representation of the grounding line migration and the ice shelf processes in future ice-sheet/ocean coupled systems would be crucial in order to reduce the uncertainties of sea ice in Southern Ocean projections.

Chapter 4 studies some of this uncertainties related to the set up of ice sheet

model when estimating the volume losses and sea level rise contribution of outlet glaciers. In particular this has been done for an idealized geometry with similar characteristics than Pine Island Glacier, where lateral buttressing is expected to exert an important control in the grounding line stability. More precisely, it has been tested two different friction laws: Weertman and Schoof friction laws, and two different englacial stress approximations: SSA and SSA*, in 100-year long simulations using the Elmer/Ice model. Based on the MISMIP+ set up, the different tests consist in producing grounding line retreats under the action of a prescribed ocean melting function, departing in all simulations from a relatively similar steady state.

According to our results, no significant differences have been founded depending on the SSA or the SSA* approximation applied. However, much more significant differences has been obtained concerning the friction laws tested in the simulations. The use of a relatively less complex Weertman friction law predicts about 50% smaller contribution to sea level rise after the 100 years simulation with respect to the use the more physical-based Schoof friction law. These differences are comparable to the differences related to the coupling of the ice sheet model with an ocean model according to a recent study in a similar glacier geometry (De Rydt and Gudmundsson, 2016). Based on our results we can conclude that friction physics applied in buttressing-driven glaciers like Pine Island might be as important as coupling with an ocean component.

The quantification of this result is subject to the validity of the melting parametrization proposed in the MISMIP+ set up. The prescribed cavity-draft dependent melting function applied in our experimental set up introduces differences in the melting perturbations which affect differently the model simulations based on different friction laws. Basically, the melting parametrization results in the here called *cavity-draft-melting feedback*, which consists in a retroaction between the melting rates and the cavity draft differences between the simulations. Further melting rates are obtained for upstream grounding line positions, therefore resulting in further grounding line retreats and larger melting rates. Therefore it should be stated here that a robust quantification of the friction law sensitivity to the melting perturbation would require further work in the melting rate perturbation to be applied in the simulations in order to reduce the impact of the *cavity-draft-melting feedback*. For instance, it might be considered a melting parametrization providing a fixed total integrated melt rate, which could be independent on the cavity draft at any time-step during the grounding line retreat. This could be easily achieved by introducing an optimization parameter to be iteratively determined at any time-step in order to match the prefixed integrated melt rate at the interior of the ice shelf cavity.

In any case, it has been shown by studying the *melting efficiency coefficient* that Schoof-based simulations are strictly more sensitive to melting perturbations than the Weertman-based one. Indeed, Coulomb-based friction laws, including the dependence of the basal traction on the effective pressure like in the Schoof friction law, are expected to better account for the smooth transition of the basal

friction in the vicinity of the grounding line, specially in deep marine ice-sheet glaciers. In addition, this friction law could be combined with more sophisticated hydrological systems, which is not possible in Weertman friction laws as there are not any explicit dependence on the effective pressure. Therefore, future ice-sheet models in the coupled systems should consider the use of a Coulomb-type friction laws, differently than it has been widely practiced in most of sea level rise estimates (Favier et al., 2014; Joughin et al., 2014).

The obtained strong sensitivity of the grounding line migration when applying an effective pressure-based friction law suggests that more effort should be considered in the improvements of the representation of the basal interactions of the glacier with hydrological systems. It would be interesting to study the sensitivity of the glacier dynamics to changes in the basal hydrology of the glacier in this particular set up. This is the objective of a new model inter-comparison exercise in a completely different experimental set up namely Subglacial Hydrology Model Inter-Comparison (SHMIP). Performing these tests in our particular set up would require further investigations in order to understand the expected magnitude of the changes in the basal hydrology of the Antarctic outlet glaciers, and how this will impact the glacier dynamics As shown above, according to our results, there are still large uncertainities in the estimation of the grounding line migration and the ice volume losses of the marine-ice-sheets related to the interactions of glaciers with the unknown basal conditions beneath the glaciers.

# 3 Thesis conclusion

In conclusion, accurate projections of the Antarctic Polar Region for the next century will require of ice-sheet/ocean coupled systems. This thesis has shown that further developments is needed in the standalone components of the future coupled systems in order to represent the complexity of the different ice-ocean interactions. Apart from the widely regarded sea level rise, the Antarctic Ice Sheet may have a strong potential impact on setting the sea ice cover in the Southern Ocean. This is related to changes in the ocean surface salinity associated with an increase of the ice volume discharge by the outlet glaciers. As shown in Chapter 3, sea ice cover is being likely affected by the ongoing AIS imbalance, and this interaction is likely to continue increasing according to the projections of further AIS mass losses during the current century. According to our results, the future ocean/sea-ice components of climate models will be sensitive to these glacial freshwater changes introduced by the ice-sheet models. However, the ability of future ocean/sea-ice models to account for these changes will depend on an accurate representation of the glacial freshwater sources. For instance, the mechanisms producing sea ice volume reduction in the Amundsen sector, the largest contributor of glacial freshwater fluxes, may need an explicit representation of the ice shelf cavities in order to accurately account for the ice shelf overturning, heat and freshwater exchanges. In addition, the offshore repartition of the glacial meltwater from icebergs requires further im-

provements to include the physical interactions of icebergs with the ocean column as proposed in (Merino et al., 2016). However, in future ice-sheet/ocean coupled systems, projections of sea ice cover in the Southern Ocean will not be only controlled by the modeling of oceanic processes, but also affected by the ability of the ice-sheet model component in reproducing grounding line migrations and ice shelf processes. To achieved that, based on our sensitivity simulations with Elmer/Ice model, further development in the glacier basal interactions with the bedrock and the hydrological system should be considered by the ice-sheet modeling community. Chapter 4 shows that improvements in the basal physics of marine-ice sheet glaciers might be as crucial as the coupling with ocean component in glaciers projections like in Pine Island. These conclusions underlines that, in future climate systems, uncertainties of the grounding line dynamics of marine-ice sheet may not only contribute to uncertainties of future sea level, but also to the of Antarctic sea ice cover estimates.

Appendix A

# Short description of the numerical tools

Contents



This Appendix aims at presenting the configurations and parametrizations used in the numerical simulations performed in Chapters 2, 3 and 4. Far from being a thorough and comprehensive deep description and a complete description of the model capabilities, this present section of my thesis manuscript provides the elements to understand the different model characteristics in the context of the studies carried out during my three years of work. Interested readers may find more information about NEMO and Elmer/Ice in the corresponding manuals (Madec, 2008; Gagliardini et al., 2013).

## 1 Generalities of NEMO and OPA

Ocean simulations of this thesis have been carried out with the Nucleus for European Modeling of the Ocean (NEMO) (Madec et al., 2015). NEMO basically consists in a framework of different engines related to the ocean. The ocean engine, namely OPA, may be combined with the sea ice model (LIM) (Vancoppenolle et al., 2012), and TOP model for the biogeochemistry tracers (unused in this work)

OPA computes the ocean dynamics and thermodynamics by solving a set of primitive equations with a centered second-order finite difference approximation scheme. Basically, primitive equations consider the Navier-Stokes equations with a state equation for the density based on (Jackett and McDougall, 1997) and two equations for the active tracers, the temperature and the salinity. By definition of the primitive equations, OPA model computes the conservation of the mass, the momentum, the heat and the salinity. However, a few of assumptions are considered in order to simplify the resolution of the primitive equations:

- The gravity potential of the Earth is assumed to be parallel to the earth radius (*spherical earth approximation*).
- The ocean depth is neglected compared to the earth's radius (*thin-shell approximation*).
- The turbulent fluxes are parametrized with large scale variables (*turbulent closure hypothesis*).
- Changes in density are only applied in the computation of the bouyancy force, otherwise, density is kept constant (*Boussinesq approximation*).
- Vertical momentum equation is restricted to a balance between vertical pressure gradient and the buoyancy force, so convective processes should be parametrized (*Hydrostatic hypothesis*).
- Divergence of the velocity vector is zero *(incompressibility hypothesis*).

NEMO contains a vast number of parametrizations and numerical features that we will not explain in detail here. Here we will just refer to the parametrizations and aspects of the simulations particularly relevant to the simulations performed during this thesis. Interested reader will find a deeper description of the model, governing equations, lateral boundaries, surface fluxes, vertical discretization, subgrid parametrizations, time and space domain, or tracers dynamics in the NEMO book (Madec, 2008).

## 1.1 NEMO in the context of this work

The ocean model experiments corresponding to Chapters 2 and 3 of this present manuscript have been carried out with a particular set up based on NEMO v3.5. The OPA ocean component has been coupled with the LIM2 sea ice model and NEMO/ICB iceberg model, and forced by the Drakkar Forcing Set DFS5.2, mostly based on ERA-Interim reanalysis (Dee et al., 2011a).

In NEMO, the position of all scalars and vectors is defined in an orthogonal grid (i,j,k) function of the geospatial coordinates, longitude and latitude, and the ocean depth respectively. The model equations are solved into a global ocean domain based on the ORCA family. The ORCA grid is a global tripolar grid domain based on the semi-analytic method of Madec and Imbard (1996). It is specifically designed to avoid the presence of singularities in the computational domain. The singularity of the south pole is maintained since it is founded in the Antarctic land, in contrast to the north pole singularity, which is founded in the middle of the Arctic Ocean, is avoided by creating two mesh north poles in land (at Canada and Siberia). The resulting mesh is continuous in the mesh lines and in the scale factors over the whole ocean domain, and therefore there is no needs of composite mesh. In this work we will use the version ORCA025 with 0.25 degree of resolution at the equator, and 75 vertical levels. The vertical discretization considers predefined levels at constant

depths with the exception of the bottom levels where depth is free to vary as a function of the location. This is known as z-coordinates with partial step and it allows a better representation of small slopes and geostrophic circulation (Barnier, 2006; Penduff et al., 2007).

A list of particular physical parametrization has been chosen in our simulations. Some of the main parameters used in the ocean simulations performed during this thesis are specified in table A.1. A TKE (Turbulent Kinetic Energie) scheme (Madec, 2008) is used for the vertical diffusion and eddy viscosity. It is based on a prognostic equation for the turbulent kinetic energy and some assumptions, so no extra equations are needed. A BBL (Bottom Boundary Layer) parametrization is applied in order to improve the overflows formation by limiting the spurious vertical mixing in the big slopes of the ocean domain when working in z-coordinates. For the ice shelves, since ORCA025 does not consider explicitly the ice shelves cavities, the ISF parametrisation is applied for the Antarctic ice shelves. This is applied to the grid points adjacent to the ice shelf front in order to parametrize the ocean recirculation created at the interior of the ice shelves cavities. It consist in distributing following the vertical axis the ice shelf melt water flux between the grounding line depth and the calving front depth of a particular ice shelf. The subsequent buoyancy fluxes associated to the locally modified salinity and temperature, emulate (as shown by Pierre Mathiot, personal communication) the coastal recirculation created at the interior of the ice shelves cavities.

| Key | Property | Value |
|---|---|---|
| rn_rdt | time-step for the dynamics (s) | 1080 |
| nn_fsbc | frequency of surface boundary condition computation | 1 |
| rn_avt_rnf | value of the additional vertical mixing coefficient (m2/s) | 2.e-3 |
| rn_deds | magnitude of the damping on salinity (mm/day) | -116.667 |
| nn_bfr | type of bottom friction (0:free-slip, 1:linear friction, 2: non-linear) | 2 |
| rn_bfri2 | bottom drag coefficient | 1e-3 |
| rn_bfeb2 | bottom turbulent kinetic energy background (m2/s2) | 2.5 e-3 |
| rn_ahtbbl | lateral mixing coefficient in the bbl (m2/s) | 1000. |
| rn_gambbl | advective bbl coefficient | 10. |
| rn_aht_0 | horizontal eddy diffusivity for tracers (m2/s) | 300. |
| rn_ahm_0_blp | horizontal bilaplacian eddy viscosity (m4/s) | -1.1e11 |
| rn_avm0 | vertical eddy viscosity (m2/s) | 1.e-4 |
| rn_avt0 | vertical eddy diffusivity (m2/s) | 1.e-5 |
| rn_avevd | enhanced vertical diffusion mixing coefficient | 10. |
| rn_ediff | vertical eddy coefficient | 0.1 |
| rn_ediss | coefficient of the Kolmogoroff dissipation | 0.7 |
| rn_ebb | coefficient of the surface input of tke | 67.83 |
| rn_ebbice | coefficient of the surface input of tke under ice | 67.83 |
| rn_emin | minimum value of tke (m2/s2) | 1e-6 |
| rn_emin0 | surface minimum value of tke (m2/s2) | 1e-4 |
| rn_efr | background shear | 1e-20 |
| rn_bshear | fraction of surface tke value which penetrates below the Mixed Layer | 0.05 |
| nn_htau | type of exponential decrease of tke penetration below the ML | 1 |

Table A.1: Main values of the NEMO namelist properties used in the NEMO ocean model simulations performed in this work

Sea ice is modeled with the LIM2 version of the Louvain-la-Neuve Sea Ice Model (LIM). LIM2 is a relatively high in complexity thermodynamic-dynamic three layer sea ice model, two for the ice and one for the snow. The sea ice model interacts with the ocean model through exchanges of freshwater heat and momentum at the ocean-ice boundary. It also interacts with the atmosphere through the solar radiation, temperature or wind stress. More numerical and physical details can be

founded in Fichefet and Maqueda (1997). The more recent version of LIM model, LIM3, which accounts for an arbitrary number of categories and layers of sea ice, provides more complex physical description than LIM2. However, at the beginning of this thesis, modelling the Antarctic sea ice with LIM3 had not provided yet better results than LIM2 version, and the use of LIM3 was dismissed due to the extra complexity related to the tuning a new sea ice model.

### 1.1.1 An improved version of NEMO/ICB model

OPA and LIM2 are additionally coupled in this work with the NEMO/ICB iceberg model (Marsh et al., 2015a). NEMO/ICB is the implemented version for NEMO of the iceberg Lagrangian particle model described in Martin and Adcroft (2010), which is a reviewed version of the version from Gladstone (2001) Gladstone 2001, based on Bigg et al. (1997).

NEMO/ICB considers Lagrangian particles (representing a collection of icebergs) floating over the ocean and released from a constant and discrete number of predefined locations. The model computes the dynamics and the thermodynamics of the icebergs based on interactions with the ocean, the sea ice, and the atmospheric variables at a given time step. As a result, a given iceberg may eventually release freshwater at a given location of the ocean domain surface. Along their trajectories, icebergs reduce their volume by melting until they completely disappeared and are removed from the ocean domain. The model considers ten types of icebergs depending on their initial volume. Size categories are predefined according to observational work from Gladstone (2001). At a given location, every time step, a fixed percentage of user-defined calving mass rate is assigned to each iceberg category according again to observations from Gladstone (2001). When each category of icebergs have stored enough ice to form a Lagrangian particle of this particular category, the iceberg is released into the ocean. Equations of the iceberg dynamics and thermodynamics (Martin and Adcroft, 2010) are applied prognostically at the end of every ocean time step. Icebergs only interacts with the ocean by changing the salinity of a particular surface grid cell, and there is no impact on the ocean dynamics or volume nor in the sea ice concentration due to the presence of icebergs.

At the beginning of this work, all the iceberg models (Bigg et al., 1997; Gladstone, 2001; Martin and Adcroft, 2010), were based on physical equations only interacting with the ocean surface. However, the thickness of the icebergs, up to 250m thick in some iceberg categories, and the relatively strong vertical gradients in temperature and ocean velocities in the Southern Ocean, very marked at some periods of the year when there are shallower mixed layers, suggest the need for the inclusion of more realistic interaction with the ocean column. Motivated by the study described in Chapter 3 of this manuscript, a set of physical improvements have been developed for the first time in iceberg modeling. They consist in:

- Consider a depth-integrated ocean velocity for the iceberg dynamics computation.

- Depth integration of the melting rates equation.
- Implement a simplified parametrization in order to account for the interaction of icebergs with the shallow bathymetry.

Those modifications are widely explained in section 2.3 of this thesis.

### 1.2 Limitations of NEMO

Some of the processes of the polar regions are currently not well represented in global ocean models. This is in part due to that the biggest efforts in the development of a global models are commonly focused in reproduce the main global circulation, the gulf stream, and equatorial processes. Here in this section we list some of the limitations of ocean models and NEMO in particular in the polar region.

Even if the resolution decrease with latitude in the NEMO ORCA grid, the Rosby deformation radius at the Antarctic region is of about 5km, and resolution of ORCA025 can not fully capture the transport and stirring processes associated to the eddies over the Antarctic shelf.

Forced simulations with NEMO need the use of a salinity restoring term in the ocean surface. This is in order to limit the appearance of a salinity drift in long forced simulations. However, the restoring term can be very strong in regions where surface salinity is weakly constrained by observations, which eventually may affect the brine rejection in the polynias and therefore the dense water formation.

NEMO has shown problems in producing bottom waters, in particular through the descent of dense waters along the oceanic slopes (Hervieux, 2007; Treguier et al., 2010). The BBL parametrization improves the formation of AABW, but the spurious vertical mixing related to the use of Z-coordinates is still too strong, and bottom waters are not dense enough as suggested by observations. This is one of the main reasons of not having studied in this thesis the recent observed trends in the freshening of the AABW

Distribution of the Antarctic glacial freshwater in the ORCA configurations is not well constrained by observations and recent estimates. The corresponding fluxes of the melting of the ice shelves and icebergs are homogeneously spread around the Antarctic coastline in the ORCA025 configuration in most of cases. However, as shown in the introduction Chapter 1, the basal melting of the ice shelves presents a very distinctive pattern with most of it located in the Pacific sector. Icebergs fluxes also present a very distinctive seasonal and spatial pattern as suggested by recent observational studies (Tournadre et al., 2015). The improvement in the distribution of the glacial freshwater fluxes is one of the objectives of this present work, and it is described and motivated in Chapter 2 of this manuscript.

## 2 Elmer/Ice

All the Ice sheet simulations in this thesis have been performed with the ice-sheet model Elmer/Ice. Elmer/Ice is a layer of specific routines for glaciological prob-

lems working over a global open-source, parallel, finite elements framework namely Elmer, mainly developed by CSC group in Finland (Malinen and Råback, 2013). Among its capabilities, we can find solvers for most of glaciological modeling problems such as the ice dynamics, thermal-mechanical coupling, fabric, ice age, hydrology ..., being one the most prolific models in the glaciological community.

Elmer/Ice allows to solve the main ice dynamics equations, such as full Stokes for three-dimensional problems with different rheologies (Glen's flow, porous-compressible ice/firn/snow, anisotropic ice with fabric ...), and the Shallow Ice Approximation (SIA), Shallow Shelf Approximation (SSA), and the SSA* approximation (Cornford et al., 2013) for two-dimensional problems. In combination, the Elmer/Ice proposes different friction parametrizations of different complexity: linear friction, non-linear power-type friction law (Weertman) or non-linear effective pressure dependent Coulomb-type friction laws, such as Schoof or Budd friction laws.

Elmer/Ice has strongly contributed to the grounding line migration research, showing good capabilities in reproducing the grounding line dynamics for different problems and model inter-comparison projects (Pattyn et al., 2012, 2013) In particular, it has been successfully applied for ice dynamics problems in Antarctica (Fürst et al., 2016), Greenland (Gillet-Chaulet et al., 2012) and Pine Island in the Amundsen sector (Favier et al., 2014). And this is why Elmer/Ice fits perfectly in the context of my thesis.

## 2.1 Elmer/Ice in the context of this work

Various set up for Elmer have been tested in Chapter 4 by combining two types of friction laws and two types of englacial stress approximations for horizontal two-dimensional problems. Here in this section we will see an overview of the main particularities of the Elmer/Ice set up applied in solving the ice-sheet problems of this thesis.

### 2.1.1 Workflow of 2-horizontal-dimension problems

All the simulations performed in Chapter 4 present the same workflow (shown in Figure A.1). Here we explain the generalities of the workflow of Elmer/Ice model for two-horizontal-dimension problems.

First of all, we initialize the problem, which is simply constrained by a bedrock topography, the initial thickness of the glacier, an accumulation rate at the surface, the melting ablation at the bottom surface, and the boundary conditions. After initialization, the main time loop starts by solving the flotation of the glacier, which is constrained by the bedrock topography and the glacier thickness. The flotation criteria redefines the surface elevation of the glacier, the bottom surface of the glacier and the grounding line position. In our two-dimensional problems, the grounding line is computed based on the *hydrostatic approximation* instead of solving the namely "contact problem" as it is the case in full-Stokes simulations. This means that for SSA or SSA* simulations, the flotation condition completely determines

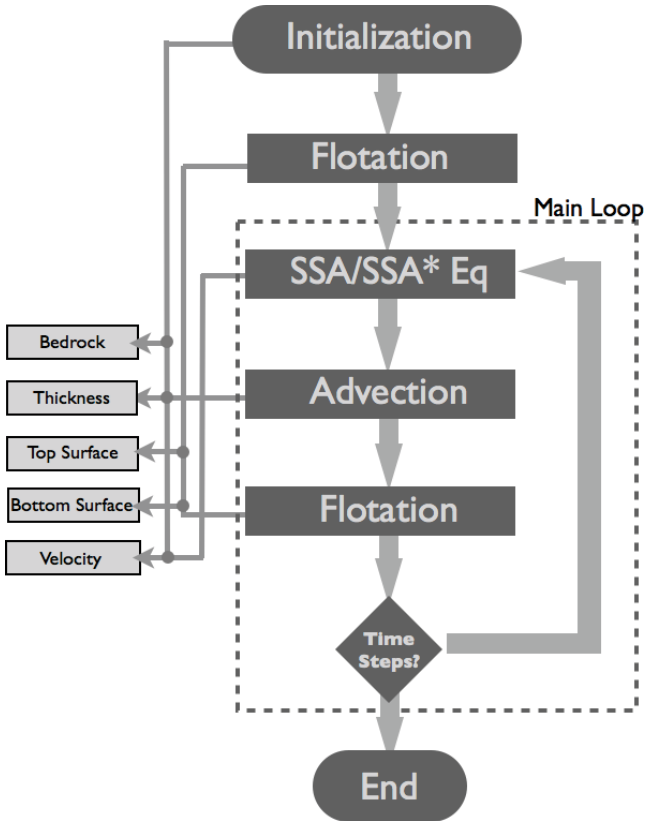


Figure A.1: Workflow corresponding to the two-horizontal-dimension problems solved in this work with Elmer/Ice model. Dark grey square boxes correspond to the different solvers, light grey boxes are the related variables modified by the solvers, dashed line limit the solvers at the interior of the main time loop.

which parts of the glacier are in contact or not with the bedrock. In full Stokes, since the vertical stresses are explicitly computed, the definition of the grounding line consists in evaluate the nodal forces exerted by the glacier and ocean force due to the sea pressure at the base of the glacier. Once the glacier is in hydrostatic balance, the ice dynamics is solved in order to compute the ice velocity. Ice dynamics solver considers an englacial stress approximation, either SSA or SSA* in our case, and the friction law at the grounded part of the bottom boundary of the glacier. In Elmer/Ice, in addition, a sub-element grounding line parametrization is used for the friction at the grounding line, which is shown to reduce the needs for element size resolution at the grounding line. This is based on the SEP3 parametrization proposed in Seroussi et al. (2014). Once the velocity field is obtained, the ice advection is solved and the ice thickness of the glacier is recomputed. If there are still time-steps to be computed, the simulation continue in the main loop, starting with the application of the hydrostatic condition.

### 2.1.2 Ice advection

Solving an advection-diffussion equation in finite elements is a recurrent problem in the literature. The application of the common Galerkin Finite Elments Method (GFEM) to advection equation results in a similar discrete expression than *central differencing* in Finite Differences Method. It can be demonstrate that *central differencing* schemes introduce truncation errors in time dependent solutions of the advection equation, which leads into spurious node to node oscillations. Solving the ice advection in Elmer/Ice needs therefore a modification of the advection scheme when solving transient problems.

There are in the bibliography various classical solutions to this problem in Finite Element Method. For instance, the Petrov-Galerkin formulation (Hughes et al., 1986) consists in changing the form of the *weight functions* with respect to the *shape functions*. In the GFEM formulation both functions are similar, which in advection problems, leads to the mentioned *central-differencing* character of the GFEM. The case of modifying the weight functions with the called *bubbles functions* is known in the literature as the Bubbles Method (Franca and Farhat, 1995). This has been implemented in most of the advective solvers of Elmer/Ice. Another solution for the instabilities is the namely Streamline Upwind Petrov Galerkin (SUPG) stabilization (Brooks and Hughes, 1982), which is based on the introduction of a particular residual-based stabilization term in the standar GFEM formulation. Basically, this term adds virtual diffusivity to the advection equation wherever the residual is expected large and the truncation errors are expected to be important. The utility of the stabilization term depends on a stabilization parameter $\tau$ which can be defined differently depending on the problem considered. The SUPG stabilization is also commonly implemented in advective solvers of Elmer/Ice. In Chapter 4, since Bubbles method appears not to perform well in this kind of rapid grounding line retreat simulations, we have applied a particular version of SUPG. This scheme, firstly implemented in Elmer/ice for the simulations of Chapter 4, consist in following

definition of $\tau$, based in Akin and Tezduyar (2004):

$$\tau_{UGN} = (\sum_{a=1}^{nodes} |\vec{v}^h \cdot \vec{\nabla}\vec{N}_a|)^2 + (\frac{2}{\alpha\Delta t})^2)^{-1/2} \tag{A.1}$$

where $\vec{v}^h$ is the ice velocity field, $\vec{\nabla}\vec{N}_a$ is the gradient of the interpolation function at each node, $\Delta t$ is the time-step and $\alpha$ is a control parameter introduced in my simulations. Parameter $\alpha$ controls the balance between the advection-dominated and the transient-dominated limits as defined in (Akin and Tezduyar, 2004). This helps the stabilization term to perform at the same time in the fastest parts of the glacier, where an advection-dominated limit works fine, and the inland boundary of the glacier where the advection-dominated limit gives instabilities due to the extremely low velocities The value of alpha for the simulations of this thesis has been determined empirically by a set of transient simulations, resulting in the value of $\alpha = 10^{-3}$.

Appendix B

# Source points of the iceberg Model

This Appendix contains the location and calving rates of the source points considered by our version of NEMO-ICB model. Those points are based on the calving fluxes distribution proposed in Depoorter et al. (2013) and have been used in the ocean simulations performed in Chapters 2 and 3

| Source Point | Latitude (°) | Longitude (°) | Calving Rate (Gt/yr) |
|---|---|---|---|
| 1 | -76.95 | 167.75 | 2.33 |
| 2 | -76.95 | 174.5 | 28.49 |
| 3 | -76.95 | 179.75 | 28.49 |
| 4 | -76.95 | -179.25 | 2.33 |
| 5 | -76.95 | -175 | 28.49 |
| 6 | -76.95 | -169.75 | 28.49 |
| 7 | -76.95 | -166.25 | 2.33 |
| 8 | -76.95 | -164.5 | 33.05 |
| 9 | -76.95 | -153.25 | 2.33 |
| 10 | -76.95 | -152.25 | 1.50 |
| 11 | -76.95 | -44.25 | 1.77 |
| 12 | -76.95 | -41.25 | 32.52 |
| 13 | -76.95 | -38.5 | 38.62 |
| 14 | -76.84 | -51.75 | 44.72 |
| 15 | -76.84 | -29.75 | 1.77 |
| 16 | -76.67 | -150.75 | 1.50 |
| 17 | -76.32 | -54 | 44.72 |
| 18 | -76.08 | -55.5 | 1.77 |
| 19 | -75.84 | -56.5 | 44.72 |
| 20 | -75.71 | -25 | 9.20 |
| 21 | -75.65 | 164.5 | 1.50 |
| 22 | -75.65 | 164.75 | 2.33 |
| 23 | -75.47 | -141.5 | 11.00 |
| 24 | -75.47 | -59.5 | 44.72 |
| 25 | -75.34 | 164.75 | 1.50 |
| 26 | -75.15 | -24.25 | 1.77 |

| | | | |
|---|---|---|---|
| 27 | -74.96 | -24.5 | 9.20 |
| 28 | -74.89 | -109.5 | 12.32 |
| 29 | -74.89 | -101.75 | 6.80 |
| 30 | -74.76 | -105.75 | 62.00 |
| 31 | -74.69 | -136 | 6.80 |
| 32 | -74.63 | -109.75 | 6.80 |
| 33 | -74.56 | -102.25 | 50.00 |
| 34 | -74.36 | -21.75 | 9.20 |
| 35 | -74.29 | -132 | 15.59 |
| 36 | -74.22 | -129 | 15.59 |
| 37 | -74.16 | -112.5 | 5.68 |
| 38 | -74.02 | -61 | 1.77 |
| 39 | -73.95 | -118.25 | 8.51 |
| 40 | -73.95 | -115.75 | 5.67 |
| 41 | -73.88 | -118.5 | 6.80 |
| 42 | -73.81 | -120.25 | 2.84 |
| 43 | -73.74 | 167 | 2.33 |
| 44 | -73.67 | -124.25 | 7.80 |
| 45 | -73.46 | -127.5 | 6.80 |
| 46 | -73.46 | -101.75 | 2.00 |
| 47 | -73.39 | -19.75 | 9.20 |
| 48 | -73.24 | -84.5 | 1.24 |
| 49 | -73.03 | -73 | 3.50 |
| 50 | -72.88 | -86.5 | 8.00 |
| 51 | -72.81 | -79 | 0.67 |
| 52 | -72.81 | -18.75 | 1.77 |
| 53 | -72.66 | -16.75 | 9.20 |
| 54 | -72.58 | -76.5 | 1.67 |
| 55 | -72.51 | -95.5 | 1.37 |
| 56 | -72.51 | -90 | 0.51 |
| 57 | -72.43 | -95.5 | 1.24 |
| 58 | -72.36 | -103.5 | 0.74 |
| 59 | -72.28 | -79 | 1.24 |
| 60 | -72.21 | -74.5 | 1.24 |
| 61 | -72.21 | -73.5 | 1.17 |
| 62 | -71.82 | -97.25 | 1.37 |
| 63 | -71.10 | -73.5 | 3.83 |
| 64 | -70.94 | -10.75 | 1.85 |
| 65 | -70.70 | -75 | 1.24 |
| 66 | -70.53 | -74.5 | 1.83 |
| 67 | -70.53 | -60.5 | 1.77 |
| 68 | -70.53 | -9.25 | 11.18 |
| 69 | -70.36 | -5.75 | 11.18 |
| 70 | -70.28 | 23.75 | 7.29 |

| | | | |
|---|---|---|---|
| 71 | -70.19 | 161.5 | 1.00 |
| 72 | -70.11 | 161 | 12.40 |
| 73 | -70.11 | -2 | 11.64 |
| 74 | -70.11 | 23.25 | 5.32 |
| 75 | -69.94 | 6.25 | 7.29 |
| 76 | -69.94 | 11 | 7.29 |
| 77 | -69.85 | 19.25 | 7.29 |
| 78 | -69.85 | 28.25 | 7.56 |
| 79 | -69.77 | 12.75 | 5.32 |
| 80 | -69.68 | -69 | 2.33 |
| 81 | -69.50 | -72.5 | 2.00 |
| 82 | -69.50 | 37 | 6.79 |
| 83 | -69.50 | 39.5 | 5.32 |
| 84 | -69.33 | 73.5 | 19.70 |
| 85 | -69.33 | 15 | 7.29 |
| 86 | -69.15 | 33 | 5.32 |
| 87 | -69.06 | 35.75 | 6.79 |
| 88 | -68.79 | -67.5 | 2.00 |
| 89 | -68.79 | 72 | 30.30 |
| 90 | -68.70 | -70 | 1.24 |
| 91 | -68.52 | 152 | 11.51 |
| 92 | -68.52 | 153 | 32.00 |
| 93 | -68.43 | -59.75 | 12.72 |
| 94 | -68.34 | 78.5 | 5.66 |
| 95 | -67.87 | 148.5 | 23.00 |
| 96 | -67.59 | -69.25 | 1.24 |
| 97 | -67.49 | 63 | 5.32 |
| 98 | -67.30 | 47.5 | 5.32 |
| 99 | -67.30 | 48.5 | 5.36 |
| 100 | -67.10 | -60.5 | 12.28 |
| 101 | -67.01 | 145.75 | 20.00 |
| 102 | -66.91 | 57.25 | 6.43 |
| 103 | -66.81 | 121 | 23.00 |
| 104 | -66.81 | 128.25 | 36.00 |
| 105 | -66.81 | 143 | 11.51 |
| 106 | -66.71 | 81.5 | 10.05 |
| 107 | -66.71 | 50 | 4.64 |
| 108 | -66.61 | 83.25 | 10.05 |
| 109 | -66.61 | 117 | 28.00 |
| 110 | -66.61 | -60.75 | 1.77 |
| 111 | -66.51 | 109.25 | 9.00 |
| 112 | -66.41 | 115 | 11.51 |
| 113 | -66.21 | 86.25 | 10.89 |
| 114 | -66.21 | 106 | 11.51 |

| | | | |
|---|---|---|---|
| 115 | -66.21 | 126 | 11.51 |
| 116 | -66.11 | 82.5 | 6.07 |
| 117 | -65.81 | 54.25 | 5.32 |
| 118 | -65.60 | 99.75 | 11.69 |
| 119 | -65.18 | 95.25 | 11.16 |
| 120 | -65.18 | 134 | 11.51 |
| 121 | -64.97 | 134.5 | 7.00 |
| 122 | -64.65 | 98 | 11.16 |
| 123 | -64.65 | 98.75 | 11.51 |
| 124 | -64.44 | -64.25 | 1.32 |

# Acronyms

**AABW** Antarctic Bottom Waters.

**ACC** Antarctic Circumpolar Current.

**ACoC** Antarctic Coastal Current.

**AIS** Antarctic Ice Sheet.

**AL** Amundsen Low.

**APIS** Antarctic Peninsula Ice Sheet.

**APR** Antarctic Polar Region.

**BMB** Basal Mass Balance.

**CDW** Circumpolar Deep Waters.

**CF** Calving Flux.

**$CO_2$** Carbon Dioxide.

**EAIS** East Antarctica Ice Sheet.

**ENSO** El Ni'no Southern Oscillation.

**GCMs** General Circulation Models.

**GFEM** Galerkin Finite Elments Method.

**GL** Grounding Line.

**GLF** Grounding Line Flux.

**GrIS** Greenland Ice Sheet.

**HSSW** High Salinity Shelf Water.

**IPCC** Intergovernmental Panel in Climate Change.

**ISD** Ice Season Duration.

**MISI** Marine Ice Sheet Instability.

**MISMIP** Marine Ice Sheet Model Inter Comparison Project.

**MISOMIP** Marine Ice Sheet Ocean Model Inter Comparison Project.

**NSDIC** National Snow and Ice Data Center.

**PIG** Pine Island Glacier.

**SAM** Southern Annular Mode.

**SIC** Sea Ice concentration.

**SIE** Sea Ice Extent.

**SLE** Sea Level Equivalent.

**SLR** Sea Level Rise.

**SMB** Surface Mass Balance.

**SO** Southern Ocean.

**SSA** Shallow Shelf Approximation.

**SSH** Sea Surface Height.

**SST** Sea Surface Temperature.

**SUPG** Streamline Upwind Petrov Galerkin.

**VAF** Volume Above Flotation.

**WAIS** West Antarctica Ice Sheet.

# Bibliography


Akin, J. E. and Tezduyar, T. E. (2004). Calculation of the advective limit of the supg stabilization parameter for linear and higher-order elements. *Computer Methods in Applied Mechanics and Engineering*, 193(21):1909–1922. (Cited on page 129.)

Arblaster, J. M. and Meehl, G. A. (2006). Contributions of external forcings to southern annular mode trends. *Journal of climate*, 19(12):2896–2905. (Cited on page 10.)

Armour, K. C., Marshall, J., Scott, J. R., Donohoe, A., and Newsom, E. R. (2016). Southern ocean warming delayed by circumpolar upwelling and equatorward transport. *Nature Geoscience*. (Cited on pages 12 and 14.)

Asay-Davis, X. S., Cornford, S. L., Galton-Fenzi, B. K., Gladstone, R. M., Gudmundsson, G. H., Holland, D. M., Holland, P. R., and Martin, D. F. (2016). Experimental design for three interrelated marine ice sheet and ocean model intercomparison projects: Mismip v. 3 (mismip+), isomip v. 2 (isomip+) and misomip v. 1 (misomip1). *Geoscientific Model Development*, 9(7):2471. (Cited on pages 29, 89, 90, 93, 96, 97 and 110.)

Baines, P. G. and Fraedrich, K. (1989). Topographic effects on the mean tropospheric flow patterns around antarctica. *Journal of the Atmospheric Sciences*, 46(22):3401–3415. (Cited on page 10.)

Bamber, J., Riva, R., and Vermeersen, B. (2008). Reassessment of the potential contribution to sea level from a collapse of the west antarctic ice sheet. In *AGU Fall Meeting Abstracts*, volume 1, page 03. (Cited on page 5.)

Barnier, B. (2006). Impact of partial steps and momentum advection schemes in a global ocean circulation model at eddy permitting resolution. In *MERSEA Annual Science Meeting*, page xx. (Cited on page 123.)

Barrand, N., Vaughan, D., Steiner, N., Tedesco, M., Kuipers Munneke, P., Broeke, M., and Hosking, J. (2013). Trends in antarctic peninsula surface melting conditions from observations and regional climate modeling. *Journal of Geophysical Research: Earth Surface*, 118(1):315–330. (Cited on page 64.)

Beckmann, A., Timmermann, R., Pereira, A. F., and Mohn, C. (2001). The effect of flow at maud rise on the sea-ice cover–numerical experiments. *Ocean Dynamics*, 52(1):11–25. (Cited on page 7.)

Bersch, M., Becker, G. A., Frey, H., and Koltermann, K. P. (1992). Topographic effects of the maud rise on the stratification and circulation of the weddell gyre. *Deep Sea Research Part A. Oceanographic Research Papers*, 39(2):303–331. (Cited on page 7.)

Bertler, N. A., Barrett, P. J., Mayewski, P. A., Fogt, R. L., Kreutz, K. J., and Shulmeister, J. (2004). El nino suppresses antarctic warming. *Geophysical Research Letters*, 31(15). (Cited on page 10.)

Bigg, G. R., Wadley, M. R., Stevens, D. P., and Johnson, J. A. (1997). Modelling the dynamics and thermodynamics of icebergs. *Cold Regions Science and Technology*, 26(2):113–135. (Cited on pages 39, 41, 56 and 124.)

Bindoff, N. L., Stott, P. A., AchutaRao, M., Allen, M. R., Gillett, N., Gutzler, D., Hansingo, K., Hegerl, G., Hu, Y., Jain, S., et al. (2013). Detection and attribution of climate change: from global to regional. (Cited on page 9.)

Bintanja, R., Van Oldenborgh, G., Drijfhout, S., Wouters, B., and Katsman, C. (2013). Important role for ocean warming and increased ice-shelf melt in antarctic sea-ice expansion. *Nature Geoscience*, 6(5):376–379. (Cited on pages 8, 15, 21, 31, 33, 39, 59, 60, 62, 68, 85, 115 and 117.)

Boening, C., Lebsock, M., Landerer, F., and Stephens, G. (2012). Snowfall-driven mass change on the east antarctic ice sheet. *Geophysical Research Letters*, 39(21). (Cited on page 13.)

Broecker, W. S. et al. (1991). The great ocean conveyor. *Oceanography*, 4(2):79–89. (Cited on pages 7 and 18.)

Broeke, M. R., Enderlin, E. M., Howat, I. M., Kuipers Munneke, P., Noël, B. P., Berg, W. J. v. d., Meijgaard, E. v., and Wouters, B. (2016). On the recent contribution of the greenland ice sheet to sea level change. *The Cryosphere*, 10(5):1933–1946. (Cited on page 23.)

Brooks, A. N. and Hughes, T. J. (1982). Streamline upwind/petrov-galerkin formulations for convection dominated flows with particular emphasis on the incompressible navier-stokes equations. *Computer methods in applied mechanics and engineering*, 32(1):199–259. (Cited on page 128.)

Caldeira, K. and Duffy, P. B. (2000). The role of the southern ocean in uptake and storage of anthropogenic carbon dioxide. *Science*, 287(5453):620–622. (Cited on page 6.)

Cassotto, R., Fahnestock, M., Amundson, J. M., Truffer, M., and Joughin, I. (2015). Seasonal and interannual variations in ice melange and its impact on terminus stability, jakobshavn isbræ, greenland. *Journal of Glaciology*, 61(225):76–88. (Cited on page 29.)

Castagno, P., Falco, P., Dinniman, M. S., Spezie, G., and Budillon, G. (2016). Temporal variability of the circumpolar deep water inflow onto the ross sea continental shelf. *Journal of Marine Systems*. (Cited on page 15.)

Cavalieri, D. and Parkinson, C. (2008). Antarctic sea ice variability and trends, 1979–2006. *Journal of Geophysical Research: Oceans*, 113(C7). (Cited on page 12.)

Church, J. A., Clark, P. U., Cazenave, A., Gregory, J. M., Jevrejeva, S., Levermann, A., Merrifield, M. A., Milne, G. A., Nerem, R. S., Nunn, P. D., et al. (2013). Sea level change. Technical report, PM Cambridge University Press. (Cited on page 24.)

Coggins, J., McDonald, A., Rack, W., and Dale, E. (2015). Sea ice trends and cyclone activity in the southern ocean. In *EGU General Assembly Conference Abstracts*, volume 17, page 8833. (Cited on page 20.)

Comiso, J. and Gordon, A. (1987). Recurring polynyas over the cosmonaut sea and the maud rise. *Journal of Geophysical Research: Oceans*, 92(C3):2819–2833. (Not cited.)

Comiso, J. C. (2010). Variability and trends of the global sea ice cover. *Sea ice*, 2:205–246. (Cited on pages 62 and 76.)

Comiso, J. C., Kwok, R., Martin, S., and Gordon, A. L. (2011). Variability and trends in sea ice extent and ice production in the ross sea. *Journal of Geophysical Research: Oceans*, 116(C4). (Cited on pages 12, 19 and 62.)

Comiso, J. C. and Nishio, F. (2008). Trends in the sea-ice cover using enhanced and compatible AMSR-E, SSM/I, and SMMR data. *Journal of Geophysical Research: Oceans*, 113(C2):C02S07. (Cited on page 38.)

Cook, A., Holland, P., Meredith, M., Murray, T., Luckman, A., and Vaughan, D. (2016). Ocean forcing of glacier retreat in the western antarctic peninsula. *Science*, 353(6296):283–286. (Cited on page 15.)

Cook, A. J. and Vaughan, D. G. (2010). Overview of areal changes of the ice shelves on the antarctic peninsula over the past 50 years. *Cryosphere*, 4(1):77–98. (Cited on page 26.)

Cornford, S. L., Martin, D. F., Graves, D. T., Ranken, D. F., Le Brocq, A. M., Gladstone, R. M., Payne, A. J., Ng, E. G., and Lipscomb, W. H. (2013). Adaptive mesh, finite volume modeling of marine ice sheets. *Journal of Computational Physics*, 232(1):529–549. (Cited on pages 29, 91 and 126.)

Couldrey, M. P., Jullion, L., Naveira Garabato, A. C., Rye, C., Herráiz-Borreguero, L., Brown, P. J., Meredith, M. P., and Speer, K. L. (2013). Remotely induced warming of antarctic bottom water in the eastern weddell gyre. *Geophysical Research Letters*, 40(11):2755–2760. (Cited on page 17.)

Curry, J. A., Schramm, J. L., and Ebert, E. E. (1995). Sea ice-albedo climate feedback mechanism. *Journal of Climate*, 8(2):240–247. (Cited on page 7.)

De Rydt, J. and Gudmundsson, G. (2016). Coupled ice shelf-ocean modeling and complex grounding line retreat from a seabed ridge. *Journal of Geophysical Research: Earth Surface*, 121(5):865–880. (Cited on pages 26, 29, 110 and 118.)

De Rydt, J., Holland, P., Dutrieux, P., and Jenkins, A. (2014). Geometric and oceanographic controls on melting beneath pine island glacier. *Journal of Geophysical Research: Oceans*, 119(4):2420–2438. (Cited on pages 26 and 97.)

DeConto, R. M. and Pollard, D. (2016). Contribution of antarctica to past and future sea-level rise. *Nature*, 531(7596):591–597. (Cited on pages 15 and 24.)

Dee, D., Uppala, S., Simmons, A., Berrisford, P., Poli, P., Kobayashi, S., Andrae, U., Balmaseda, M., Balsamo, G., Bauer, P., et al. (2011a). The era-interim reanalysis: Configuration and performance of the data assimilation system. *Quarterly Journal of the royal meteorological society*, 137(656):553–597. (Cited on page 122.)

Dee, D. P., Uppala, S. M., Simmons, A. J., Berrisford, P., Poli, P., Kobayashi, S., Andrae, U., Balmaseda, M. A., Balsamo, G., Bauer, P., Bechtold, P., Beljaars, A. C. M., van de Berg, L., Bidlot, J., Bormann, N., Delsol, C., Dragani, R., Fuentes, M., Geer, A. J., Haimberger, L., Healy, S. B., Hersbach, H., Holm, E. V., Isaksen, L., Kallberg, P., Kohler, M., Matricardi, M., McNally, A. P., Monge-Sanz, B. M., Morcrette, J.-J., Park, B.-K., Peubey, C., de Rosnay, P., Tavolato, C., Thepaut, J.-N., and Vitart, F. (2011b). The ERA-Interim reanalysis: configuration and performance of the data assimilation system. *Quarterly Journal of the Royal Meteorological Society*, 137(656):553–597. (Cited on page 40.)

Depoorter, M., Bamber, J., Griggs, J., Lenaerts, J., Ligtenberg, S., van den Broeke, M., and Moholdt, G. (2013). Calving fluxes and basal melt rates of antarctic ice shelves. *Nature*, 502(7469):89–92. (Cited on pages 25, 34, 35, 36, 39, 43, 44, 55, 57, 63, 66, 67, 68, 115, 116 and 131.)

Dinniman, M. S., Klinck, J. M., Bai, L.-S., Bromwich, D. H., Hines, K. M., and Holland, D. M. (2015). The effect of atmospheric forcing resolution on delivery of ocean heat to the antarctic floating ice shelves*,+. *Journal of Climate*, 28(15):6067–6085. (Cited on page 15.)

Dinniman, M. S., Klinck, J. M., and Hofmann, E. E. (2012). Sensitivity of circumpolar deep water transport and ice shelf basal melt along the west antarctic peninsula to changes in the winds. *Journal of Climate*, 25(14):4799–4816. (Cited on page 15.)

Dinniman, M. S., Klinck, J. M., and Smith, W. O. (2011). A model study of circumpolar deep water on the west antarctic peninsula and ross sea continental shelves. *Deep Sea Research Part II: Topical Studies in Oceanography*, 58(13):1508–1523. (Cited on page 15.)

Dolman, A., Van Der Werf, G., Van Der Molen, M., Ganssen, G., Erisman, J.-W., and Strengers, B. (2010). A carbon cycle science update since ipcc ar-4. *Ambio*, 39(5-6):402–412. (Cited on page 16.)

Doney, S. C., Fabry, V. J., Feely, R. A., and Kleypas, J. A. (2009). Ocean acidification: the other co2 problem. *Marine Science*, 1. (Cited on page 16.)

Dufour, C. O., Le Sommer, J., Zika, J. D., Gehlen, M., Orr, J. C., Mathiot, P., and Barnier, B. (2012). Standing and transient eddies in the response of the southern ocean meridional overturning to the southern annular mode. *Journal of Climate*, 25(20):6958–6974. (Cited on pages 33 and 34.)

Dupont, T. and Alley, R. (2005). Assessment of the importance of ice-shelf buttressing to ice-sheet flow. *Geophysical Research Letters*, 32(4). (Cited on page 27.)

Duprat, L. P., Bigg, G. R., and Wilton, D. J. (2016). Enhanced southern ocean marine productivity due to fertilization by giant icebergs. *Nature Geoscience*. (Cited on page 17.)

Durand, G., Gagliardini, O., Zwinger, T., Le Meur, E., and Hindmarsh, R. C. (2009). Full stokes modeling of marine ice sheets: influence of the grid size. *Annals of Glaciology*, 50(52):109–114. (Cited on page 29.)

Durand, G. and Pattyn, F. (2015). Reducing uncertainties in projections of antarctic ice mass loss. *The Cryosphere*, 9(6):2043–2055. (Cited on page 88.)

Dutrieux, P., De Rydt, J., Jenkins, A., Holland, P. R., Ha, H. K., Lee, S. H., Steig, E. J., Ding, Q., Abrahamsen, E. P., and Schröder, M. (2014). Strong sensitivity of pine island ice-shelf melting to climatic variability. *Science*, 343(6167):174–178. (Cited on page 15.)

Eisenman, I., Meier, W. N., and Norris, J. R. (2014). A spurious jump in the satellite record: has Antarctic sea-ice expansion been overestimated? *The Cryosphere*, 8(4):1289–1296. (Cited on page 38.)

Fahrbach, E., Hoppema, M., Rohardt, G., Boebel, O., Klatt, O., and Wisotzki, A. (2011). Warming of deep and abyssal water masses along the greenwich meridian on decadal time scales: The weddell gyre as a heat buffer. *Deep Sea Research Part II: Topical Studies in Oceanography*, 58(25):2509–2523. (Cited on page 17.)

Fan, T., Deser, C., and Schneider, D. P. (2014). Recent antarctic sea ice trends in the context of southern ocean surface climate variations since 1950. *Geophysical Research Letters*, 41(7):2419–2426. (Cited on pages 10 and 38.)

Favier, L., Durand, G., Cornford, S., Gudmundsson, G., Gagliardini, O., Gillet-Chaulet, F., Zwinger, T., Payne, A., and Le Brocq, A. (2014). Retreat of pine island glacier controlled by marine ice-sheet instability. *Nature Climate Change*, 4(2):117–121. (Cited on pages 27, 29, 89, 110, 119 and 126.)

Ferreira, D., Marshall, J., Bitz, C. M., Solomon, S., and Plumb, A. (2015). Antarctic ocean and sea ice response to ozone depletion: A two-time-scale problem. *Journal of Climate*, 28(3):1206–1226. (Cited on page 19.)

Fichefet, T. and Maqueda, M. (1997). Sensitivity of a global sea ice model to the treatment of ice thermodynamics and dynamics. *Journal of Geophysical Research: Oceans*, 102(C6):12609–12646. (Cited on page 124.)

Fichefet, T. and Morales Maqueda, M. A. M. (1997). Sensitivity of a global sea-ice model to the treatment of ice thermodynamics and dynamics. *Journal of Geophysical Research: Oceans*, 102(C6):12609–12646. (Cited on pages 40 and 63.)

Franca, L. P. and Farhat, C. (1995). Bubble functions prompt unusual stabilized finite element methods. *Computer Methods in Applied Mechanics and Engineering*, 123(1):299–308. (Cited on page 128.)

Fransson, A., Chierici, M., and Torstensson, A. (2014). Ocean acidification state in western antarctic surface waters: controls and interannual variability. (Cited on page 17.)

Fretwell, P., Pritchard, H. D., Vaughan, D. G., Bamber, J., Barrand, N., Bell, R., Bianchi, C., Bingham, R., Blankenship, D., Casassa, G., et al. (2013). Bedmap2: improved ice bed, surface and thickness datasets for antarctica. *The Cryosphere*, 7(1). (Cited on pages 4, 7 and 36.)

Frieler, K., Clark, P. U., He, F., Buizert, C., Reese, R., Ligtenberg, S. R., Van Den Broeke, M. R., Winkelmann, R., and Levermann, A. (2015). Consistent evidence of increasing antarctic accumulation with warming. *Nature Climate Change*, 5(4):348–352. (Cited on page 13.)

Fukasawa, M., Freeland, H., Perkin, R., Watanabe, T., Uchida, H., and Nishina, A. (2004). Bottom water warming in the north pacific ocean. *Nature*, 427(6977):825–827. (Cited on page 18.)

Fürst, J. J., Durand, G., Gillet-Chaulet, F., Tavard, L., Rankl, M., Braun, M., and Gagliardini, O. (2016). The safety band of antarctic ice shelves. *Nature Climate Change*, 6(5):479–482. (Cited on pages 25, 26 and 126.)

Fyfe, J. C., Saenko, O. A., Zickfeld, K., Eby, M., and Weaver, A. J. (2007). The role of poleward-intensifying winds on southern ocean warming. *Journal of Climate*, 20(21):5391–5400. (Cited on page 14.)

Gagliardini, O., Cohen, D., Råback, P., and Zwinger, T. (2007). Finite-element modeling of subglacial cavities and related friction law. *Journal of Geophysical Research: Earth Surface*, 112(F2). (Cited on pages 29, 92 and 93.)

Gagliardini, O., Durand, G., Zwinger, T., Hindmarsh, R., and Le Meur, E. (2010). Coupling of ice-shelf melting and buttressing is a key process in ice-sheets dynamics. *Geophysical Research Letters*, 37(14). (Cited on pages 25 and 67.)

Gagliardini, O., Zwinger, T., Gillet-Chaulet, F., Durand, G., Favier, L., De Fleurian, B., Greve, R., Malinen, M., Martín, C., Råback, P., et al. (2013). Capabilities and performance of elmer/ice, a new-generation ice sheet model. *Geoscientific Model Development*, 6(4):1299–1318. (Cited on page 121.)

Gagne, M.-E., Gillett, N. P., and Fyfe, J. C. (2015). Observed and simulated changes in Antarctic sea-ice extent over the past 50 years. *Geophysical Research Letters*, 42(1):2014GL062231. (Cited on page 38.)

Galton-Fenzi, B. (2010). Modelling the interaction between antarctica and the southern ocean. *Centre for Australian Weather and Climate Research, GPO Box 1289, Melbourne, VIC 3001, Australia*, page 33. (Cited on page 97.)

Gill, A. (1973). Circulation and bottom water production in the weddell sea. In *Deep Sea Research and Oceanographic Abstracts*, volume 20, pages 111–140. Elsevier. (Cited on page 15.)

Gillet-Chaulet, F., Gagliardini, O., Seddik, H., Nodet, M., Durand, G., Ritz, C., Zwinger, T., Greve, R., and Vaughan, D. G. (2012). Greenland ice sheet contribution to sea-level rise from a new-generation ice-sheet model. *The Cryosphere*, 6(6):1561–1576. (Cited on pages 91 and 126.)

Gladstone, R. (2001). *A modelling and remote sensing study of Antarctic icebergs.* PhD thesis, University of East Anglia. (Cited on page 124.)

Gladstone, R. M., Bigg, G. R., and Nicholls, K. W. (2001). Iceberg trajectory modeling and meltwater injection in the southern ocean. *Journal of Geophysical Research: Oceans (1978–2012)*, 106(C9):19903–19915. (Cited on pages 39, 41, 42, 43 and 47.)

Glen, J. W. (1955). The creep of polycrystalline ice. In *Proceedings of the Royal Society of London A: Mathematical, Physical and Engineering Sciences*, volume 228, pages 519–538. The Royal Society. (Cited on page 90.)

Gloersen, P. (1995). Modulation of hemispheric sea-ice cover by enso events. *Nature*, 373(6514):503–506. (Cited on page 20.)

Goldberg, D., Holland, D., and Schoof, C. (2009). Grounding line movement and ice shelf buttressing in marine ice sheets. *Journal of Geophysical Research: Earth Surface*, 114(F4). (Cited on page 27.)

Goldberg, D., Little, C., Sergienko, O., Gnanadesikan, A., Hallberg, R., and Oppenheimer, M. (2012). Investigation of land ice-ocean interaction with a fully coupled ice-ocean model: 1. model description and behavior. *Journal of Geophysical Research: Earth Surface*, 117(F2). (Cited on page 97.)

Goosse, H. and Zunz, V. (2014a). Decadal trends in the antarctic sea ice extent ultimately controlled by ice–ocean feedback. *The Cryosphere*, 8(2):453–470. (Cited on pages 21, 30 and 62.)

Goosse, H. and Zunz, V. (2014b). Decadal trends in the Antarctic sea-ice extent ultimately controlled by ice-ocean feedback. *The Cryosphere*, 8(2):453–470. (Cited on page 38.)

Gordon, A. L. (1978). Deep antarctic convection west of maud rise. *Journal of Physical Oceanography*, 8(4):600–612. (Cited on page 7.)

Gorodetskaya, I. V., Tsukernik, M., Claes, K., Ralph, M. F., Neff, W. D., and Van Lipzig, N. P. (2014). The role of atmospheric rivers in anomalous snow accumulation in east antarctica. *Geophysical Research Letters*, 41(17):6199–6206. (Cited on page 13.)

Grégorio, S., Penduff, T., Sérazin, G., Molines, J.-M., Barnier, B., and Hirschi, J. (2015). Intrinsic variability of the atlantic meridional overturning circulation at interannual-to-multidecadal time scales. *Journal of Physical Oceanography*, 45(7):1929–1946. (Cited on page 40.)

Griffies, S. M., Biastoch, A., Böning, C., Bryan, F., Danabasoglu, G., Chassignet, E. P., England, M. H., Gerdes, R., Haak, H., Hallberg, R. W., et al. (2009). Coordinated ocean-ice reference experiments (cores). *Ocean Modelling*, 26(1):1–46. (Cited on pages 41 and 63.)

Grinsted, A. (2013). An estimate of global glacier volume. *The Cryosphere*, 7(1):141–151. (Cited on page 24.)

Gudmundsson, G. (2012). Ice-shelf buttressing and the stability of marine ice sheets. *The Cryosphere Discussions*, 6:3937–3962. (Cited on page 93.)

Gudmundsson, G., Krug, J., Durand, G., Favier, L., and Gagliardini, O. (2012a). The stability of grounding lines on retrograde slopes. *The Cryosphere*, 6:1497–1505. (Cited on page 25.)

Gudmundsson, G., Krug, J., Durand, G., Favier, L., and Gagliardini, O. (2012b). The stability of grounding lines on retrograde slopes. *The Cryosphere*, 6:1497–1505. (Cited on pages 27 and 88.)

Hall, A. and Visbeck, M. (2002). Synchronous variability in the southern hemisphere atmosphere, sea ice, and ocean resulting from the annular mode*. *Journal of Climate*, 15(21):3043–3057. (Cited on page 19.)

Harig, C. and Simons, F. J. (2015). Accelerated west antarctic ice mass loss continues to outpace east antarctic gains. *Earth and Planetary Science Letters*, 415:134–141. (Cited on page 12.)

Haumann, F. A., Notz, D., and Schmidt, H. (2014). Anthropogenic influence on recent circulation-driven antarctic sea ice changes. *Geophysical Research Letters*, 41(23):8429–8437. (Cited on page 19.)

Hellmer, H. H., Jacobs, S. S., and Jenkins, A. (1998). *Oceanic erosion of a floating Antarctic glacier in the Amundsen Sea*. Wiley Online Library. (Cited on page 15.)

Hellmer, H. H., Kauker, F., Timmermann, R., Determann, J., and Rae, J. (2012). Twenty-first-century warming of a large antarctic ice-shelf cavity by a redirected coastal current. *Nature*, 485(7397):225–228. (Cited on pages 17 and 26.)

Hellmer, H. H. and Olbers, D. J. (1989). A two-dimensional model for the thermohaline circulation under an ice shelf. *Antarctic Science*, 1(04):325–336. (Cited on page 83.)

Hervieux, G. (2007). Numerical sensitivity studies of dense overflows in the drakkar framework. In *Geophysical Research Abstracts*, volume 9, page 03861. (Cited on page 125.)

Heuzé, C. (2015). *Antarctic Bottom Water in CMIP5 models: characteristics, formation, evolution*. PhD thesis, Ph. D. thesis, School of Environmental Sciences, University of East Anglia. (Cited on pages 18, 30, 31 and 33.)

Hindmarsh, R. (1996). Sliding of till over bedrock: scratching, polishing, comminution and kinematic-wave theory. *Annals of Glaciology*, 22(1):41–47. (Cited on page 27.)

Hindmarsh, R. C. (1993). Qualitative dynamics of marine ice sheets. In *Ice in the climate system*, pages 67–99. Springer. (Cited on page 27.)

Hindmarsh, R. C. (2006). The role of membrane-like stresses in determining the stability and sensitivity of the antarctic ice sheets: back pressure and grounding line motion. *Philosophical Transactions of the Royal Society of London A: Mathematical, Physical and Engineering Sciences*, 364(1844):1733–1767. (Cited on page 27.)

Holland, D. (2001). Explaining the weddell polynya–a large ocean eddy shed at maud rise. *Science*, 292(5522):1697–1700. (Cited on page 7.)

Holland, P. R., Bruneau, N., Enright, C., Losch, M., Kurtz, N. T., and Kwok, R. (2014). Modeled trends in antarctic sea ice thickness. *Journal of Climate*, 27(10):3784–3801. (Cited on pages 19, 20 and 38.)

Holland, P. R., Jenkins, A., and Holland, D. M. (2008). The response of ice shelf basal melting to variations in ocean temperature. *Journal of Climate*, 21(11):2558–2572. (Cited on page 97.)

Holland, P. R. and Kwok, R. (2012a). Wind-driven trends in antarctic sea-ice drift. *Nature Geoscience*, 5(12):872–875. (Cited on pages 10 and 19.)

Holland, P. R. and Kwok, R. (2012b). Wind-driven trends in Antarctic sea-ice drift. *Nature Geoscience*, 5(12):872–875. (Cited on page 38.)

Hoppe, C. J., Hassler, C. S., Payne, C. D., Tortell, P. D., Rost, B., and Trimborn, S. (2013). Iron limitation modulates ocean acidification effects on southern ocean phytoplankton communities. *PLoS One*, 8(11):e79890. (Cited on page 17.)

Hosking, J. S., Orr, A., Marshall, G. J., Turner, J., and Phillips, T. (2013). The influence of the amundsen–bellingshausen seas low on the climate of west antarctica and its representation in coupled climate model simulations. *Journal of Climate*, 26(17):6633–6648. (Cited on pages 11 and 19.)

Houghton, J. T., Jenkins, G. J., and Ephraums, J. (1990). Climate change: the ipcc scientific assessment. *American Scientist;(United States)*, 80(6). (Cited on page 23.)

Howard, W. R., Havenhand, J., Parker, L., Raftos, D., Ross, P., Williamson, J., and Matear, R. (2009). Ocean acidification. *A marine climate change impacts and adaptation report card for Australia*. (Cited on page 16.)

Hughes, T. (1973). Is the west antarctic ice sheet disintegrating? *Journal of Geophysical Research*, 78(33):7884–7910. (Cited on pages 12 and 87.)

Hughes, T. J. (1981). The weak underbelly of the west antarctic ice-sheet. (Cited on page 68.)

Hughes, T. J., Franca, L. P., and Balestra, M. (1986). A new finite element formulation for computational fluid dynamics: V. circumventing the babuška-brezzi condition: A stable petrov-galerkin formulation of the stokes problem accommodating equal-order interpolations. *Computer Methods in Applied Mechanics and Engineering*, 59(1):85–99. (Cited on page 128.)

Hunke, E. C. and Comeau, D. (2011). Sea-ice and iceberg dynamic interaction. *Journal of Geophysical Research: Oceans (1978–2012)*, 116(C5). (Cited on page 49.)

Iken, A. (1981). The effect of the subglacial water pressure on the sliding velocity of a glacier in an idealized numerical model. *Journal of Glaciology*, 27(97):407–421. (Cited on page 92.)

Irvine-Fynn, T. D., Hodson, A. J., Moorman, B. J., Vatne, G., and Hubbard, A. L. (2011). Polythermal glacier hydrology: a review. *Reviews of Geophysics*, 49(4). (Cited on page 64.)

Iudicone, D., Speich, S., Madec, G., and Blanke, B. (2008). The global conveyor belt from a southern ocean perspective. *Journal of Physical Oceanography*, 38(7):1401–1425. (Cited on page 7.)

Jacka, T. H. and Giles, A. B. (2007). Antarctic iceberg distribution and dissolution from ship-based observations. *Journal of Glaciology*, 53(182):341–356. (Cited on page 42.)

Jackett, D. R. and McDougall, T. J. (1997). A neutral density variable for the world's oceans. *Journal of Physical Oceanography*, 27(2):237–263. (Cited on page 121.)

Jacobs, S., Giulivi, C., and Mele, P. (2002). Freshening of the ross sea during the late 20th century. *Science*, 297(5580):386–389. (Cited on page 62.)

Jacobs, S., Helmer, H., Doake, C., Jenkins, A., and Frolich, R. (1992). Melting of ice shelves and the mass balance of antarctica. *Journal of Glaciology*, 38(130):375–387. (Cited on page 26.)

Jacobs, S. S., Amos, A. F., and Bruchhausen, P. M. (1970). Ross sea oceanography and antarctic bottom water formation. In *Deep Sea Research and Oceanographic Abstracts*, volume 17, pages 935–962. Elsevier. (Cited on page 15.)

Jacobs, S. S. and Giulivi, C. F. (2010). Large multidecadal salinity trends near the pacific-antarctic continental margin. *Journal of Climate*, 23(17):4508–4524. (Cited on page 17.)

Jacobs, S. S., Hellmer, H. H., and Jenkins, A. (1996). Antarctic ice sheet melting in the southeast pacific. *Geophysical Research Letters*, 23(9):957–960. (Cited on pages 15 and 117.)

Jacobs, S. S., Jenkins, A., Giulivi, C. F., and Dutrieux, P. (2011). Stronger ocean circulation and increased melting under pine island glacier ice shelf. *Nature Geoscience*, 4(8):519–523. (Cited on pages 12, 15 and 82.)

Jenkins, A. (1999). The impact of melting ice on ocean waters. *Journal of physical oceanography*, 29(9):2370–2381. (Cited on page 83.)

Jenkins, A. and Holland, D. (2007). Melting of floating ice and sea level rise. *Geophysical Research Letters*, 34(16). (Cited on page 25.)

Jenkins, A. and Jacobs, S. (2008). Circulation and melting beneath george vi ice shelf, antarctica. *Journal of Geophysical Research: Oceans*, 113(C4). (Cited on page 15.)

Johnson, G. C. (2008). Quantifying antarctic bottom water and north atlantic deep water volumes. *Journal of Geophysical Research: Oceans*, 113(C5). (Cited on page 18.)

Jones, C. and Sellar, A. (2016). *Development of the 1st version of the UK Earth system model*. `http://www.jwcrp.org.uk/research-activity/ukesm-devesm.asp`, [Accessed: 2016]. (Cited on page 59.)

Jongma, J. I., Driesschaert, E., Fichefet, T., Goosse, H., and Renssen, H. (2009). The effect of dynamic–thermodynamic icebergs on the southern ocean climate in a three-dimensional model. *Ocean Modelling*, 26(1):104–113. (Cited on page 39.)

Joughin, I., Shean, D. E., Smith, B. E., and Dutrieux, P. (2016). Grounding line variability and subglacial lake drainage on pine island glacier, antarctica. *Geophysical Research Letters*. (Cited on page 26.)

Joughin, I., Smith, B. E., and Holland, D. M. (2010). Sensitivity of 21st century sea level to ocean-induced thinning of pine island glacier, antarctica. *Geophysical Research Letters*, 37(20). (Cited on pages 29 and 110.)

Joughin, I., Smith, B. E., and Medley, B. (2014). Marine ice sheet collapse potentially under way for the thwaites glacier basin, west antarctica. *Science*, 344(6185):735–738. (Cited on pages 27, 29, 89, 110 and 119.)

Jullion, L., Jones, S., Naveira Garabato, A., and Meredith, M. P. (2010). Wind-controlled export of antarctic bottom water from the weddell sea. *Geophysical Research Letters*, 37(9). (Cited on page 17.)

Jullion, L., Naveira Garabato, A. C., Meredith, M. P., Holland, P. R., Courtois, P., and King, B. A. (2013). Decadal freshening of the antarctic bottom water exported from the weddell sea. *Journal of Climate*, 26(20):8111–8125. (Cited on page 18.)

Kang, S. M., Polvani, L. M., Fyfe, J., Son, S.-W., Sigmond, M., and P Correa, G. (2013). Modeling evidence that ozone depletion has impacted extreme precipitation in the austral summer. *Geophysical Research Letters*, 40(15):4054–4059. (Cited on page 10.)

Kennicutt II, M., Chown, S. L., Cassano, J., Liggett, D., Peck, L., Massom, R., Rintoul, S., Storey, J., Vaughan, D., Wilson, T., et al. (2015). A roadmap for antarctic and southern ocean science for the next two decades and beyond. *Antarctic Science*, 27(1):3. (Cited on page 19.)

Klinck, J. M., Hofmann, E. E., Beardsley, R. C., Salihoglu, B., and Howard, S. (2004). Water-mass properties and circulation on the west antarctic peninsula continental shelf in austral fall and winter 2001. *Deep Sea Research Part II: Topical Studies in Oceanography*, 51(17):1925–1946. (Cited on page 15.)

Kohut, J., Hunter, E., and Huber, B. (2013). Small-scale variability of the cross-shelf flow over the outer shelf of the ross sea. *Journal of Geophysical Research: Oceans*, 118(4):1863–1876. (Cited on page 15.)

Kostov, Y., Marshall, J., Hausmann, U., Armour, K. C., Ferreira, D., and Holland, M. M. (2016). Fast and slow responses of southern ocean sea surface temperature to sam in coupled climate models. *Climate Dynamics*, pages 1–15. (Cited on page 15.)

Krug, J., Durand, G., Gagliardini, O., and Weiss, J. (2015). Modelling the impact of submarine frontal melting and ice mélange on glacier dynamics. *The Cryosphere*, 9:989–1003. (Cited on page 29.)

Kusahara, K. (2016). Cryosphere: Warming ocean erodes ice sheets. *Nature Climate Change*, 6(1):22–23. (Cited on page 26.)

Le Quéré, C., Rödenbeck, C., Buitenhuis, E. T., Conway, T. J., Langenfelds, R., Gomez, A., Labuschagne, C., Ramonet, M., Nakazawa, T., Metzl, N., et al. (2007). Saturation of the southern ocean co2 sink due to recent climate change. *science*, 316(5832):1735–1738. (Cited on pages 7 and 10.)

Lefebvre, W. and Goosse, H. (2008). An analysis of the atmospheric processes driving the large-scale winter sea ice variability in the southern ocean. *Journal of Geophysical Research: Oceans*, 113(C2). (Cited on pages 19 and 62.)

Lefebvre, W., Goosse, H., Timmermann, R., and Fichefet, T. (2004). Influence of the southern annular mode on the sea ice–ocean system. *Journal of Geophysical Research: Oceans*, 109(C9). (Cited on pages 19 and 38.)

Leguy, G., Asay-Davis, X., and Lipscomb, W. (2014). Parameterization of basal friction near grounding lines in a one-dimensional ice sheet model. *The Cryosphere*, 8(4):1239–1259. (Cited on page 92.)

Lenaerts, J., Den Broeke, M., Berg, W., Meijgaard, E. v., and Kuipers Munneke, P. (2012). A new, high-resolution surface mass balance map of antarctica (1979–2010) based on regional atmospheric climate modeling. *Geophysical Research Letters*, 39(4). (Cited on page 68.)

Lenn, Y.-D. and Chereskin, T. K. (2009). Observations of ekman currents in the southern ocean. *Journal of Physical Oceanography*, 39(3):768–779. (Cited on page 42.)

Lenton, A., Tilbrook, B., Law, R., Bakker, D. C., Doney, S. C., Gruber, N., Hoppema, M., Ishii, M., Lovenduski, N. S., Matear, R. J., et al. (2013). Sea-air co 2 fluxes in the southern ocean for the period 1990-2009. *Biogeosciences Discussions*, 10:285–333. (Cited on page 10.)

Li, C., von Storch, J.-S., and Marotzke, J. (2013). Deep-ocean heat uptake and equilibrium climate response. *Climate Dynamics*, 40(5-6):1071–1086. (Cited on page 14.)

Li, X., Rignot, E., Mouginot, J., and Scheuchl, B. (2016a). Ice flow dynamics and mass loss of totten glacier, east antarctica from 1989 to 2015. *Geophysical Research Letters*. (Cited on pages 13 and 26.)

Li, Y., Ji, R., Jenouvrier, S., Jin, M., and Stroeve, J. (2016b). Synchronicity between ice retreat and phytoplankton bloom in circum-antarctic polynyas. *Geophysical Research Letters*, 43(5):2086–2093. (Cited on page 4.)

Lichey, C. and Hellmer, H. H. (2001). Modeling giant-iceberg drift under the influence of sea ice in the weddell sea, antarctica. *Journal of Glaciology*, 47(158):452–460. (Cited on page 49.)

Ligtenberg, S., Van de Berg, W., Van den Broeke, M., Rae, J., and Van Meijgaard, E. (2013). Future surface mass balance of the antarctic ice sheet and its influence on sea level change, simulated by a regional atmospheric climate model. *Climate dynamics*, 41(3-4):867–884. (Cited on page 25.)

Liu, J., Curry, J. A., and Martinson, D. G. (2004). Interpretation of recent antarctic sea-ice variability. *Geophysical Research Letters*, 31(2). (Cited on page 38.)

Liu, Y., Moore, J. C., Cheng, X., Gladstone, R. M., Bassis, J. N., Liu, H., Wen, J., and Hui, F. (2015). Ocean-driven thinning enhances iceberg calving and retreat of antarctic ice shelves. *Proceedings of the National Academy of Sciences*, 112(11):3263–3268. (Cited on page 68.)

Lliboutry, L. (1968). General theory of subglacial cavitation and sliding of temperate glaciers. *Journal of Glaciology*, 7(49):21–58. (Cited on page 92.)

Lovenduski, N. S., Long, M. C., Gent, P. R., and Lindsay, K. (2013). Multi-decadal trends in the advection and mixing of natural carbon in the southern ocean. *Geophysical Research Letters*, 40(1):139–142. (Cited on page 10.)

MacAyeal, D. R., Rommelaere, V., Huybrechts, P., Hulbe, C. L., Determann, J., and Ritz, C. (1996). An ice-shelf model test based on the ross ice shelf, antarctica. *Annals of Glaciology*, 23(1):46–51. (Cited on page 91.)

Madec, G. (2008). Nemo ocean general circulation model reference manuel. In *Internal Report*. LODYC/IPSL Paris. (Cited on pages 121, 122 and 123.)

Madec, G. (2014). *NEMO ocean engine*. Number 27 in Note du Pole de modelisation. Institut pierre-simon laplace (ipsl) edition. (Cited on pages 40 and 63.)

Madec, G. et al. (2015). Nemo ocean engine. (Cited on page 121.)

Madec, G. and Imbard, M. (1996). A global ocean mesh to overcome the north pole singularity. *Climate Dynamics*, 12(6):381–388. (Cited on page 122.)

Maheshwari, M., Singh, R. K., Oza, S. R., and Kumar, R. (2013). An investigation of the southern ocean surface temperature variability using long-term optimum interpolation sst data. *ISRN Oceanography*, 2013. (Cited on page 14.)

Malinen, M. and Råback, P. (2013). Elmer finite element solver for multiphysics and multiscale problems. *Multiscale Modelling Methods for Applications in Materials Science: CECAM Tutorial, 16-20 September 2013, Forschungszentrum Jülich, Lecture Notes*, 19:101. (Cited on page 126.)

Mantyla, A. W. and Reid, J. L. (1983). Abyssal characteristics of the world ocean waters. *Deep Sea Research Part A. Oceanographic Research Papers*, 30(8):805–833. (Cited on page 61.)

Marsh, R., Ivchenko, V., Skliris, N., Alderson, S., Bigg, G. R., Madec, G., Blaker, A. T., Aksenov, Y., Sinha, B., Coward, A. C., et al. (2015a). Nemo–icb (v1. 0): interactive icebergs in the nemo ocean model globally configured at eddy-permitting resolution. *Geoscientific Model Development*, 8(5):1547–1562. (Cited on pages 34, 115 and 124.)

Marsh, R., Ivchenko, V. O., Skliris, N., Alderson, S., Bigg, G. R., Madec, G., Blaker, A. T., Aksenov, Y., Sinha, B., Coward, A. C., Le Sommer, J., Merino, N., and Zalesny, V. B. (2015b). NEMO-ICB (v1.0): interactive icebergs in the NEMO ocean model globally configured at eddy-permitting resolution. *Geosci. Model Dev.*, 8(5):1547–1562. (Cited on pages 39, 40, 41, 54, 63 and 81.)

Marshall, G. J. (2003). Trends in the southern annular mode from observations and reanalyses. *Journal of Climate*, 16(24):4134–4143. (Cited on page 9.)

Marsland, S. and Wolff, J.-O. (2001). On the sensitivity of southern ocean sea ice to the surface freshwater flux: a model study. *Journal of Geophysical Research: Oceans*, 106(C2):2723–2741. (Cited on pages 8, 15, 21, 33, 39, 53, 79, 82 and 117.)

Martin, D., Asay-Davis, X., Cornford, S., Price, S., Ng, E., and Collins, W. (2015). A tale of two forcings: Present-day coupled antarctic ice-sheet/southern ocean dynamics using the popsicles model. In *EGU General Assembly Conference Abstracts*, volume 17, page 7564. (Cited on page 29.)

Martin, T. and Adcroft, A. (2010). Parameterizing the fresh-water flux from land ice to ocean with interactive icebergs in a coupled climate model. *Ocean Modelling*, 34(3):111–124. (Cited on pages 39, 41, 56 and 124.)

Massonnet, F., Mathiot, P., Fichefet, T., Goosse, H., Beatty, C. K., Vancoppenolle, M., and Lavergne, T. (2013). A model reconstruction of the antarctic sea ice thickness and volume changes over 1980–2008 using data assimilation. *Ocean Modelling*, 64:67–75. (Cited on page 20.)

Matear, R. J., O'Kane, T. J., Risbey, J. S., and Chamberlain, M. (2015). Sources of heterogeneous variability and trends in antarctic sea-ice. *Nature communications*, 6. (Cited on page 19.)

Meehl, G. A., Arblaster, J. M., Bitz, C. M., Chung, C. T., and Teng, H. (2016). Antarctic sea-ice expansion between 2000 and 2014 driven by tropical pacific decadal climate variability. *Nature Geoscience*. (Cited on page 20.)

Meier, W., Gallaher, D., and Campbell, G. (2013). New estimates of arctic and antarctic sea ice extent during september 1964 from recovered nimbus i satellite imagery. *The Cryosphere*, 7(2):699–705. (Cited on page 19.)

Mercer, J. H. (1968). Glacial geology of the reedy glacier area, antarctica. *Geological Society of America Bulletin*, 79(4):471–486. (Cited on page 12.)

Meredith, M. P., Woodworth, P. L., Chereskin, T. K., Marshall, D. P., Allison, L. C., Bigg, G. R., Donohue, K., Heywood, K. J., Hughes, C. W., Hibbert, A., et al. (2011). Sustained monitoring of the southern ocean at drake passage: Past achievements and future priorities. *Reviews of Geophysics*, 49(4). (Cited on page 17.)

Merino, N., Le Sommer, J., Durand, G., Jourdain, N. C., Madec, G., Mathiot, P., and Tournadre, J. (2016). Antarctic icebergs melt over the southern ocean: climatology and impact on sea ice. *Ocean Modelling*. (Cited on pages 37, 63, 64, 67, 69 and 120.)

Mo, K. C. and Higgins, R. W. (1998). The pacific-south american modes and tropical convection during the southern hemisphere winter. *Monthly Weather Review*, 126(6):1581–1596. (Cited on page 20.)

Moffat, C., Owens, B., and Beardsley, R. C. (2009). On the characteristics of circumpolar deep water intrusions to the west antarctic peninsula continental shelf. *Journal of Geophysical Research: Oceans*, 114(C5). (Cited on page 15.)

Monaghan, A. J., Bromwich, D. H., Fogt, R. L., Wang, S.-H., Mayewski, P. A., Dixon, D. A., Ekaykin, A., Frezzotti, M., Goodwin, I., Isaksson, E., et al. (2006). Insignificant change in antarctic snowfall since the international geophysical year. *Science*, 313(5788):827–831. (Cited on page 68.)

Morlighem, M., Bondzio, J., Seroussi, H., Rignot, E., Larour, E., Humbert, A., and Rebuffi, S. (2016). Modeling of store gletscher's calving dynamics, west greenland, in response to ocean thermal forcing. *Geophysical Research Letters*. (Cited on page 29.)

Mouginot, J., Rignot, E., and Scheuchl, B. (2014). Sustained increase in ice discharge from the amundsen sea embayment, west antarctica, from 1973 to 2013. *Geophysical Research Letters*, 41(5):1576–1584. (Cited on page 12.)

Nakayama, Y., Timmermann, R., Schröder, M., and Hellmer, H. H. (2015). Data analysis and modeling of the amundsen sea embayment. In *Towards an Interdisciplinary Approach in Earth System Science*, pages 131–136. Springer. (Cited on page 15.)

NIAS, I. J., CORNFORD, S. L., and PAYNE, A. J. (2016). Contrasting the modelled sensitivity of the amundsen sea embayment ice streams. *Journal of Glaciology*, pages 1–11. (Cited on page 29.)

Nihashi, S. and Cavalieri, D. J. (2006). Observational evidence of a hemispheric-wide ice–ocean albedo feedback effect on antarctic sea-ice decay. *Journal of Geophysical Research: Oceans*, 111(C12). (Cited on page 7.)

Nihashi, S. and Ohshima, K. I. (2015). Circumpolar mapping of antarctic coastal polynyas and landfast sea ice: relationship and variability. *Journal of climate*, 28(9):3650–3670. (Cited on page 3.)

Oke, P. R. and England, M. H. (2004). Oceanic response to changes in the latitude of the southern hemisphere subpolar westerly winds. *Journal of Climate*, 17(5):1040–1054. (Cited on page 14.)

Olbers, D., Borowski, D., Völker, C., and WOeLFF, J.-O. (2004). The dynamical balance, transport and circulation of the antarctic circumpolar current. *Antarctic science*, 16(04):439–470. (Cited on page 8.)

Orsi, A., Johnson, G., and Bullister, J. (1999). Circulation, mixing, and production of antarctic bottom water. *Progress in Oceanography*, 43(1):55–109. (Cited on page 61.)

Orsi, A. H. and Wiederwohl, C. L. (2009). A recount of ross sea waters. *Deep Sea Research Part II: Topical Studies in Oceanography*, 56(13):778–795. (Cited on page 15.)

Paolo, F. S., Fricker, H. A., and Padman, L. (2015). Volume loss from antarctic ice shelves is accelerating. *Science*, 348(6232):327–331. (Cited on pages 25, 26, 62 and 85.)

Parkinson, C. and Cavalieri, D. (2012a). Antarctic sea ice variability and trends, 1979–2010. *The Cryosphere*, 6(4):871–880. (Cited on pages 12 and 19.)

Parkinson, C. L. and Cavalieri, D. J. (2012b). Antarctic sea-ice variability and trends, 1979-2010. *The Cryosphere*, 6(4):871–880. (Cited on page 38.)

Pattyn, F. and Durand, G. (2013). Why marine ice sheet model predictions may diverge in estimating future sea level rise. *Geophysical research letters*, 40(16):4316–4320. (Cited on pages 88 and 91.)

Pattyn, F., Huyghe, A., De Brabander, S., and De Smedt, B. (2006). Role of transition zones in marine ice sheet dynamics. *Journal of Geophysical Research: Earth Surface*, 111(F2). (Cited on page 27.)

Pattyn, F., Perichon, L., Durand, G., Favier, L., Gagliardini, O., Hindmarsh, R. C., Zwinger, T., Albrecht, T., Cornford, S., Docquier, D., et al. (2013). Grounding-line migration in plan-view marine ice-sheet models: results of the ice2sea mismip3d intercomparison. *Journal of Glaciology*, 59(215):410–422. (Cited on pages 29, 88, 91, 96, 99, 110 and 126.)

Pattyn, F., Schoof, C., Perichon, L., Hindmarsh, R., Bueler, E., Fleurian, B. d., Durand, G., Gagliardini, O., Gladstone, R., Goldberg, D., et al. (2012). Results of the marine ice sheet model intercomparison project, mismip. *The Cryosphere*, 6(3):573–588. (Cited on pages 29, 88 and 126.)

Pauling, A. G., Bitz, C. M., Smith, I. J., and Langhorne, P. J. (2016). The response of the southern ocean and antarctic sea ice to freshwater from ice shelves in an earth system model. *Journal of Climate*, 29(5):1655–1672. (Cited on pages 8, 21, 31, 59, 60, 62, 85 and 115.)

Payne, A. J., Vieli, A., Shepherd, A. P., Wingham, D. J., and Rignot, E. (2004). Recent dramatic thinning of largest west antarctic ice stream triggered by oceans. *Geophysical Research Letters*, 31(23). (Cited on page 29.)

Penduff, T., Juza, M., Barnier, B., Zika, J., Dewar, W. K., Treguier, A.-M., Molines, J.-M., and Audiffren, N. (2011). Sea level expression of intrinsic and forced ocean variabilities at interannual time scales. *Journal of Climate*, 24(21):5652–5670. (Cited on page 40.)

Penduff, T., Le Sommer, J., Barnier, B., Tréguier, A.-M., Molines, J.-M., and Madec, G. (2007). Influence of numerical schemes on current-topography interactions in 1/4 global ocean simulations. *Ocean Science Discussions*, 4(3):491–528. (Cited on page 123.)

Peng, G., Meier, W., Scott, D., and Savoie, M. (2013). A long-term and reproducible passive microwave sea ice concentration data record for climate studies and monitoring. *Earth System Science Data*, 5(2):311–318. (Cited on pages 45 and 47.)

Perovich, D. K. (2011). The changing arctic sea ice cover. *Oceanography*. (Cited on page 62.)

Petty, A. A., Feltham, D. L., and Holland, P. R. (2013). Impact of atmospheric forcing on antarctic continental shelf water masses. *Journal of Physical Oceanography*, 43(5):920–940. (Cited on pages 15 and 16.)

Polvani, L. M. and Smith, K. L. (2013a). Can natural variability explain observed antarctic sea ice trends? new modeling evidence from cmip5. *Geophysical Research Letters*, 40(12):3195–3199. (Cited on pages 19 and 62.)

Polvani, L. M. and Smith, K. L. (2013b). Can natural variability explain observed Antarctic sea-ice trends? New modeling evidence from CMIP5. *Geophysical Research Letters*, 40(12):3195–3199. (Cited on page 38.)

Prinn, R. G. (2013). Development and application of earth system models. *Proceedings of the National Academy of Sciences*, 110(Supplement 1):3673–3680. (Cited on page 59.)

Pritchard, H., Ligtenberg, S., Fricker, H., Vaughan, D., Van den Broeke, M., and Padman, L. (2012a). Antarctic ice-sheet loss driven by basal melting of ice shelves. *Nature*, 484(7395):502–505. (Cited on pages 15, 25 and 88.)

Pritchard, H., Ligtenberg, S., Fricker, H., Vaughan, D., Van den Broeke, M., and Padman, L. (2012b). Antarctic ice-sheet loss driven by basal melting of ice shelves. *Nature*, 484(7395):502–505. (Cited on pages 62, 67, 82 and 85.)

Purkey, S. G. and Johnson, G. C. (2012). Global contraction of antarctic bottom water between the 1980s and 2000s*. *Journal of Climate*, 25(17):5830–5844. (Cited on page 18.)

Purkey, S. G. and Johnson, G. C. (2013). Antarctic bottom water warming and freshening: Contributions to sea level rise, ocean freshwater budgets, and global heat gain*. *Journal of Climate*, 26(16):6105–6122. (Cited on pages 12, 17 and 18.)

Rahmstorf, S. and Ganopolski, A. (1999). Long-term global warming scenarios computed with an efficient coupled climate model. *Climatic change*, 43(2):353–367. (Cited on page 18.)

Raphael, M., Marshall, G., Turner, J., Fogt, R., Schneider, D., Dixon, D., Hosking, J., Jones, J., and Hobbs, W. (2016). The amundsen sea low: Variability, change, and impact on antarctic climate. *Bulletin of the American Meteorological Society*, 97(1):111–121. (Cited on page 11.)

Raphael, M. N. and Hobbs, W. (2014). The influence of the large-scale atmospheric circulation on antarctic sea ice during ice advance and retreat seasons. *Geophysical Research Letters*, 41(14):5037–5045. (Cited on page 19.)

Raupach, M. R., Marland, G., Ciais, P., Le Quéré, C., Canadell, J. G., Klepper, G., and Field, C. B. (2007). Global and regional drivers of accelerating co2 emissions. *Proceedings of the National Academy of Sciences*, 104(24):10288–10293. (Cited on page 16.)

Reid, P., Stammerjohn, S., Massom, R., Scambos, T., and Lieser, J. (2015). The record 2013 southern hemisphere sea-ice extent maximum. *Annals of Glaciology*, 56(69):99–106. (Cited on page 19.)

Richter, A., Horwath, M., and Dietrich, R. (2015). Comment on zwally and others (2015)-mass gains of the antarctic ice sheet exceed losses. *Journal of Glaciology*, pages 1–3. (Cited on page 13.)

Rignot, E., Bamber, J. L., Van Den Broeke, M. R., Davis, C., Li, Y., Van De Berg, W. J., and Van Meijgaard, E. (2008). Recent antarctic ice mass loss from radar interferometry and regional climate modelling. *Nature Geoscience*, 1(2):106–110. (Cited on page 39.)

Rignot, E., Jacobs, S., Mouginot, J., and Scheuchl, B. (2013). Ice-shelf melting around antarctica. *Science*, 341(6143):266–270. (Cited on pages 25, 34, 35, 39, 44, 63, 66 and 67.)

Rignot, E. and Jacobs, S. S. (2002). Rapid bottom melting widespread near antarctic ice sheet grounding lines. *Science*, 296(5575):2020–2023. (Cited on page 44.)

Rignot, E., Mouginot, J., Morlighem, M., Seroussi, H., and Scheuchl, B. (2014). Widespread, rapid grounding line retreat of pine island, thwaites, smith, and kohler glaciers, west antarctica, from 1992 to 2011. *Geophysical Research Letters*, 41(10):3502–3509. (Cited on page 26.)

Rignot, E., Vaughan, D. G., Schmeltz, M., Dupont, T., and MacAyeal, D. (2002). Acceleration of pine island and thwaites glaciers, west antarctica. *Annals of Glaciology*, 34(1):189–194. (Cited on page 26.)

Rignot, E., Velicogna, I., Van den Broeke, M., Monaghan, A., and Lenaerts, J. (2011). Acceleration of the contribution of the greenland and antarctic ice sheets to sea level rise. *Geophysical Research Letters*, 38(5). (Cited on pages 8, 12, 15, 62 and 67.)

Rintoul, S. R. (2007). Rapid freshening of antarctic bottom water formed in the indian and pacific oceans. *Geophysical Research Letters*, 34(6). (Cited on page 17.)

Roemmich, D., Church, J., Gilson, J., Monselesan, D., Sutton, P., and Wijffels, S. (2015). Unabated planetary warming and its ocean structure since 2006. *Nature Climate Change*. (Cited on page 61.)

Rott, H., Skvarca, P., and Nagler, T. (1996). Rapid collapse of northern larsen ice shelf, antarctica. *Science*, 271(5250):788. (Cited on page 68.)

Sallée, J.-B., Matear, R. J., Rintoul, S. R., and Lenton, A. (2012). Localized subduction of anthropogenic carbon dioxide in the southern hemisphere oceans. *Nature Geoscience*, 5(8):579–584. (Cited on page 61.)

Sasgen, I., Konrad, H., Ivins, E., Van den Broeke, M., Bamber, J., Martinec, Z., and Klemann, V. (2013). Antarctic ice-mass balance 2003 to 2012: regional reanalysis of grace satellite gravimetry measurements with improved estimate of glacial-isostatic adjustment based on gps uplift rates. *The Cryosphere*, 7:1499–1512. (Cited on page 12.)

Scambos, T. and Shuman, C. (2015). Comment on zwally and others (2015)-mass gains of the antarctic ice sheet exceed losses. *Journal of Glaciology*, pages 1–5. (Cited on page 13.)

Scambos, T. A., Bohlander, J., Shuman, C. u., and Skvarca, P. (2004). Glacier acceleration and thinning after ice shelf collapse in the larsen b embayment, antarctica. *Geophysical Research Letters*, 31(18). (Cited on pages 13, 26 and 67.)

Scheuchl, B., Mouginot, J., Rignot, E., Morlighem, M., and Khazendar, A. (2016). Grounding line retreat of pope, smith, and kohler glaciers, west antarctica, measured with sentinel-1a radar interferometry data. *Geophysical Research Letters*. (Cited on page 26.)

Schodlok, M., Hellmer, H., Rohardt, G., and Fahrbach, E. (2006). Weddell sea iceberg drift: Five years of observations. *Journal of Geophysical Research: Oceans (1978–2012)*, 111(C6). (Cited on page 49.)

Schoof, C. (2005). The effect of cavitation on glacier sliding. In *Proceedings of the Royal Society of London A: Mathematical, Physical and Engineering Sciences*, volume 461, pages 609–627. The Royal Society. (Cited on page 92.)

Schoof, C. (2007a). Ice sheet grounding line dynamics: Steady states, stability, and hysteresis. *Journal of Geophysical Research: Earth Surface*, 112(F3). (Cited on pages 27, 87 and 88.)

Schoof, C. (2007b). Marine ice-sheet dynamics. part 1. the case of rapid sliding. *Journal of Fluid Mechanics*, 573:27–55. (Cited on page 89.)

Schoof, C. (2010). Coulomb friction and other sliding laws in a higher-order glacier flow model. *Mathematical Models and Methods in Applied Sciences*, 20(01):157–189. (Cited on pages 29 and 93.)

Screen, J. A. (2011). Sudden increase in antarctic sea ice: Fact or artifact? *Geophysical Research Letters*, 38(13). (Cited on pages 19 and 62.)

Sen Gupta, A. and England, M. H. (2006). Coupled ocean-atmosphere-ice response to variations in the southern annular mode. *Journal of Climate*, 19(18):4457–4486. (Cited on page 19.)

Seroussi, H., Morlighem, M., Rignot, E., Mouginot, J., Larour, E., Schodlok, M., and Khazendar, A. (2014). Sensitivity of the dynamics of pine island glacier, west antarctica, to climate forcing for the next 50 years. *Cryosphere*, 8(5). (Cited on pages 29 and 128.)

Shepherd, A., Ivins, E. R., Geruo, A., Barletta, V. R., Bentley, M. J., Bettadpur, S., Briggs, K. H., Bromwich, D. H., Forsberg, R., Galin, N., et al. (2012). A reconciled estimate of ice-sheet mass balance. *Science*, 338(6111):1183–1189. (Cited on pages 12, 24, 39, 62, 67, 68, 82 and 116.)

Shi, D., Xu, Y., Hopkinson, B. M., and Morel, F. M. (2010). Effect of ocean acidification on iron availability to marine phytoplankton. *Science*, 327(5966):676–679. (Cited on page 16.)

Shindell, D. T. and Schmidt, G. A. (2004). Southern hemisphere climate response to ozone changes and greenhouse gas increases. *Geophysical Research Letters*, 31(18). (Cited on page 10.)

Shu, Q., Song, Z., and Qiao, F. (2015). Assessment of sea ice simulations in the cmip5 models. *The Cryosphere*, 9(1):399–409. (Cited on pages 33 and 59.)

Sigmond, M. and Fyfe, J. (2010). Has the ozone hole contributed to increased antarctic sea ice extent? *Geophysical Research Letters*, 37(18). (Cited on page 19.)

Silva, T., Bigg, G., and Nicholls, K. (2006). Contribution of giant icebergs to the southern ocean freshwater flux. *Journal of Geophysical Research: Oceans*, 111(C3). (Cited on pages 34 and 39.)

Simmonds, I. and Jacka, T. (1995). Relationships between the interannual variability of antarctic sea ice and the southern oscillation. *Journal of Climate*, 8(3):637–647. (Cited on page 20.)

Simpkins, G. R., Ciasto, L. M., Thompson, D. W., and England, M. H. (2012). Seasonal relationships between large-scale climate variability and antarctic sea ice concentration. *Journal of Climate*, 25(16):5451–5469. (Cited on page 20.)

Simpkins, G. R. and Karpechko, A. Y. (2012). Sensitivity of the southern annular mode to greenhouse gas emission scenarios. *Climate dynamics*, 38(3-4):563–572. (Cited on page 10.)

Stammerjohn, S., Martinson, D., Smith, R., Yuan, X., and Rind, D. (2008a). Trends in antarctic annual sea ice retreat and advance and their relation to el niño–southern oscillation and southern annular mode variability. *Journal of Geophysical Research: Oceans*, 113(C3). (Cited on page 62.)

Stammerjohn, S., Massom, R., Rind, D., and Martinson, D. (2012a). Regions of rapid sea ice change: An inter-hemispheric seasonal comparison. *Geophysical Research Letters*, 39(6). (Cited on page 20.)

Stammerjohn, S., Massom, R., Rind, D., and Martinson, D. (2012b). Regions of rapid sea-ice change: An inter-hemispheric seasonal comparison. *Geophysical Research Letters*, 39(6):L06501. (Cited on page 80.)

Stammerjohn, S. E., Martinson, D. G., Smith, R. C., Yuan, X., and Rind, D. (2008b). Trends in Antarctic annual sea-ice retreat and advance and their relation to El Nino-Southern Oscillation and Southern Annular Mode variability. *Journal of Geophysical Research*, 113(C3). (Cited on pages 39, 62 and 78.)

Stewart, A. L. and Thompson, A. F. (2015). Eddy-mediated transport of warm circumpolar deep water across the antarctic shelf break. *Geophysical Research Letters*, 42(2):432–440. (Cited on page 49.)

Stocker, T., Qin, D., Plattner, G., Tignor, M., Allen, S., Boschung, J., Nauels, A., Xia, Y., Bex, B., and Midgley, B. (2013). Ipcc, 2013: climate change 2013: the physical science basis. contribution of working group i to the fifth assessment report of the intergovernmental panel on climate change. (Cited on pages 6, 7, 17, 23, 24, 25, 28 and 59.)

Stocker, T. F., Qin, D., Plattner, G.-K., Tignor, M., Allen, S. K., Boschung, J., Nauels, A., Xia, Y., Bex, V., and Midgley, P. M. (2014). Climate change 2013: The physical science basis. (Cited on pages 23, 26 and 88.)

Swart, N. and Fyfe, J. (2013). The influence of recent antarctic ice sheet retreat on simulated sea ice area trends. *Geophysical Research Letters*, 40(16):4328–4332. (Cited on pages 8, 21, 31, 39, 59, 60, 62, 68, 85 and 115.)

Takahashi, T., Sutherland, S. C., Wanninkhof, R., Sweeney, C., Feely, R. A., Chipman, D. W., Hales, B., Friederich, G., Chavez, F., Sabine, C., et al. (2009). Climatological mean and decadal change in surface ocean pco 2, and net sea–air co 2 flux over the global oceans. *Deep Sea Research Part II: Topical Studies in Oceanography*, 56(8):554–577. (Cited on page 7.)

Talbot, M. (1988). Oceanic environment of george vi ice shelf, antarctic peninsula. *Ann. Glaciol*, 11:161–164. (Cited on page 15.)

Thoma, M., Jenkins, A., Holland, D., and Jacobs, S. (2008). Modelling circumpolar deep water intrusions on the amundsen sea continental shelf, antarctica. *Geophysical Research Letters*, 35(18). (Cited on pages 15 and 82.)

Thomas, R. H. and Bentley, C. R. (1978). A model for holocene retreat of the west antarctic ice sheet. *Quaternary Research*, 10(2):150–170. (Cited on page 27.)

Thompson, D. W., Solomon, S., Kushner, P. J., England, M. H., Grise, K. M., and Karoly, D. J. (2011). Signatures of the antarctic ozone hole in southern hemisphere surface climate change. *Nature Geoscience*, 4(11):741–749. (Cited on page 62.)

Timmermann, R. and Goeller, S. (2016). Towards a regional coupled ice sheet-ocean model for antarctica. (Cited on page 29.)

Tournadre, J. and Accensi, M. (2015). The ALTIBERG iceberg data base version 1. Doc Tech. 2015-01 IFREMER/LOS. (Cited on page 115.)

Tournadre, J., Bouhier, N., Girard-Ardhuin, F., and Remy, F. (2015). Large icebergs characteristics from altimeter waveforms analysis. *Journal of Geophysical Research: Oceans*, 120(3):1954–1974. (Cited on pages 34, 41, 49 and 125.)

Tournadre, J., Bouhier, N., Girard-Ardhuin, F., and Remy, F. (2016). Antarctic icebergs distributions 1992–2014. *Journal of Geophysical Research: Oceans*, 121(1):327–349. (Cited on page 34.)

Tournadre, J., Girard-Ardhuin, F., and Legrésy, B. (2012). Antarctic icebergs distributions, 2002–2010. *Journal of Geophysical Research: Oceans (1978–2012)*, 117(C05004). (Cited on pages 39, 46, 47, 49 and 50.)

Tournadre J., N. Bouhier, F. G.-A. a. F. R. (2015). Antarctic icebergs distributions 1992-2014. *J. Geophys. Res.* (Cited on pages 39, 46, 47 and 48.)

Tréguier, A.-M., Deshayes, J., Le Sommer, J., Lique, C., Madec, G., Penduff, T., Molines, J.-M., Barnier, B., Bourdalle-Badie, R., and Talandier, C. (2014). Meridional transport of salt in the global ocean from an eddy-resolving model. *Ocean Science*, 10(2):243–255. (Cited on page 34.)

Treguier, A. M., Le Sommer, J., Molines, J.-M., and De Cuevas, B. (2010). Response of the southern ocean to the southern annular mode: Interannual variability and multidecadal trend. *Journal of Physical Oceanography*, 40(7):1659–1668. (Cited on page 125.)

Trenberth, K. E., Smith, L., Qian, T., Dai, A., and Fasullo, J. (2007). Estimates of the global water budget and its annual cycle using observational and model data. *Journal of Hydrometeorology*, 8(4):758–769. (Cited on page 10.)

Tsai, V. C., Stewart, A. L., and Thompson, A. F. (2015). Marine ice-sheet profiles and stability under coulomb basal conditions. *Journal of Glaciology*, 61(226):205–215. (Cited on pages 29, 89 and 93.)

Turner, J. (2004). The el niño–southern oscillation and antarctica. *International Journal of Climatology*, 24(1):1–31. (Cited on page 20.)

Turner, J., Colwell, S. R., Marshall, G. J., Lachlan-Cope, T. A., Carleton, A. M., Jones, P. D., Lagun, V., Reid, P. A., and Iagovkina, S. (2005). Antarctic climate change during the last 50 years. *International journal of Climatology*, 25(3):279–294. (Cited on page 10.)

Turner, J., Comiso, J. C., Marshall, G. J., Lachlan-Cope, T. A., Bracegirdle, T., Maksym, T., Meredith, M. P., Wang, Z., and Orr, A. (2009a). Non-annular atmospheric circulation change induced by stratospheric ozone depletion and its role in the recent increase of antarctic sea ice extent. *Geophysical Research Letters*, 36(8). (Cited on pages 19 and 62.)

Turner, J., Comiso, J. C., Marshall, G. J., Lachlan-Cope, T. A., Bracegirdle, T., Maksym, T., Meredith, M. P., Wang, Z., and Orr, A. (2009b). Non-annular atmospheric circulation change induced by stratospheric ozone depletion and its role in the recent increase of Antarctic sea-ice extent. *Geophysical Research Letters*, 36(8):L08502. (Cited on page 38.)

Turner, J., Hosking, J. S., Bracegirdle, T. J., Marshall, G. J., and Phillips, T. (2015a). Recent changes in antarctic sea ice. *Philosophical Transactions of the Royal Society of London A: Mathematical, Physical and Engineering Sciences*, 373(2045):20140163. (Cited on page 38.)

Turner, J., Hosking, J. S., Marshall, G. J., Phillips, T., and Bracegirdle, T. J. (2016). Antarctic sea ice increase consistent with intrinsic variability of the amundsen sea low. *Climate Dynamics*, 46(7-8):2391–2402. (Cited on page 11.)

Turner, J., Summerhayes, C., Sparrow, M., Mayewski, P., Convey, P., di Prisco, G., Gutt, J., Hodgson, D., Speich, S., Worby, T., et al. (2015b). Antarctic climate change and the environment–2015 update. Antarctic Treaty Consultative Meeting. (Cited on page 19.)

Uotila, P., Holland, P. R., Vihma, T., Marsland, S. J., and Kimura, N. (2014). Is realistic antarctic sea-ice extent in climate models the result of excessive ice drift? *Ocean Modelling*, 79:33–42. (Cited on page 38.)

van den Berk, J. and Drijfhout, S. (2014). A realistic freshwater forcing protocol for ocean-coupled climate models. *Ocean Modelling*, 81:36–48. (Cited on pages 39 and 44.)

van den Broeke, M. (2005). Strong surface melting preceded collapse of antarctic peninsula ice shelf. *Geophysical Research Letters*, 32(12). (Cited on page 64.)

van den Broeke, M., Bamber, J., Ettema, J., Rignot, E., Schrama, E., van de Berg, W. J., van Meijgaard, E., Velicogna, I., and Wouters, B. (2009). Partitioning recent greenland mass loss. *science*, 326(5955):984–986. (Cited on page 25.)

Vancoppenolle, M., Bouillon, S., Fichefet, T., Goosse, H., Lecomte, O., Morales Maqueda, M., and Madec, G. (2012). Lim, the louvain-la-neuve sea ice model. *Notes du Pôle de modélisation*, (31). (Cited on page 121.)

Vaughan, D. G., Bamber, J. L., Giovinetto, M., Russell, J., and Cooper, A. P. R. (1999). Reassessment of net surface mass balance in antarctica. *Journal of climate*, 12(4):933–946. (Cited on page 5.)

Velicogna, I., Sutterley, T., and Van Den Broeke, M. (2014). Regional acceleration in ice mass loss from greenland and antarctica using grace time-variable gravity data. *Geophysical Research Letters*, 41(22):8130–8137. (Cited on page 24.)

Wåhlin, A., Yuan, X., Björk, G., and Nohr, C. (2010). Inflow of warm circumpolar deep water in the central amundsen shelf*. *Journal of Physical Oceanography*, 40(6):1427–1434. (Cited on page 15.)

Walker, D. P., Brandon, M. A., Jenkins, A., Allen, J. T., Dowdeswell, J. A., and Evans, J. (2007). Oceanic heat transport onto the amundsen sea shelf through a submarine glacial trough. *Geophysical Research Letters*, 34(2). (Cited on page 82.)

Weertman, J. (1974). Stability of the junction of an ice sheet and an ice shelf. *Journal of Glaciology*, 13(67):3–11. (Cited on pages 5, 12, 27 and 87.)

Wesche, C. and Dierking, W. (2015). Near-coastal circum-antarctic iceberg size distributions determined from synthetic aperture radar images. *Remote Sensing of Environment*, 156:561–569. (Cited on pages 48 and 49.)

Wijk, E. M. and Rintoul, S. R. (2014). Freshening drives contraction of antarctic bottom water in the australian antarctic basin. *Geophysical Research Letters*, 41(5):1657–1664. (Cited on pages 12 and 18.)

Williams, N. L., Feely, R. A., Sabine, C. L., Dickson, A. G., Swift, J. H., Talley, L. D., and Russell, J. L. (2015). Quantifying anthropogenic carbon inventory

changes in the pacific sector of the southern ocean. *Marine Chemistry*, 174:147–160. (Cited on page 8.)

Wouters, B., Martin-Espanol, A., Helm, V., Flament, T., van Wessem, J., Ligtenberg, S., van den Broeke, M., and Bamber, J. (2015). Dynamic thinning of glaciers on the southern antarctic peninsula. *Science*, 348(6237):899–903. (Cited on page 13.)

Yan, Q., Wang, H., Johannessen, O. M., and Zhang, Z. (2014). Greenland ice sheet contribution to future global sea level rise based on cmip5 models. *Advances in Atmospheric Sciences*, 31(1):8–16. (Cited on page 24.)

Yang, Y., Hansson, L., and Gattuso, J. (2016). Data compilation on the biological response to ocean acidification: an update. *Earth System Science Data*, 8(1):79. (Cited on page 16.)

Zhang, J. (2007). Increasing antarctic sea ice under warming atmospheric and oceanic conditions. *Journal of Climate*, 20(11):2515–2529. (Cited on pages 20, 30, 38 and 62.)

Zwally, H. J., Comiso, J. C., Parkinson, C. L., Cavalieri, D. J., and Gloersen, P. (2002). Variability of antarctic sea ice 1979–1998. *Journal of Geophysical Research: Oceans*, 107(C5). (Cited on page 12.)

Zwally, H. J., Li, J., Robbins, J. W., Saba, J. L., Yi, D., and Brenner, A. C. (2015). Mass gains of the antarctic ice sheet exceed losses. *Journal of Glaciology*, 61(230):1019–1036. (Cited on page 13.)

## Abstract:

The next generation of climate models will include an ice-sheet model in order to improve the ice sheet mass balance projections by accounting for the ice dynamics and ice-oceans interactions. On the one hand, the Southern Ocean (SO) is indeed driving the acceleration of the Antarctic outlet glaciers via an increase in the basal melting of the ice shelves. On the other hand, the increasing ice discharge from Antarctic Ice Sheet (AIS) contributes to the current sea level rise and is likely to become the largest cryospheric contributor to sea level rise by the end of the current century. In addition, the related freshening may have significant implications on future sea-ice cover and on bottom water formation. However, it is not clear yet how the ocean and ice-sheet components of future coupled systems will account for the ice-ocean interactions, which are both causes and consequences of the AIS mass imbalance. Here in this work, different aspects of the standalone ocean and ice-sheet components have been investigated. A first step of this thesis has been focused in the representation of the glacial freshwater fluxes in current ocean models. Based on recent glaciological estimates, the ice shelf basal melting fluxes have been spatially distributed in an ORCA025 grid, and the calving rates have been applied into an improved version of the NEMO-ICB iceberg model. This preliminary study has been used to produce a monthly iceberg meltwater climatology, to be used to force current ocean models. This work shows the importance of representing the iceberg meltwater fluxes when modeling sea ice, which can be inexpensively achieve by using our climatology. The improvements in the representation of the glacial freshwater fluxes have been considered in the study of the ocean model response to the Antarctic mass imbalance. This study considers a realistic perturbation in the glacial freshwater forcing as close as possible as it will be represented in future ice-sheet/ocean models. According to our results, up to 50% of the recent Antarctic sea ice volume changes might be caused by the observed decadal AIS mass imbalance rate. Glacial freshwater forcing appears to be crucial to correctly represent the ice-ocean interactions and projecting sea ice cover of future coupled systems. However, the estimation of the glacial freshwater input in future climate models will be strongly dependent upon the capacity of ice-sheet models to reproduce the grounding line migrations of marine ice sheet glaciers. Current ice-sheet models present large uncertainties related to different parametrizations. In the context of the future climate models, we have studied the sensitivity of ocean-driven grounding line retreats to the application of two different friction laws and two different englacial stress approximations. The model responses almost indistinctively to either the SSA or the SSA* englacial stress approximations. However, differences in the contribution of the glacier to the sea level rise can be up to 50% depending on the friction law considered. The more physically constrained Schoof friction law is significantly more reactive to the ocean perturbations than Weertman law and should be considered in future coupled systems. This work underlines that uncertainties related to the ice sheet model estimates of grounding line migrations may not only contribute to uncertainties in sea level projections, but also the sea ice cover through the ice-ocean interaction in future ocean models.This conclusion suggests the need for improving the representation of both the ice shelf basal melting and the glacier interaction with the bedrock, in order to improve the climate projections of future climate models, in which the spatial and seasonal distribution of the glacial freshwater fluxes may play an important role in setting the sea ice cover.

## Resumé:

Les prochains modèles climatiques comprendront un modèle de calotte polaire afin de prendre en compte la dynamique de la glace et les interactions glace-océans dans leurs projections. D'une part, l'océan Austral (SO) pilote l'accélération des glaciers de l'Antarctique via une augmentation de la fonte basale des ice shelves. D'autre part, l'accélération de la décharge de glace de la calotte Antarctique (AIS) contribue à la montée du niveau de la mer et est susceptible de devenir le plus grand contributeur d'ici la fin du siècle. En outre, l'adoucissement relié, peut avoir des répercussions importantes sur la glace de mer et sur la formation des eaux profondes. Cependant, on ne sait pas encore comment les modèles d'océan et de calotte polaire des futurs systèmes couplés vont représenter les interactions glace-océan, causes et conséquences du déséquilibre de masse de l'AIS. Dans ce travail, les différents aspects des modèles d'océan et calotte polaire ont été étudiés. Une première étape de cette thèse a été centrée sur à la représentation des flux d'eau douce glaciaires dans les modèles océaniques actuels. Basé sur des estimations glaciologiques, la fonte basale des ice shelves a été répartie sur une grille de ORCA025, et les taux de production d'icebergs ont été appliqués dans une version améliorée du modèle d'iceberg NEMO-ICB. Cette étude préliminaire a été utilisée pour produire une climatologie d'eau de fonte provenant des icebergs, valable pour forcer les modèles d'océan actuels. Ce travail montre l'importance de représenter les flux d'eau de fonte des icebergs pour modéliser la glace de mer, qui peut être obtenu en utilisant notre climatologie. Ces améliorations ont été prises en compte dans l'étude de la réponse du modèle d'océan à la perte de masse de AIS. Cette étude considère une perturbation réaliste de l'eau douce glaciaire aussi près que possible de sa représentation dans les futurs modèles couplés calotte/océan. Selon nos résultats, jusqu'à 50% des changements récents de volume de glace de mer pourraient être causés par le bilan de masse de l'AIS. Le forçage en eau douce glaciaire semble être crucial pour représenter correctement les interactions glace-océan et projeter la glace de mer dans les futurs systèmes couplés. Cependant, l'estimation de l'apport d'eau douce glaciaire dans les modèles climatiques futurs sera fortement affectée par la capacité des modèles de calotte polaire à reproduire les migrations de la ligne d'échouage autour de la calotte. Les modèles de calotte actuels présentent de grandes incertitudes liées aux différents réglages. Dans le contexte des futurs modèles climatiques, nous avons étudié la sensibilité des retraits de lignes d'èchouage forcés par l'océan à l'utilisation de deux lois de frottement différentes et de deux différentes approximations du stress glacier. Les modèle réagit de façon presque similaire aux approximations SSA ou SSA *. Par contre, les différences dans la contribution du glacier à l'élévation du niveau de la mer peuvent être jusqu'à 50% en fonction de la loi de frottement considérée. La loi de friction de Schoof, la plus physique, est nettement plus réactive aux perturbations océaniques que la loi de Weertman, et devrait être pris en compte dans les systèmes couplés futurs. Ce travail souligne que les incertitudes liées aux estimations de migration de la ligne d'échouage dans les modéles de calotte peuvent contribuer non seulement à des incertitudes du futur niveau de la mer, mais aussi de la glace de mer à travers des interactions glace-océan dans les futures modèles climatiques. Une telle conclusion suggère la nécessité d'améliorer la représentation de la fonte basale des ice shelves et du frottement du glacier, afin d'améliorer les projections des modèles climatiques, dans lequel la distribution spatiale et saisonnière des eau douce glaciaires peut jouer un rôle important sur la glace de mer.